1-1-2012

Explicit Finite Element Modeling of the Human Lumbar Spine

Milind Rao
University of Denver

Explicit Finite Element Modeling of the Human Lumbar Spine

Abstract

Validated finite element (FE) models of the functional spinal unit (FSU) and lumbar spine are essential in design-phase device development and in assessing the mechanics associated with normal spine function and degenerative disc disease (DDD), as well as the impact of fusion and total disc replacement (TDR). Although experimental data from fully intact specimens can be used for model calibration and validation, the contributions from the individual structures (disc, facets, and ligaments) may be inappropriately distributed. Hence, creation of decompression conditions or device implantations that require structure removal may not have the proper resulting mechanics. An explicit FE formulation may be advantageous compared to standard analysis due to efficiency in handling complex, changing contact conditions and the ability to evaluate either rigid or deformable body contact. Also, probabilistic studies based on these deterministic FE formulations are of great interest currently as model input parameters (such as properties of nucleus, annulus, ligament stiffness and facet material and geometric orientation) have been characterized experimentally, but contain substantial variability. The use of these FE formulations is not only valuable from an intact spine point of view, but also relevant in understanding and improving the design outcome of procedures like the total disc replacement (TDR). It has been shown that clinical outcome and the incidence of adjacent level disease is linked to the range of motion achieved by the introduction of these disc replacement devices like the ProDisc-L (Synthes Spine, West Chester, PA). Placement of the spherical center of the device as close as possible to the anatomical axis of rotation of the segment is essential in achieving optimal performance.

Accordingly, an explicit FE model of the lumbosacral spine and FSU's L2-L3 and L4-L5 using subject-specific *in vitro* data was developed using sequential transection of each structure. In addition, the objective of this dissertation was to develop a computationally efficient, probabilistic explicit FE model of the lumbar spine, to evaluate spine mechanics for the FSU's L2-L3 and L4-L5. This probabilistic modeling approach was used to assess the capability of efficient probabilistic analyses to predict performance incorporating disc and ligament material variability as well as geometric variability of the facet joint. A well calibrated deterministic and probabilistic model can be used as an excellent computational tool to predict the behavior of the spine with implants like the ProDisc-L. This dissertation also investigates the effect of altering the position of the Prodisc-L implanted in a FE model on ROM during flexion-extension, lateral bending, and axial rotation. Specifically, ROM, bone impingement, implant impingement, and facet forces were evaluated with varying anterior-posterior and medial-lateral placement of the TDR implant.

The uniqueness of this work is the method developed to tune the individual structures in calibrating the FE model using sequential sectioning. This strong calibration against subject-specific *in vitro* data developed confidence in the predictive power of this FE model. For an applied torque, the rotational root mean squared error between the model predictions and the experimental results were within 0.15deg averaged during flexion and extension. The probabilistic analysis compared some of the advanced reliability and probabilistic techniques with the Monte Carlo simulation which is considered the gold standard. The efficient methods accurately estimated the results from Monte Carlo simulation in approximately 5% of computational time. This study on the implanted spine performed on four different spine models showed the importance of using FE techniques as a pre-op templating tool in decision making process for spinal procedures.

Document Type

Dissertation

Degree Name

Ph.D.

Department

Mechanical Engineering

First Advisor

Paul J. Rullkoetter, Ph.D.

Second Advisor

Peter Laz

Third Advisor

Matthew Gordon

Keywords

Calibration and validation, FEA, Finite element analysis, Probabilistic analysis, Spine, Total disc replacement

Subject Categories

Biomedical Engineering and Bioengineering | Mechanical Engineering

Publication Statement

Copyright is held by the author. User is responsible for all copyright compliance.

EXPLICIT FINITE ELEMENT MODELING OF THE HUMAN LUMBAR SPINE

_____

A Dissertation

Presented to

the Faculty of Engineering and Computer Science

University of Denver

_____

In Partial Fulfillment

of the Requirements for the Degree

Doctor of Philosophy

_____

by

Milind Rao

November 2012

Advisor: Dr. Paul J. Rullkoetter

Author: Milind Rao
Title: EXPLICIT FINITE ELEMENT MODELING OF THE HUMAN LUMBAR
SPINE
Advisor: Dr. Paul J. Rullkoetter
Degree Date: November 2012

Abstract

Validated finite element (FE) models of the functional spinal unit (FSU) and

lumbar spine are essential in design-phase device development and in assessing the

mechanics associated with normal spine function and degenerative disc disease (DDD),

as well as the impact of fusion and total disc replacement (TDR). Although experimental

data from fully intact specimens can be used for model calibration and validation, the

contributions from the individual structures (disc, facets, and ligaments) may be

inappropriately distributed. Hence, creation of decompression conditions or device

implantations that require structure removal may not have the proper resulting mechanics.

An explicit FE formulation may be advantageous compared to standard analysis due to

efficiency in handling complex, changing contact conditions and the ability to evaluate

either rigid or deformable body contact. Also, probabilistic studies based on these

deterministic FE formulations are of great interest currently as model input parameters

(such as properties of nucleus, annulus, ligament stiffness and facet material and

geometric orientation) have been characterized experimentally, but contain substantial

variability. The use of these FE formulations is not only valuable from an intact spine

point of view, but also relevant in understanding and improving the design outcome of

procedures like the total disc replacement (TDR). It has been shown that clinical outcome

and the incidence of adjacent level disease is linked to the range of motion achieved by

the introduction of these disc replacement devices like the ProDisc-L (Synthes Spine, West Chester, PA). Placement of the spherical center of the device as close as possible to the anatomical axis of rotation of the segment is essential in achieving optimal performance.

Accordingly, an explicit FE model of the lumbosacral spine and FSU's L2-L3 and L4-L5 using subject-specific *in vitro* data was developed using sequential transection of each structure. In addition, the objective of this dissertation was to develop a computationally efficient, probabilistic explicit FE model of the lumbar spine, to evaluate spine mechanics for the FSU's L2-L3 and L4-L5. This probabilistic modeling approach was used to assess the capability of efficient probabilistic analyses to predict performance incorporating disc and ligament material variability as well as geometric variability of the facet joint. A well calibrated deterministic and probabilistic model can be used as an excellent computational tool to predict the behavior of the spine with implants like the ProDisc-L. This dissertation also investigates the effect of altering the position of the Prodisc-L implanted in a FE model on ROM during flexion-extension, lateral bending, and axial rotation. Specifically, ROM, bone impingement, implant impingement, and facet forces were evaluated with varying anterior-posterior and medial-lateral placement of the TDR implant.

The uniqueness of this work is the method developed to tune the individual structures in calibrating the FE model using sequential sectioning. This strong calibration against subject-specific *in vitro* data developed confidence in the predictive power of this FE model. For an applied torque, the rotational root mean squared error between the

model predictions and the experimental results were within 0.15° averaged during flexion and extension. The probabilistic analysis compared some of the advanced reliability and probabilistic techniques with the Monte Carlo simulation which is considered the gold standard. The efficient methods accurately estimated the results from Monte Carlo simulation in approximately 5% of computational time. This study on the implanted spine performed on four different spine models showed the importance of using FE techniques as a pre-op templating tool in decision making process for spinal procedures.

Acknowledgements

The best moments of my doctoral journey have been shared with many people. It has been a great privilege to spend several years in the Department of Mechanical and Materials Engineering at the University of Denver, and its teaching and non-teaching staff will always remain dear to me. To begin with, special thanks goes to my excellent supervisory team, Prof. Paul Rullkoetter and Dr. Peter Laz for making the process of doing a PhD both an invaluable and enjoyable experience. Thank you for all your support and guidance throughout the project. I also want to extend my thanks to Synthes Spine, especially Dana Coombs and Mike Bushelow for funding my PhD in part. Dr. Cain and Dr. Lafleur from the University of Colorado Hospital were of immense help with their clinical insight. It was a great collaborative effort with Dr. Randy Ching and his team at the Applied Biomechanics Lab, University of Washington. It's been a pleasure working with my labmates (past and present) at the Computational Biomechanics Lab – Clare, Mark, Chad, Sean, Tariq, James, Chandru, AZ, and Justin. Finally, I would like to thank my parents and my brother for tirelessly supporting me through all the life changing events that eventually led me where I am. Thanks to my family for letting me do it 'my way' and for encouraging me at every point in life. This acknowledgement will be incomplete without thanking my friends who helped me achieve great work-life balance.

Table of Contents

List of Figures

List of Tables

Chapter 1: Introduction

The vertebral column is a bony structure comprised of the vertebrae. The lumbar vertebrae are the largest segments of the movable part of the vertebral column. The lumbar spine - or low back - is the third major region of the vertebral column. Most people have five bones or vertebrae in the lumbar spine, although it is not unusual to have six. Each vertebra is stacked on top of the other and between each vertebra is a gel-like cushion called a disc (intervertebral disc). The discs help to absorb pressure, distribute stress, and keep the vertebrae from grinding against each other. A functional spinal unit (FSU) is the smallest physiological motion unit of the spine to exhibit biomechanical characteristics similar to those of the entire spine. An FSU consists of two adjacent vertebrae, the disc and all adjoining ligaments between them and excludes other connecting tissues such as muscles (White AA, 1980).

Low back pain is a chronic and acute medical condition that affects a large portion of the population. Lumbar back pain may result from injury or degeneration of the spinal structures like the discs, ligaments, and facet joints (Adams, 2011). A herniated disc – also referred to as a bulging, ruptured, or slipped disc – is a condition that occurs when an intervertebral disc extrudes into the spinal canal. As a disc degenerates over time as part of the natural aging process, the inner disc material can extrude into the spinal canal causing pain to radiate all the way down the legs and into the feet. Artificial or total

disc replacement (TDR) is a procedure that aims to maintain the intervertebral disc height while restoring the physiologic motion a person would have with a healthy disc.

Experimental testing of spinal segments has historically been conducted to understand overall spine mechanics but does not necessarily help us gain insight on the evaluation of the individual structures like the contribution of ligaments in the overall stability of the spine. On the other hand, if accurately developed, numerical simulations can be used in conjunction with experimental testing. In the recent past, computational technology and numerical simulations have changed the traditional approach of conducting biomechanics research. With the help of sophisticated finite element (FE) models and tools, researchers are seeking answers to fundamental and complex biomechanical phenomena in the field of orthopedic biomechanics. One of the most important steps in the development of FE models of the spine involves the process of geometry creation and assigning material properties to the spinal structures (Viceconti et al., 2005), (Oreskes et al., 1994). Previous FE work has largely consisted of implicit methods that provide static solutions. For quasistatic and dynamic simulations, explicit FE methods have been developed to solve for kinematics and contact mechanics more accurately.

1.1 Aims and Objectives of this Work

The aim of this dissertation was to create lumbar spine models to evaluate natural and implanted spine mechanics. The objectives of this dissertation in particular are:

1. Perform subject-specific model calibration/tuning to *in vitro* experiment.

Understanding the importance of *in vitro* testing and the contribution of each spinal structure on the mechanical stability of the spine is critical for development of surgical protocols and the postoperative treatment of the spinal injuries. The stepwise reduction or addition of soft tissues will prove helpful to quantify the contribution of each functional structure.

2. Evaluate spine mechanics considering variability sources in material and geometric properties.

    The probabilistic FE model is a good platform to understand the uncertainty and variability associated with material and geometric properties.

3. Develop a design-phase computational platform (pre-operational templating tool) to assess device performance.

    The FE model can be used to evaluate the effect of altering the position/placement of an artificial disc implanted in an FSU on the Range of Motion (ROM).

    This work represents a stepwise calibration of a lumbar spine FE model and the prediction of spine mechanics. Chapter 3 of the dissertation focuses on deterministic calibration and verifications with experimental kinematic data from patient-specific testing performed at the University of Washington for multiple geometries. The FE models are calibrated and used for the prediction of combined motions. Many model input parameters, e.g. properties of nucleus, annulus, facets, ligament stiffness and reference strain, have been characterized experimentally, but contain substantial

variability. Chapter 4 includes probabilistic methods to assess the effects of material and geometric uncertainty in the functional spinal unit (FSU). Lastly, Chapter 5 focuses on the application of these FE models to evaluate the influence of disc replacement device positioning on the mechanics of the lumbar spine. The organization of this dissertation is summarized in Figure 1.1.

CT Scans
(Spine A)

ScanIP⁺

Hypermesh*

Assign material properties
(Soft tissues)

Abaqus** solver (Explicit)

Results from FE analysis
(Deterministic)

Matches experimental results
for Spine A?

Reassign material properties
(Using optimization routine)

No

Yes

Apply geometric and material variability

Run probabilistic analysis

Results from FE analysis
(Probabilistic)

Develop pre-op templating tool
using deterministic and probabilistic analysis

Chapter 3

Chapter 4

Chapter 5

⁺Simpleware, Exeter, UK

*Altair Engineering, Inc, MI, USA

** Abaqus, Inc., Providence, RI, USA

Figure 1.1: Dissertation workflow

Chapter 2: Background and Literature Review

2.1 Overview

The human spine consists of seven cervical vertebrae, twelve thoracic vertebrae, five lumbar vertebrae, one sacrum vertebrae (five fused bones), and three to four fused coccygeal segments. When the spine is viewed in the frontal plane, it generally appears straight and symmetrical about the sagittal plane. When viewed in the sagittal plane, four normal curves are seen. These curves are convex anteriorly in the cervical and lumbar regions whereas convex posteriorly in the thoracic region giving the spinal column increased stability and flexibility (Figure 2.1). Each vertebral body is separated by the intervertebral discs and the spinal ligaments (Figure 2.2).

2.2 Components of the Human Lumbar Spine

The smallest physiological motion unit of the spine, the FSU has a complicated geometry, and most of the material properties of their different components (vertebral bodies, intervertebral disc, spinal ligaments, and facet cartilages) show nonlinear behavior, especially the soft tissues. In the next subsections, the various components of the FSU have been discussed in detail.

<u>Vertebral Body</u>

A typical vertebra consists of two essential parts—viz., an anterior segment, the body, and a posterior part, the vertebral or neural arch; these enclose a foramen, the vertebral foramen. The vertebral arch consists of a pair of pedicles and a pair of laminae, and supports seven processes—viz., four articular, two transverse, and one spinous. The lumbar vertebrae (Figure 2.3) are the largest segments of the movable vertebral column. The body is large, wider from side to side than anterior-posterior, and a little thicker in front than behind. It is flattened or slightly concave above and below, concave behind, and deeply constricted in front and at the sides. The vertebral endplates, usually categorized as a part of the vertebral body, marks the boundary with the adjacent intervertebral discs and are thin plates of cortical bone, perforated by many small holes which allow the passage of metabolites from bone to the central regions of the intervertebral discs (Roberts et al., 1989). The pedicles are the strongest portion of the lumbar vertebrae and are directed backward from the upper part of the body; consequently, the inferior vertebral notches are of considerable depth. The laminae are broad, short, and strong; the foramen is triangular, larger than in the thoracic, but smaller than in the cervical region. The spinous process is thick, broad, and somewhat quadrilateral; it projects backward and ends in a rough, uneven border, thickest below where it is occasionally notched. The superior and inferior articular processes are well-defined, projecting respectively upward and downward from the junctions of pedicles and laminae. The facets on the superior processes are concave, and look backward and

7

medial; those on the inferior are convex, and are directed forward and lateral. The former are wider apart than the latter, since in the articulated column the inferior articular processes are embraced by the superior processes of the subjacent vertebra. The transverse processes are usually long, slender, and horizontal.

Like every bone, the vertebral body is divided into the trabecular bone and the cortical bone. It is shown that the dense network of trabeculae offers great resistance to compression because the removal of the cortical bone layer doesn't weaken the structure greatly (McBroom RJ 1985). The load-bearing role of the cortex increases in old vertebrae, which lose bone faster from trabeculae than from the cortex (Adams 2011).

Understanding of the mechanical behavior induced in human intervertebral body bones during physiological activities is of great importance both clinically as well as for research purposes. In clinical practice, it can be extremely useful to plan the individual's rehabilitation after a subject-specific spinal procedure involving the bones. In research, it is important to investigate the mechanobiological phenomenon especially at the bone-screw interface in case of procedures like spinal fusion.

Prior FE models of the intervertebral body have used three kinds of modeling approaches: 1. Vertebral bodies represented as shell elements representing it as rigid bodies to achieve reduced computational time (Moramarco et al., 2010); 2. vertebral bodies represented as solid elements divided into outer cortical region and inner trabecular region with their respective two material definition (Schmidt et al., 2006); and

3. vertebral bodies with the generation of material mapped subject-specific bones from CT data (Sylvestre et al, 2007).

Intervertebral Disc

The intervertebral disc is comprised of the annulus fibrosus (AF) and the nucleus pulposus in the center (Figure 2.4). The AF consists of several concentric layers of fibrocartilage with annular fibers embedded in the ground matrix. These annular fibers are at a tilt angle to the vertical axis (Horton, 1958). The strong composite of annulus fibrosus ground matrix and annular fibers encloses the nucleus pulposus that helps to distribute pressure evenly across the disc. The nucleus pulposus contains loose fibers suspended in a gel with the consistency of jelly.

It has been seen that the AF contains *type I* and *type II* collagen (Bogduk 1997). It has been found that the tissues experiencing tensile or compressive loading show the strong presence of *type I* collagen (Bogduk, 1997). It was also found that the outer layers of the AF have very little *type II* collagen and mainly *type I*. However, at the 'transition zone' between the nucleus and the annulus, *type II* collagen has been observed (Eyre and Muir, 1976). It has been seen that the tilt angle of the annular fibers contain reasonable amount of variation. Even though for modeling and numerical analysis purposes, some researchers vary the tilt angle radially through the annulus (Cassidy et al. 1989), most use a single value to represent this angle. The values used are typically in the range of 50 to 80° (Shirazi-Adl *et al.* 1986, Bogduk, 1997). Accordingly, the primary role of the disc is

9

to transmit loads arising from body weight and muscle activity through the spinal column. They provide flexibility to the vertebral column allowing bending, flexion and torsion.

Research on the intervertebral disc as a whole and its associated structures can be categorized into groups performing experiments on discs and motion segments associated to the disc (Guerin 2006, Thompson et al., 2000, Osti et al., 1990), development of analytical and mathematical models (Elliott 2000) and development of finite element models (Ayturk 2011, Natarajan 1994). Experimental studies provide important data in the form of force, displacements, and pressures. However, it becomes almost impossible to provide kinetic data using experimental techniques. Analytical and mathematical models provide great accuracy in representing the material properties of the disc (McNally and Arridge, 1995), but doesn't necessarily provide accurate representation of the disc geometry. Finite element models not only provide a more realistic geometric and material representation of the disc, but also permit a high control over the method and magnitude of load application. FE models allow simulation of various disc defects and surgical procedures with the possibility of using the same model for several solution runs. It can also be used to determine the internal stress state of the disc and can help to track the changes in pressure inside the nucleus.

Uniaxial and biaxial testing has been performed on specimen from various regions of the annulus fibrosus (ground matrix and collagen fibers). Measurement of their force-deflection relationship has been reported in several works (Wagner 2004, Bass et

al., 2004). Continuum material models of the annulus fibrosus have also been developed that include representations of the extrafibrillar matrix and fibers (Holzapfel et al., 2001) and also the ground matrix and fiber interaction (Elliott et al., 2001). Although experimental data exists, very few groups have simulated and carried out FE analysis of the experimental uniaxial and biaxial setup. It has also been shown that the material properties are different for different locations of the AF (Fujita et al., 1997). It is seen that not only does the location matter, but also the orientation of the specimen (circumferential, radial or axial) from inside the AF matters because of the directional collagen fibers present inside the AF (Guerin et al., 2006).

A common approach to the material modeling of the disc has been to represent them as a linear elastic material formulation that is used to describe both the bulk response of the annulus fibrosus (mainly the annulus ground substance) (Kumaresan et al., 1999); however, the AF behaves nonlinearly and anisotropically under physiological loading (Fujita et al., 1997). Classical linear elastic material theories apply to small strains of approximately (less than 2–5%). Hyperelastic materials exhibit nonlinear elastically recoverable behavior under the application of large strains due to rearrangements in the microstructure, such as reorientation of the fiber directions with deformation. Hyperelastic theory deals with material strains greater than these and is a material description commonly applied to large strain materials such as rubbers. Hyperelastic materials are also incompressible or near incompressible. Hence, representing the AF as anisotropic hyperelastic material model is more appropriate. The

11

fibers in the AF have been modeled in the past as spring elements (Zander et al., 2004) that involves manually placing one dimensional spring elements between two nodes throughout the geometry of the AF. Anisotropic hyperelastic material definition also captures the changes in the preferred fiber directions that reduce the manual spring geometry creation.

Spinal Ligaments

In the human spine, ligaments mainly provide structural stability. The ligament system can be divided into two; the intrasegmental and intersegmental systems. The intrasegmental system holds two vertebrae together. The intrasegmental system includes the ligamentum flavum (LFL), interspinous (ISL), intertransverse (ITL), and the facet capsular (FCL) ligaments. The intersegmental system holds many vertebrae together. The intersegmental system includes the anterior and posterior longitudinal ligaments (ALL and PLL), and the supraspinous ligament (SSL) (Figure 2.2).

The spinal ligaments provide limits to the physiological motion of the spine and protect the spinal cord by preventing motion of the spine outside these limits (White and Panjabi, 1978). Many studies have documented the geometry (Brolin et al, 2004, Pintar et al. 1992, Sharma 1976 Tkaczuk 1968) and the attachment sites (Panjabi et al., 1991) of the spinal ligaments. In addition to the geometric representation of the ligaments, several researchers discuss about the material representation of each ligament in the form of force-deflection or stress-strain plots.

12

White and Panjabi (1978) mentioned the difficulty involved in determining the dimensions and properties of the ligaments. This was primarily due to the difficulties in delineating the boundaries of the ligaments from surrounding soft tissue in the spine. These factors explain the variability observed in the morphology and properties of the spinal ligaments. Chazal et al. (1985) obtained data on the geometry of the spinal ligaments as well as the tensile testing information of 43 human spinal ligaments from fresh cadavers with ages between 30 and 80 years (average age 53). Panjabi et al., 1991 performed anatomic study to determine 3-D morphological information about the attachments points, lengths, directions and cross-sectional areas of the ligaments in the lumbar spine. It has been also been reported that the ligaments of the lumbar spine exist in a state of prestress when *in vivo* (Tkaczuk, 1968). Prestress in the ligament is the force per unit cross-sectional area present when the spine is in the neutral position. The prestress depends on the ligament age and type and vertebrae retract by about 10% when cut. The amount of prestress is directly dependent on the magnitude of intradiscal pressure (Tkaczuk, 1968). This data was used by many groups as the starting point for their FE model but contained substantial variability.

The ligament geometry of most FE models of the human spine has been represented as point to point one-dimensional spring or connector elements (Zander et al., 2004). However, findings show that the ligaments support complex loading patterns with nonuniform plane stress distributions rather than simple axial stresses (Dickey et al., 1996). Unlike the knee FE models where it is common to represent the ligaments as

three-dimensional elements (Weiss et al., 2005), the spinal ligaments (especially the anterior and posterior longitudinal ligaments) are more commonly represented as tension only 'fabric' (two dimensional) elements (Bowden et al., 2008).

Facet cartilages

The zygapophyseal, or facet joint is a complicated biomechanical structure in the spine and understanding its mechanical performance plays an important role in studying the overall spine mechanics. At each spinal level, there is a pair of facet joints located on the postero-lateral aspects of each motion segment. These facet joints are enclosed in a capsular membranous ligament called the 'facet capsular ligament', which is one of the spinal ligaments. The facet joints, along with the intervertebral discs and spinal ligaments, connect the adjacent vertebrae at all levels and provide support for the transfer of loads applied to the spinal column (Figure 2.5). This articulation ensures the mechanical stability and also overall mobility of the spine, while protecting the spinal cord running through it. At each spinal level, the bilateral facet joints are positioned symmetrically relative to the mid-sagittal plane in the postero-lateral regions of the spine (Figure 2.5).

The bony articulating facet joints effectively support the compressive loads and the facet capsular ligament resists tensile forces that are developed across the joint when it undergoes rotations and translations (Adams et al.,1983, Ahmed et al. 1990, Kalichman et al., 2007). The bony facet has an avascular layer of hyaline cartilage covering the

14

articular faces with varying thickness across spinal regions (Yoganandan, 2003). The cartilage is thinner at the edges of the opposing surfaces and gradually increases to its thickest (approximately 1mm) towards the center of the articulating joint, in both the antero-posterior and medio-lateral regions of the joint (Womack 2008).

Recently, there has been a growing interest in the understanding of the facet joints – its biomechanics and physiology. The existing finite element simulations of the spinal facet joint structure include facet bone, capsular ligament and air gap between the cartilages. Researchers have looked at modeling the mechanical environment of the bony geometry and the different tissues in the facet joint (Botolin et al., 2001, Siepe 2010). Goel et al. 1993 and Zander et al., 2004, represented the facet joint as three-dimensional 8-noded interface elements (gap elements) capable of supporting compression only load normal to its surface. In the literature, the contact between the facet joints were also represented as three-dimensional 8-noded hexahedral elements by simulating frictionless surface-to-surface contact elements (Schmidt et al., 2007). Kumaresan et al. (1998) simulated the facet joint in four different models, in two of which the articular cartilage and synovial fluid were not included and in the other two the synovial fluid was simulated by 8-noded incompressible hyperelastic solid or hydrostatic incompressible fluid elements. Both Sharma et al. (1995) and Kumaresan et al. (1998) marked the facet articular surface areas as rectangles and squares, respectively, and they partitioned these areas into zones in which facet contact occurs in order to evaluate contact pressure distributions in the facet joint during flexion, extension, and lateral bending. Womack et

15

al. (2011) investigated four different representations of the articular surface geometry, two anatomy-based thickness distributions, a constant thickness and a flat surface model.

2.3 Clinical Description of Motion and Experimental Setup

Spinal movement is usually measured in degrees of range of motion (ROM). All movements starts from a neutral position, standing up straight, arms to your sides and eyes straight ahead. This is considered as zero degrees. The four movements measured are flexion, extension, lateral bending and axial rotation. Flexion is forward bending; extension is bending backward; lateral bending is side bending; and axial rotation is a twisting motion of the spine (Figure 2.6).

According to the ISO standard for the coordinate systems (ISO/DIS 2631, Mechanical vibration and impacts: evaluation of the effect of whole body vibration in the human; general requirements [Part 1 (08/95)]), the three-dimensional, orthogonal, right-handed coordinate system shall have the following axis designations: X forward or ventral, Y to the left, and Z above or cranial. The transverse plane of the spine corresponds to the x-y plane of the coordinate system, the sagittal plane to the x–z plane, and the frontal plane to the y–z plane (Figure 2.6). With the appropriate definition of the coordinate system the loading components corresponds to the following: lateral bending to the right/left is a pure moment in the $\pm Mx$ direction; flexion/extension is a pure moment in the $\pm My$ direction; and axial rotation to the left/right is a pure moment in the $\pm Mz$ direction. As for the forces: anterior/posterior shear is a force in the $\pm Fx$ direction;

16

left/right lateral shear is a force in the ± Fy direction; and compression in the ± *Fz direction.*

The first loading frames for spine testing were developed by Brown et al. (1957) and Markolf (1972). Advancements in testing on monosegmental and short polysegmental spine specimens in special loading frames with pure moment were introduced using pulleys (Goel 1987, Panjabi 1991). These loading frames either used dead weights or an in-house pneumatic system. In such testing setups, either the load applications or the motions were often constrained and the quality of testing was compromised. Even though these testing systems were technically sophisticated for material testing, they could not reproduce physiological loading. Most *in vitro* testing often neglected the application of muscle forces except the two groups who found that there was a strong influence on the kinematics in the presence of muscle forces (El-Bohy 1989, Panjabi 1989). Spine testers were then developed allowing most kinds of biomechanical, quasi-static, three-dimensional, *in vitro* investigations with monosegmental or entire spines. In most of these testing devices, application of muscle forces and external loads was possible and during the test, the spine was capable of moving unconstrained in all directions (Wen et al., 1993, Wilke et al., 1994). Thereafter several groups have performed *in vitro* pure moments and combined motions experiments using their custom single axis or multi-axis spine simulators that have tested intact as well as instrumented spines with and without the presence of external loads like the follower load (Gornet 2011, Patwardhan 1999, Lee 2010, Gédet 2007).

17

2.4 Prior Deterministic Finite Element Models – FSU and Lumbosacral Spine

The use of FSU models has rapidly grown over the last few years and this section is not intended to include an exhaustive list of studies in this area. However, similarities and differences between models and modeling approaches are discussed here.

FE model development of the FSU includes the modeling of all its components like the spinal ligaments, intervertebral disc, facet joints, and the bony geometry. The primary challenge of modeling this is the estimation of geometry and the assignment of material properties. Several groups have theoretically created the model by adopting the geometry and material properties from experiments performed on individual components (Goel et al., 1993; Lavaste et al., 1992; Pitzen et al., 2001; Shirazi-Adl, 1991; Zander et al., 2001, 2002). These models were created and validated by comparing the torque-rotation responses with experimental data from literature but not necessarily calibrated or stepwise tuned to a subject-specific dataset.

Imaging data that includes CT, MRI and micro-CT's have often been used to extract data for assigning properties of the vertebrae. In most cases, bony material properties have been assigned to the whole region rather than on an element-to-element basis. The values used for the bone (cortical and cancellous) have been relatively consistent (Table 2.1). A value of 12,000 MPa, which was first proposed by Shirazi-Adl et al (1984), has been widely used for the cortical region This value is relatively high, particularly when compared to the range used in many subject-specific vertebral models (Jones and Wilcox 2008).

The inclusion of the ligaments and the facet joints into the FSU adds additional complexity, but extensive research has been done in characterizing the individual behavior of these components (previous sections).From Table 2.1 shows that there exists considerable uncertainty in the values assigned to the ligaments (geometric and material). The ligaments play an important role in the FSU behavior, particularly in bending, and therefore there is a need to accurately characterize these soft tissues.

The geometry of the disc in an FSU has been simplified as an axisymmetric structure (Shirazi-Adl et al., 1986, Natali and Meroi, 1990). A linear elastic material formulation has been extensively used (Table 2.1) to describe the bulk response of the annulus fibrosus (especially the response of the annulus ground substance) (Kurowski and Kubo, 1986; Shirazi-Adl et al., 1986, Goel et al., 1995, Ueno and Liu, 1987, Kumaresan et al., 1999); however, this material has been shown to behave nonlinearly under loading (Acaroglu et al., 1995, Best et al., 1994, Fujita et al., 1997). More recently, nonlinear hyperelastic material definitions have been used to represent the ground matrix of the AF (Rohlmann et al., 2007).

A number of different approaches have been used to simulate the facet interaction. While some groups have modeled a separate cartilage layer by assigning properties (Williams et al., 2007), some have used gap elements whose stiffness changes as the gap closes (Goel et al., 2005, Rohlmann et al., 2007). In both cases, these surfaces have generally been assumed to be frictionless (Williams et al., 2007, Rohlmann et al.,

20077, Schmidt et al., 2007) or a low coefficient of friction has been applied (Bellini et al., 2007, Fantigrossi et al., 2007).

With all these components modeled and the degrees of freedom in the model increasing, the tuning and validation of the model outputs becomes critical and more challenging. Numerous authors employ a validation process that compares the whole segment behavior against published experimental data (Moramarco et al., 2010). A number of studies have performed testing on cadaveric specimens and used this data to directly compare the kinematics with the predicted FE results (Guan et al., 2006, Goel et al., 2005, Kumaresan et al., 1999). In most cases, the predicted torque-rotation was found to match the experimental results. Since most of the models exhibit a nonlinear behavior, it becomes critical to compare the kinematics not only at the endpoints but also though the loading cycle. Guan et al. compared the range of motion prediction through the entire loading cycle to capture the nonlinearity (Guan et al., 2006). This added a greater degree of confidence in the process of calibration. The FE model by Zander et al. predicted the intradiscal pressure and found good agreement with the measured pressure (Zander et al., 2001). In addition to the intact spine modeling, various surgical procedures like posterior decompression, discectomy, total disc replacement were compared and validated (Pitzen et al., 2001, Goel et al., 2005). These models compared well with the experimental values. Most of these analyses were static finite element modeling but Wilcox et al. compared displacements measured across disc and vertebral components using high

speed video with predictions from a dynamic finite element model under impact loading and found agreement within the resolution of the image data (Wilcox et al., 2006).

More sophisticated studies have been performed by employing a calibration process that aims to find the values of a set of parameters which define the material properties of the different structures in the model that achieve the best match between the FE model and the *in vitro* response of the lumbar FSU (Ayturk et al., 2011, Ezquerro et al., 2011, and Schmidt et al., 2007). The experimental data referenced for models created by Ezquerro (2011) was from the results on biomechanical response published by Heuer et al. (2006). In these models dissection stages started with the intact segment and progressively reduced the structure until there remained only the annulus fibrosus and vertebral bodies. Ezquerro et al. calibrated the model by perturbing only the material properties in the optimization process. However, there exist geometric parameters such as the ligament attachment sites, orientation of the facets, direction or dispersion of the collagen fibers inside the AF. There exists a degree of uncertainty associated with these parameters that need consideration as much as the material properties.

As an extension to the FSU models, maintaining the material and geometric properties, several groups have developed computational model to simulate the behavior of normal spine mechanics (Moramarco et al., 2010), instrumented spine mechanics (Rohlmann et al., 2001), and the behavior of degenerated spinal structures (Zander et al., 2004) under physiological loadings and constraint conditions.

All of these studies have taken the first step towards model validation by comparing a generic model and cadaveric testing, but as yet direct subject-specific stepwise segment model validation has not been well understood.

2.5 Probabilistic Methods and Prior Probabilistic Finite Element Models

In probabilistic modeling, input variables are realistic distributions and output distributions are predicted based on the assigned variability. Monte Carlo simulations are the most common type of probabilistic method. In this method, input variables are assigned random values based on the assigned variability. Distributions of output are predicted and the accuracy of the solution is dependent on the number of iterations. High computational cost is associated with the Monte Carlo method but it is also a robust solution method. More computationally efficient and advanced methods include First-Order Reliability Method (FORM), and Second-order Reliability Method (SORM). Reliability methods are typically characterized by the use of analytical techniques that finds a particular point in the design space which can be related (at least approximately) to the probability of failure, defined by a limit state. This point is often referred to as the Most Probable Point (MPP) or the design point. The First-Order Reliability Method (FORM) and Second-order Reliability Method (SORM) are Most Probable Point (MPP) search methods that use an optimization strategy to find the closest MPP on each constraint to the current design, called the Mean Value Point (MVP). While FORM works primary on first order analysis, SORM uses a first-order analysis and the principle

curvatures of the failure function (second-order analysis) to determine the probability of failure at the MPP. Multi-variable optimization is used to calculate the MPP and requires far fewer iterations than the Monte Carlo method. The FORM method and has been shown to perform well for estimations near the mean. It only requires *n+1* iterations, where *n* is the number of random variables.

Sensitivity factors can identify which input parameters are most important to a given output measure (e.g.: disc properties, ligament stiffness, facet cartilage orientation, etc.). More specifically, the FORM method allows for the calculation of α sensitivity factor, which is a relative measure of how much a performance measure is affected by an input parameter. In lumbar spine modeling, sensitivity analysis are mostly used to study the impact of variability in material properties (Lee and Teo, 2005) or deviations in the position and the size of artificial disc implants or pedicle screws (Rohlmann et al., 2001, 2008). These studies have looked at the role of spinal structures on the physiological response by assessing the sensitivity of a model to the input parameters. Many groups have looked at probabilistic model of the FSU and three-segment spine (Lee and Teo, 2005, Rohlmann et al., 2001, 2008), however the lessons learned and results observed from these FSU analysis have not been used in L1-Sacrum spine modeling. The probabilistic framework used for Chapters 4 of this study was implemented using Isight (Simulia, Providence, RI). A more detailed description of the statistic and probabilistic methods can be found in Halder and Mahadevan (2000), Wu et al. (1990), Abaqus manual.

2.6 Pre-operative Templating of the ProDisc-L

Accurate positioning of the ProDisc-L implant is vital to the success of a Total disc replacement (TDR) surgery (Jamali et al., 2009). Traditionally, preoperative planning has been performed on standard radiographs with various techniques, including the use of clear plastic templates (Knight et al., 1992, Linclau et al., 1993). In the recent past, digital templating was proposed as a method to electronically overlay templates from a digital library on clinical radiographs for arthroplasty (Bono et al., 2004). The primary advantage of this technique is the speed and precision of this technique, elimination of hard copy printouts of radiographs along with their associated costs. Although digital templating has become a commonly used tool in hip arthroplasty surgeries and total knee replacement surgeries (Olsen 2009, Trickett et al, 2009), its importance in spinal disc replacement surgeries isn't fully clear.

As spinal discs degenerate, they may become painful, thus limiting function and mechanics which eventually may decrease the quality of life. The gold standard in prevention of pain related to disc degeneration has been lumbar inter-body fusion. TDR, also called as artificial disc replacement, surgery is one of the latest advancements in spine surgery. This surgery is recommended only after extensive non-surgical therapies have failed to significantly provide pain relief. Planning of spinal surgeries is done using a series of coronal, lateral or frontal radiographs. They also include side bending radiographs to trace the incidence of unwanted motions. However, this process involves

several difficult decisions by the surgeon such as proper implant sizing and alignment, choice of the instrumentation systems and types of constructs allowed by each construct. To further complicate the process, the surgeon also has to decide on the optimum placement of these implants that will clinically provide the maximum range of motion (ROM) at the index level without damaging the anatomical constructs like the facet joints. To estimate the TDR procedure and the instrumentation variables, surgery simulators and computer models has been developed in addition to a basic digital image templating (Aubin et al., 2008). Computer models based on finite element (FE) methods (Lafage et al, 2004) and kinetic flexible mechanisms (Desroches et al., 2007) have been developed. Predictions of surgical outcomes using computer modeling along with anemphasis to the biomechanical models present a unique approach. Also, patient-specific FE models of the spine can provide assessments of mechanics associated with degenerative disc disease (DDD) (Schmidt et al., 2007), as well as the impact of fusion (Yan et al., 2011), TDR (Rundell et al., 2008) and facet arthroplasty treatments (Lee et al., 1991).

2.7 Explicit Finite Element Modeling

There are open source, custom-developed and commercial FE solvers to perform computational analysis. Recently, Abaqus[TM] (Dassault Systemes, Providence, RI) has been used extensively in the life sciences domain focusing mainly on computational biomechanics. The Abaqus FE analysis product suite contains a wide variety of materials,

procedures, and load types to simulate the human body, medical implants, and the manner in which the system is used. The work presented in this dissertation was performed using the explicit dynamics FE solution method within the available Abaqus solver. In the finite-element method, a physical structure to be analyzed is divided into a number (often large) of discrete elements. The complete structure may be complex and irregularly shaped, but the individual discretized elements are easy to analyze. The explicit dynamics procedure performs a large number of small time increments efficiently. It used a central-difference time integration rule that is relatively inexpensive because there is no solution for a set of simultaneous equations. The explicit central-difference operator satisfies the dynamic equilibrium equations at the beginning of the increment, t; the accelerations calculated at time t are used to advance the velocity solution to time $t + \Delta t/2$ and the displacement solution to time $t + \Delta t$. Finally, using Newton's second law of motion, the nodal accelerations at the beginning of the current increment (t) are calculated using:

$$\ddot{u}(t) = \mathrm{M}^{-1} \left[\mathrm{P}(t) \cdot \mathrm{I}(t) \right]$$
<div style="text-align:right">Equation 2.1</div>

Where $\ddot{u}(t)$ is the current nodal accelerations, M is the lumped mass matrix, and P and I are the external applied and internal element forces, respectively. The Explicit procedure assumes that using small enough time increments (Δt), the nodal accelerations are constant. This can be used to determine the change in velocity at the middle of the current increment $\mathring{u}_{(t+\Delta t/2)}$ based solely on the velocity from the middle of the previous increment $\mathring{u}_{(t-\Delta t/2)}$ using the equation:

<div style="text-align:center">26</div>

$$\mathring{u}_{(t+\Delta t/2)} = \mathring{u}_{(t-\Delta t/2)} + (\Delta t_{(t+\Delta t)} + \Delta t_{(t)})/2 \cdot \ddot{u}(t) \qquad \text{Equation 2.2}$$

The velocities are integrated through time and added to the displacements at the beginning of the increment to determine the displacements at the end of the increment using:

$$u_{(t+\Delta t)} = u_{(t)} + \Delta t_{(t+\Delta t)} \cdot v_{(t+\Delta t/2)} \qquad \text{Equation 2.3}$$

Once the nodal accelerations are determined from Equation 2.1, the velocities and displacements are advanced "explicitly" through time (i.e. based only on the displacements, velocities, and accelerations at the beginning of the increment) using Equations 2.2 and 2.3, which makes the analysis conditionally stable with small enough time increments. Once the nodal displacements have been determined for the current increment, the element strains, strain rates, and stresses can be determined from the material constitutive relationships for each element type, populating the matrix of internal nodal forces $I_{(t+\Delta t)}$ for the next increment $(t + \Delta t)$.

As seen above, the explicit procedure integrates through time using a large number of small time increments. The central-difference operator is conditionally stable, and the stability limit for the operator (with no damping) is given in terms of the highest frequency (ω_{max}) of the system as

$$\Delta t \leq \frac{2}{\omega max}$$

An approximation to the stability limit is often written as the smallest transit time of a dilatational wave across any of the elements in the mesh

$$\Delta t \approx \frac{Lmin}{Cd}$$

Where L_{min} is the smallest element dimension in the mesh and c_d is the dilatational wave speed. C_d is calculated as the square root of the Young's modulus *(E)* over the mass density *(ρ)*. This indicates that the stable time increment will need to be smaller with a stiffer material (higher E), leading to longer total run times. Conversely, if the density is higher, the wave speed of the material decreases and the total run time decreases.

The explicit procedure which is driven by small increments (governed by the stability limit) is advantageous because it allows the solution to proceed without iterations and without requiring tangent stiffness matrices to be formed. It also simplifies the treatment of contact. The explicit dynamics procedure is ideally suited for analyzing high-speed dynamic events, but many of the advantages of the explicit procedure also apply to the analysis of slower (quasi-static) processes. To reduce the number of increments required, analysts can speed up the simulation compared to the time of the actual process—that is, the analyst can artificially reduce the time period. This has the potential to introduce errors. If the simulation speed is increased too much, the increased inertia forces will change the predicted response (in an extreme case the problem will exhibit wave propagation response). The only way to avoid this error is to choose a speed-up that is not too large. The concept of increasing the simulation speed is called "mass scaling," that reduces the ratio of the event time to the time for wave propagation across an element while leaving the event time fixed, which allows rate-dependent behavior to be included in the analysis. Mass scaling has exactly the same effect on

inertia forces as speeding up the time of simulation. Mass scaling can also be accomplished by altering the density; however, the fixed and variable mass scaling capabilities provide more versatile methods of scaling the mass of the entire model or specific element sets in the model.

In this work, special care was taken and well controlled mesh was generated (thereby maximizing L_e). Also, the material properties (E, ρ) were adjusted to an acceptable level while monitoring the model predictions.

2.8 Conclusions

From the review of literature, it was seen that a well validated and developed FE model of the human lumbosacral spine would provide valuable information and enable a variety of clinically relevant investigations. Although the calibration method may be time consuming, it is important to conduct a stepwise calibration at the FSU level. The model needs to be well tuned in relation to the experimental response of different anatomical dissections of the functional spinal unit. This technique would also involve appropriate representation of the components like the disc stiffness, ligament properties and facet contact modeling.

In order to carry out this investigation, deterministic and probabilistic finite element modeling and analysis technique of the human lumbar spine was proposed. The technique used here for developing a computational model increases the confidence in the validation process. To account for the material and geometric uncertainties, probabilistic

and reliability techniques will be employed in this work using Monte Carlo simulation and computationally efficient methods like FORM. This will make sure that we not only validate the deterministic model but also look at a wide population of specimens. Additionally, this FE model will be a great platform to understand the influence of TDR on the spinal mechanics in terms of range of motion, templating for implant selection, decision making between fusion and TDR etc

Table 2.1: Values of the elastic modulus used for the main components of the lumbar spine FE models

	Elastic modulus of vertebral bone components (MPa)			Elastic modulus of intervertebral disc components (MPa)			Elastic modulus of ligaments (MPa)						
	Cortical	Cancellous	Posterior	Ground matrix	Collagen fibers	Nucleus	ALL	PLL	LFL	FCL	ISL	SSL	ITL
Ayturk et al., 2011	E11=E22=8000,E33=12000 ²	Orthotropic	3500	Fiber reinforced Yeoh material		1	Exponential force-displacement curves						
Ezquerro et al., 2011	Orthotropic		3500	Hyperelastic (Mooney Rivlin)			Non-linear elastic material						
Moramarco et al., 2010	Rigid body	Rigid body		Hyperelastic									
Sylvestre et al., 2007	8000-14000²	375-2000²	-	8	550	2	7.8	1	1.5	43.8	35.1	3	10
Kim, 2007	12000	100	3500	4	Variable	Not modeled	20	70	50	20	28	28	50
Bellini et al., 2007	12000	340	3500	E_rad=35, E_ten=8, E_axial=2		1	7.8	10	17	7.5	10	8	10
Hato et al., 2007	10000	750	-	Hyperelastic	7.5	Incompress, Fluid	Non-linear behavior						
De Visser et al., 2007	5000	74	Inner 74, outer 5000	4	450	1	20	20	10	10	10	10	10
Williams et al., 2007	12000	100	3500	2.56	Non-linear	1.56	11.9	12.5	2.4	7.7	3.4	3.4	3.4
Fantigrossi et al., 2007	12000	340	3500	4.2	500	1	Non-linear elastic spring elements						
Schmidt et al., 2006	Orthotropic	Orthotropic	3500	Mooney–Rivlin	Stress-strain curve	Mooney–Rivlin	Calibrated force–deflection-curves						
Rohlmann et al., 2006	10000	200	3500	Hyperelastic	Non-linear	Incompress, Fluid	Non-linear behavior						
Zander et al., 2001	6000	500	-	Hyperelastic	Non-linear	Incompress, Fluid							
Goel et al., 1995	12000	100	3500	4.2	175/450(15%¹)	4	7.8/20(12%¹)	10/20(11%¹)	15/20(6.2%¹)	7.5/32.9(25%¹)	10/12(14%¹)	8/15(20%¹)	10/58(18%¹)
Lavaste et al., 1992	12000	100	1000	2	500	4	10	10	10	10	10	10	10

Notes:
¹ Bi-linear elastic model used, bracketed values show strain value at cut-off between first and second value
² Element-specific values taken from CT greyscale
Where the models have included degeneration/osteoporotic variations, only the values for healthy tissue are shown
More recent studies have adapted material values from the above mentioned work

31
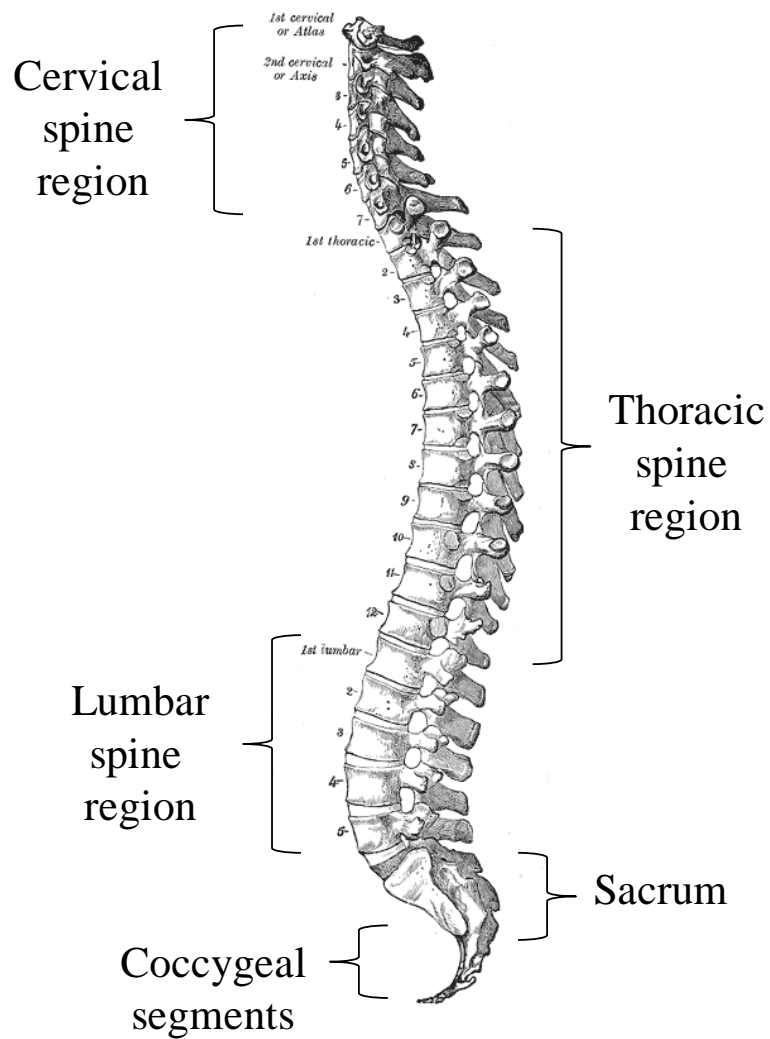
Figure 2.1: The human vertebral column with various regions (Adopted from www.bartleby.com)
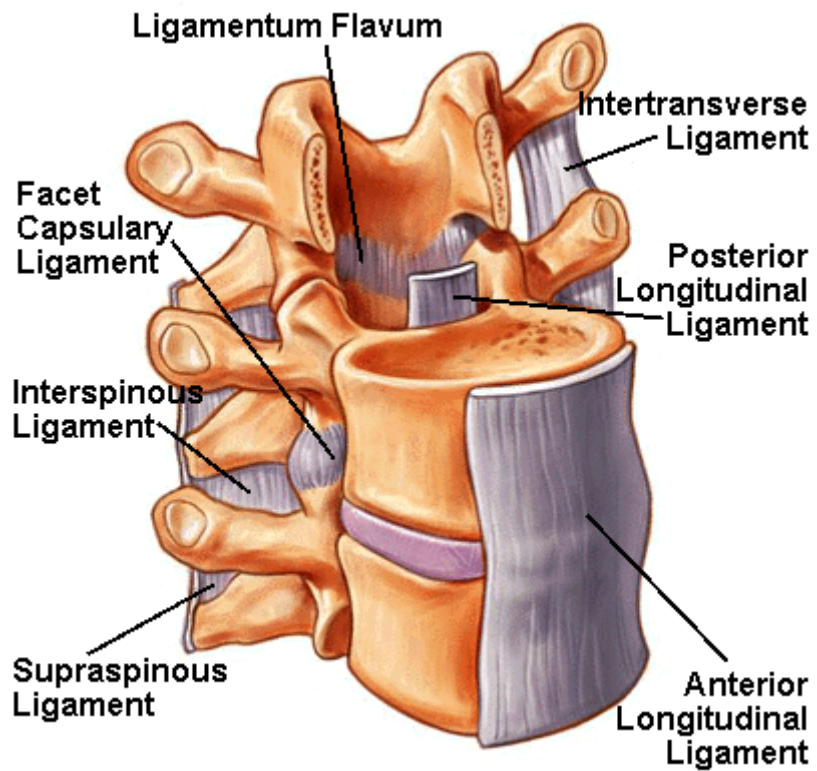
Figure 2.2: The functional spinal unit (FSU) separating the bones by disc and the
spinal ligaments (Adopted from www.spineuniverse.com)
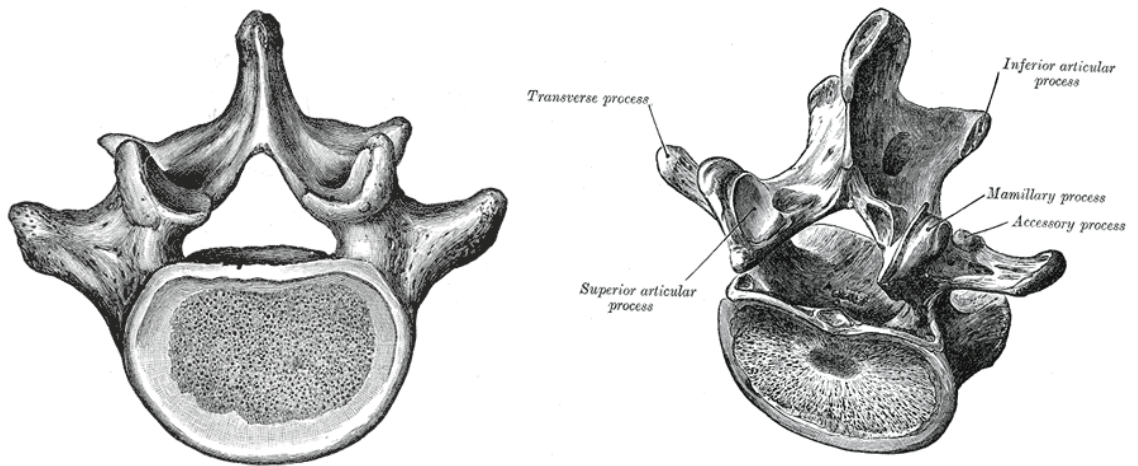
Figure 2.3: A lumbar vertebra from above and behind (Adopted from Gray's Anatomy of the Human Body)
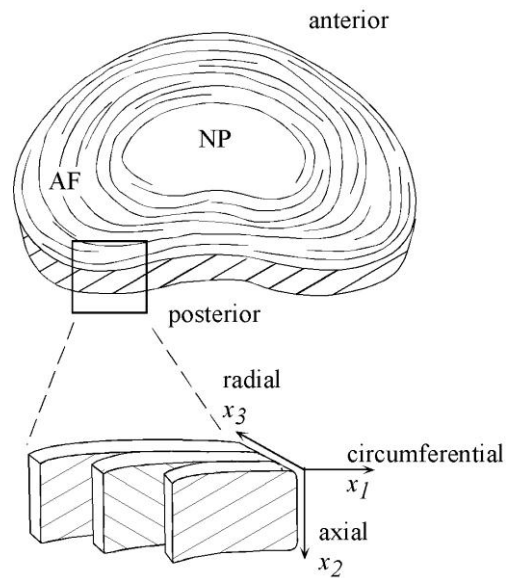
Figure 2.4: The intervertebral disc comprising of the annulus fibrosus (AF) and the nucleus pulposus (NP) in the center and showing the different directions of the multiple AF layers (Adopted from www.spineuniverse.com)
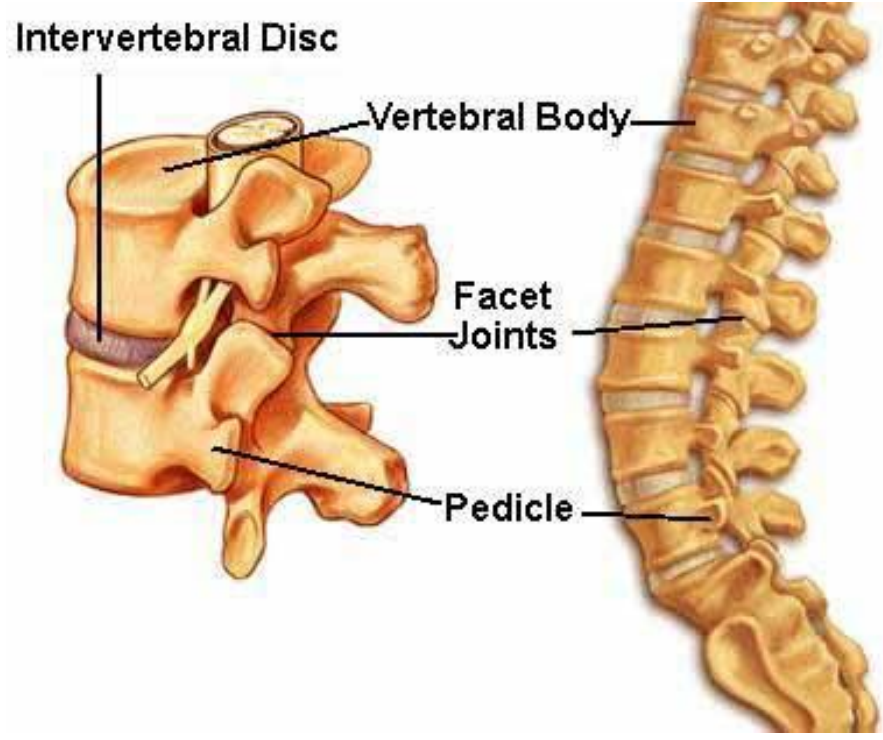
Figure 2.5: The FSU and the vertebral column with the facet joints and the pedicles (Adopted from Netterimages.com)
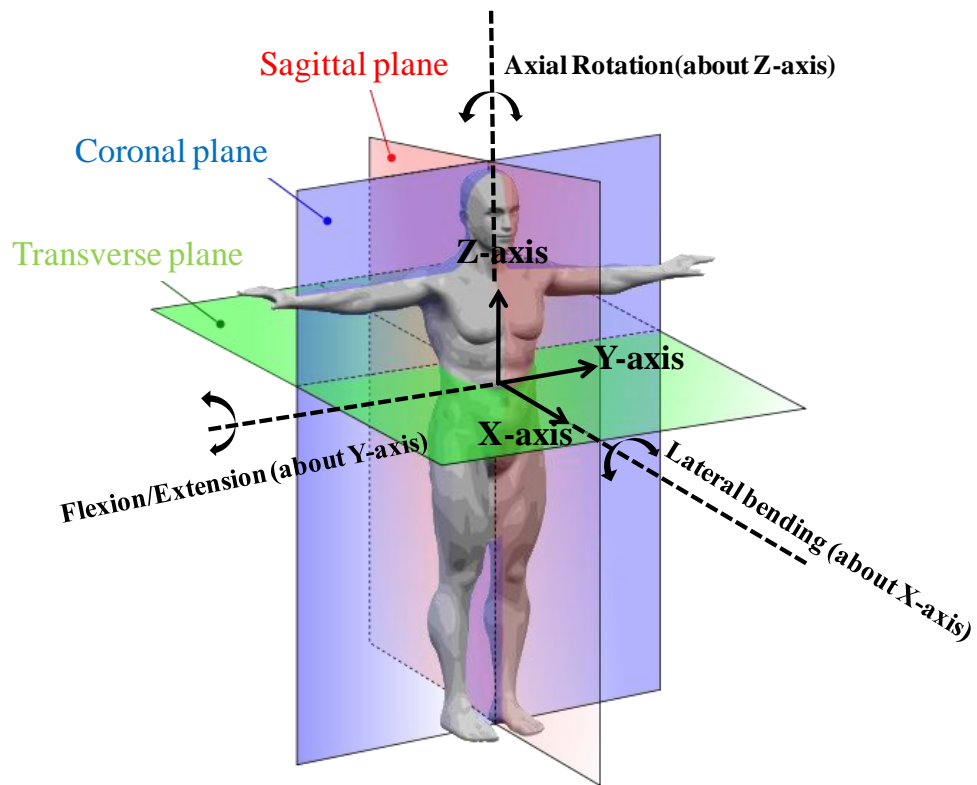
Figure 2.6: Anatomic planes with the clinical directions and motions of the spine (Adopted from Wikipedia.com)

Chapter 3: Calibration and Validation of a Finite Element Model of the Human Lumbar Spine

3.1 Background and Motivation

The previous chapter described the fundamental aspects of spine anatomy and computational spine biomechanics. This chapter presents an approach to calibrate a finite element (FE) model of the human lumbar spine to patient-specific *in vitro* data. A strongly calibrated and validated FE model of the spine will be extremely valuable as a predictive tool in answering clinically relevant questions.

3.2 Introduction

Understanding the functional spinal unit (FSU) is essential in assessing the mechanics associated with normal spine function, spinal loading (Stokes and Gardner-Morse, 2001) degenerative disc disease (DDD) (Schmidt et al., 2007), simulations of surgery (Aubin et al., 2003) as well as the impact of fusion, and total disc replacement (Lee et al., 1991). The FSU is comprised of bones and complex soft tissues, such as intervertebral discs (IVD), muscles and ligaments. Damage or degeneration of structures of the FSU is a common phenomenon resulting in instability of the spine (Oxland et al., 1991). Prior *in vitro* studies have focused on understanding the behavior of isolated

structures such as ligaments (Chazal et al., 1985, Pintar et al., 1992), muscles (Wilke et al., 1995), facet joints (Wilson et al., 2006), IVD (Polga et al., 2004), but the contribution of each structure to the overall kinematics of the spine is essential (Panjabi et al., 1975)..

Heuer et al. performed *in vitro* testing to study the biomechanical effect of stepwise anatomy reduction for several loading magnitudes (Heuer et al., 2007).

Conventionally, finite element (FE) models have been used to answer clinically relevant questions in the field of knee, ankle, and spine biomechanics (Halloran et al., 2005, Anderson et al., 2007, Goel et al., 1993). In the past, several FE models of the lumbosacral spine have been developed to simulate the behavior of normal spine mechanics (Moramarco et al., 2010), instrumented spine mechanics (Rohlmann et al., 2001), and the behavior of degenerated spinal structures (Zander et al., 2004). Many models have been developed and validated with *in vitro* data from literature to quantify the overall mechanics of the lumbosacral segment (Moramarco et al., 2010, Shirazi-Adl et al., 1994, Ezquerro et al., 2004). However, it is important to create FE models using patient-specific *in vitro* data involving a stepwise addition of spinal structures resulting in a well performed calibration and structure validation. Additionally, a validated explicit FE formulation has advantages over an implicit FE formulation due to its efficiency in handling complex, changing contact conditions, the ability to evaluate either rigid or deformable body contact, and to reduce the analysis time to make optimization and probabilistic studies feasible.

Previous efforts have applied a FE-model calibration process starting with the basic disc only configuration and then stepwise adding and validating the model (Ezquerro et al., 2011, Schmidt et al., 2007, Shirazi-Adl et al., 1986a). However, those models focused on modeling a single FSU and no attempt was made in calibrating the entire lumbosacral segment. Accordingly, the objective of the present study was to develop and validate a patient-specific explicit FE model of the human lumbosacral spine. Stepwise addition of spinal structures based on *in vitro* testing carried out at the University of Washington was used to calibrate a healthy lumbosacral spine (none to mild disc degeneration) identified as *Spine A*. Analogous to the testing, models were developed for individual FSU's (L2-L3 and L4-L5) and a multi-segment lumbar spine (L1-Sacrum). The load-deflection characteristics, contact mechanics and efficiency of the FSU's were evaluated using a deterministic approach. As an extension to this methodology, another spine model from a different patient was developed identified as *Spine B*. Given the similarity in the method used to develop these two spine models and for the purpose of brevity, the methods, results and discussions from *Spine A* have only been documented as a part of this dissertation.

3.3 Methods

3.3.1 *In Vitro* Testing

A series of *in vitro* tests were conducted on a fresh-frozen intact lumbosacral spine. The spine was identified as *Spine A* (33 years old male subject in healthy spine

condition). To prepare the spine for computed tomographic (CT) scanning, the specimen underwent gross dissection to remove unnecessary spinal levels, residual rib attachments, and soft tissues structures. Four non-metallic (radio-opaque) CT marker beads (4-mm diameter, SureMark, Simi Valley, CA) were embedded into each vertebral level to serve as fiducial (reference) markers for subsequent registration of the measured vertebral kinematics. Placement of the beads was performed by burring shallow, hemispherical holes into the vertebral body, lamina or transverse processes, then securing each bead in the hole with cyanoacrylate glue.

Pure-moment, combined motion, and compressive tests were performed according to the following testing protocol. Pure-moment (flexion-extension, lateral bending, axial rotation) and combined motions testing was performed using a custom multi-axis spine motion simulator (Figure 3.1) in tandem with a Vicon 3-D motion analysis 4-camera system (Vicon Motion Systems, Lake Forest, CA) to track segmental spinal motions. Pure bending moments were applied to each specimen via three independently controlled rotary actuators (HD Systems, Hauppauge, NY) that were digitally controlled to induce sagittal-, coronal-, or transverse-plane rotational moments while allowing the spine to freely displace in X, Y and Z via air bearings. The applied loads to the test specimen were recorded using a six-axis load cell (ATI Industrial Automation, Apex, NC) connected to a data acquisition board (National Instruments, Austin, TX) sampling at a rate of 100 Hz. In addition to pure-moment testing on the spine simulator, two FSUs were also tested to obtain axial compressive stiffness of the IVD. An MTS servohydraulic test

frame (MTS Corp., Eden Prairie, MN) was used to perform the testing. A load cell (Robert A. Denton, Inc., Rochester Hills, MI) recorded the axial compressive forces, while the MTS linear variable differential transformer (MTS Corp., Eden Prairie, MN) measured the actuator displacement.

For the FSU testing, a sequential sectioning protocol was performed to remove spinal structures while repeating tests to evaluate the contribution of the sectioned structures to the overall mechanics of the motion segment (Table 3.1).

3.3.2 Finite Element Model Development

A three-dimensional explicit FE model of *Spine A* was developed in Abaqus/Explicit (Abaqus, Inc., Providence, RI, USA) from a series of coronal CT images (in-plane resolution of 0.375 mm/pixel; 512 X 512 pixels; 0.625mm slice thickness). The visible bony structures of the vertebral bodies were manually segmented and exported as 3D surface geometries using ScanIP (Simpleware, Exeter, UK). Similar to the marker beads (fiducial markers) glued to the bone in the experiment, rigid body spheres were modeled on the vertebral bodies exactly at the position as seen in the experiment. To reduce computational cost, bones and articulating facet surfaces were considered rigid for all analyses with facet contact defined by a previously verified pressure-overclosure relationship.

Seven of the load-bearing ligamentous structures crossing each of the FSU were represented by connector elements (Figure 3.1) including the anterior and posterior

longitudinal ligament (ALL, PLL), supraspinous and intraspinous ligament (SSL, ISL), intertransverse ligament (ITL), facet capsular ligament (FCL) and ligamentum flavum (LFL). These ligaments were modeled by multiple nonlinear, tension only connector elements in series and parallel. Most of the ligament attachment sites were based of the dissection performed after testing. Few attachment sites were adopted from literature based descriptions (Panjabi et al., 1991).

Based on the dissected geometry of the IVD (Figure 3.2), the annulus fibrosus (AF) comprised of three major regions (anterior, posterior and laterals) modeled as 8-noded hexahedral elements and a fluid-filled cavity representing the nucleus (Figure 3.2). A common approach to the material modeling of the disc is to represent them as linear elastic material formulation that is used to describe both the bulk response of the annulus fibrosus and the response of the annulus ground substance (Kumaresan et al., 1999); however, the AF behaves nonlinearly and anisotropically under physiological loading (Fujita et al., 1997). Classical linear elastic material theories apply to small strains of approximately (less than 2–5%). Hyperelastic materials exhibit nonlinear elastically recoverable behavior under the application of large strains due to rearrangements in the microstructure, such as reorientation of the fiber directions with deformation. Accordingly, the regions of the AF were represented as anisotropic hyperelastic (Holzapfel) with C_{10}, D, k_1, k_2 and *kappa* being the material constants. In a separate analysis, uniaxial tensile tests were simulated with specimens from different regions of the AF to match the micro behavior of the AF (Appendix A1.2). FE analysis of simple

tensile tests of AF strips cut along (simulation) the axial and circumferential directions were used for this analysis. On a macro level, in the FSU model, the AF was represented as two families of collagen fibers embedded in a soft incompressible ground matrix.

The lumbosacral L1-sacrum model incorporated intervertebral bodies L1 through sacrum separated by IVD, ligaments, and facet joints at each level (Figure 3.2). Four fiducial markers were modeled on each bone from L1 through sacrum. The annulus fibrosus at each level and the ligaments between each bone were represented by their own set of material constants giving the freedom to tune the property at each level.

3.3.3 Finite Element Analysis and Calibration

For the FSU testing, a stepwise reduction of structures protocol was followed. In contrast, to validate the FSU's, Abaqus/Explicit analyses were performed using a stepwise addition of structures approach starting with the most basic configuration of the bones separated by the IDV. The facet cartilages were then added in the model followed by the facet capsules (FCL), ITL, ALL, PLL, LFL, ISL, and SSL. Pure moment analysis in the principal axes – Flexion-Extension (Flex-Ext), Lateral bending (LB), and axial rotation (AR) were performed force controlled to a moment limit of 10Nm (in the intact FSU configuration) or, in the case of a "hybrid" analysis, to the maximum angle limit recorded during the specimen's intact configuration. Except for the intact configuration analysis, the inferior bone was kept fixed and displacement was applied to the fiducial markers modeled on the superior bone to reproduce the hybrid tests. Displacements were

applied to the fiducial markers in the form of translations and rotations to mimic the experiment. The finite element analysis was repeated after the addition of each spinal structure to evaluate the contribution of the sectioned structures to the overall stability of the segment. Reaction moment (RM) from the analysis was compared to the moment measured during the testing. In addition to pure moments, compressive tests were simulated on two FSU's where the load was ramped up to 1000N to obtain a relationship between load and displacement.

In any given analysis, anywhere between twelve to twenty five input parameters were included in the optimization based on the structural configuration that was being evaluated: C_{10}, K_1, K_2 and *kappa* for three regions of the AF, seven ligament stiffness, three translations (along X-, Y-, Z-axis) of the facet cartilage and three rotations (about X-, Y-, Z-axis) of the facet cartilage. Using literature values to define initial and maximal bounds for stiffness (Pintar et al., 1992), input parameters were perturbed with the adaptive simulated annealing global optimization algorithm within Isight (Dassault Systems, Providence, RI) to minimize the Root Mean Squared (RMS) error between the model-predicted curves and experimental force-deflection or reaction moment-time curves.

For the L1-Sacrum analysis, the sacrum was kept fixed in all degrees-of-freedom. In these analyses, each follower load point (at the center of mass of the bone) was manually adjusted such that the application of the 450N preload did not introduce segmental angular displacements. This assured that the follower load modeling was

44

providing only a compressive load to the specimen, and moment applied to the bone L1 would be a pure bending moment. In the presence of 450N follower load (FL) (only for flexion and extension loading), pure moment of 10Nm was applied to L1. A manual optimization of the follower load path was performed to minimize the intervertebral rotations at the end of FL application. As a starting point, similar to FSU optimization, the input parameters were perturbed with the adaptive simulated annealing algorithm to minimize the RMS error between the model-predicted torque-rotation curves. The multisegmental FE model was calibrated for pure moment as well as combined motion cases (including moment with follower load). Based on the geometry and initial orientation of the facets, an automated optimization was performed using Isight followed by manual tuning.

3.4 Results

3.4.1 Stepwise Calibration and Optimization

Representative optimization results for *Spine A* FSU L4-L5 are shown in Figure 3.3a for flexion-and axial rotation with two different setups – 'disc only' and 'without ISL, SSL and PLL' that correspond to the experiment. The reaction moment was predicted in time to perform optimization on the structure properties to reproduce the collected experimental data. In these plots, the reaction moment is plotted on the Y-axis with the X-axis being the loading cycle time (Appendix A1.5-A1.13). As expected with the model tuning, the FE model prediction was in good agreement with the experiment.

45

Compressive load was applied to two FSUs and following the optimization process, the force-displacement results closely matched the experimental data (Figure 3.3b). In the FE model, compressive force of 1000N caused displacements of 1.10 and 1.33 mm FSU L2-L3 and FSU L4-L5 respectively. In addition to the actual model tuning, uniaxial tensile testing was performed on small specimens (~20x10x5mm) of the annulus fibrosus to obtain force-deflection characteristics as shows in Appendix A1.2-A1.4.

In the case of the "hybrid" analyses, displacement control analyses were setup by prescribing displacements to the fiducial markers from the experimental data. Capturing the change in stiffness response, the required torque (reaction moment) to achieve the intact case angle limit was computed for each of the stepwise structure addition configuration. The results from the optimization process matched well with the experiment and are shown in the form of bar graphs for the L2-L3 and L4-L5 FSU's in Figure 3.4 and Figure 3.5 respectively.

3.4.2 Intact FSU Kinematics

For the intact case, material property optimization of L2-L3 and L4-L5 FSU's were performed using the torque-rotation behavior in flexion-extension, lateral bending and axial rotation. These analyses were performed force controlled with applied torques of 10 N-m. Torque-rotation response comparison of the model with the experiment for FSU L2-L3 and L4-L5 is shown in Figure 3.6 top and bottom respectively. The non-linearity of the FSU was excellently represented by tuning the soft tissue properties to

46

experimental *in vitro* data (Table 3.1). The resulting range of motion or amount of rotation corresponding to the 10 N-m of loading for the intact FSU cases is summarized in Table 3.2. Lastly, root mean squared errors (RMSE) were computed over the torque-rotation curves for each loading degree of freedom (Table 3.2). RMSE for all loading cases across various FSU's was between 0.05 and 0.25° with the average being in the range of 0.09 to 0.17°.

For the intact FSU optimization results explained above, the tuned ligament stiffness were as shown in Table 3.3. The deflection was kept constant while the force was varied to change the stiffness slope. The reference strain was manually adjusted once before the optimization routine was implemented. For the disc only compression analysis, no significant differences were found for C_{10} with variation in AF region (Table 3.4). The value of C_{10}, which directly relates to the stiffness of the ground matrix, increased from 0.4 to 1.57 MPa anterior to posterior. However, the anterior, lateral and posterior regions showed significant differences with respect to K_1 and K_2. The lateral regions of the AF showed an increase in *kappa* value which shows a difference in the microstructure between the anterior/posterior and the lateral regions. Low values of *kappa* − 0.06 and 0.07 in the anterior and posterior regions respectively show that the collagen fibers in the AF are perfectly aligned (no dispersion). However, a value of 0.17 in the lateral region indicates that the collagen fibers are more randomly distributed as compared to the other regions.

3.4.3 L1-Sacrum Calibration and Optimization

Comparison of the calibrated and experimental torque-rotation curves are presented for each segment and the whole spine are shown in Figures 3.7-3.9 for follower load and flexion-extension. Pure moment evaluations were performed for lateral bending (left and right) and axial rotations (clockwise and counterclockwise). The representative torque-rotation curves are presented in Figure 3.10 and Figure 3.11 The image to the right of each curve indicates the FSU level or whole spine being evaluated. The flexion-extension analyses included a 450N follower load applied along a manually optimized path that maintained intersegmental rotation as close as possible to zero at the end of follower load application. In general, the calibrated curves compared well with the experimental behavior. The model calibration tended to match or err with slightly stiffer behavior.

3.4.4 L1-Sacrum Prediction and Kinematics

As a measure of predictive capability, the model, calibrated with the single degree of freedom analyses, predicted the experimental behavior for a combined flexion (7Nm) and lateral bending (7Nm) loading conditions. Results of the combined loading comparison are shown in Figure 3.12-3.15 for the flexion-extension components, lateral bending components and axial rotation components. The torque-rotation RMSE between the model predictions and the experimental results were within 0.15°. Additional plots during different loading conditions are represented in Appendix A1.16-A1.23.

3.5 Discussion

The purpose of this study was to create a calibrated FE model of the human lumbosacral spines (FSU and multisegmental) using *in vitro* subject-specific scan and experimental testing data. Patient-specific FE model validation provides improved realism over validation to literature data by considering subject-specific anatomical representations and mechanical behavior. This study utilized a rigorous stepwise structure addition process and applied optimization at each step to match model response to the experimental protocol. The process ensures that the contribution of each structure is appropriately represented in the various degrees of freedom. This is especially relevant for evaluations of implants, as structures are often resected as part of the surgical procedures. By appropriately capturing the contribution of each structure, engineers and designers can have greater confidence that the instrumented evaluations are appropriately characterizing the contributions of the implant and structures.

This model development included several notable improvements compared to previously developed spine models in terms of an optimization workflow using Isight and Abaqus, and an improved representation of structures. The Isight optimization software was able to directly interface with Abaqus .odb results files. This communication facilitated the data exchange including multifactorial objective functions, e.g. torque-rotation behavior in multiple degrees of freedom. A robust optimization algorithm, adaptive simulating annealing was able to consider uphill movements and was successful

in determining global optima. Each analysis took anywhere between three minutes (disc only configuration) to 20 minutes (intact FSU). The optimization routine performed around 300 iterations to converge to the objective function. The entire lumbosacral spine lasted anywhere between two to three hours based on the loading condition.

Some of the FE models of the spine have represented the soft tissue material properties of the annulus fibrosus (AF) as a combination of ground matrix with fibers placed in a criss-cross orientation. However, that representation was not able to appropriately capture the contributions of the ground matrix and fibers, and was also labor intensive to create. The current model utilizes an anisotropic hyperelastic material for the annulus, with optimized parameter values that capture the experimental disc only data. Additionally, a pilot analysis was performed using 2-D fiber-reinforced membrane representations of ligaments (Appendix A1.15).

The explicit finite element analyses were run with an aggressive stable time increment to decrease analysis times for the many iterations required for the optimization procedure. In some cases, small oscillations were observed in the results which can be removed by running the analyses slower.

In closing, this study developed calibrated computational models to appropriately capture the behavior of individual structures and collectively reproduce the behavior of the lumbar spine. By appropriately representing the *in vitro* testing during a sequential resection protocol, a computation tool has been validated that can be used in performing

design phase assessments of implant design concepts and in providing insight into a variety of spine mechanics related research questions.
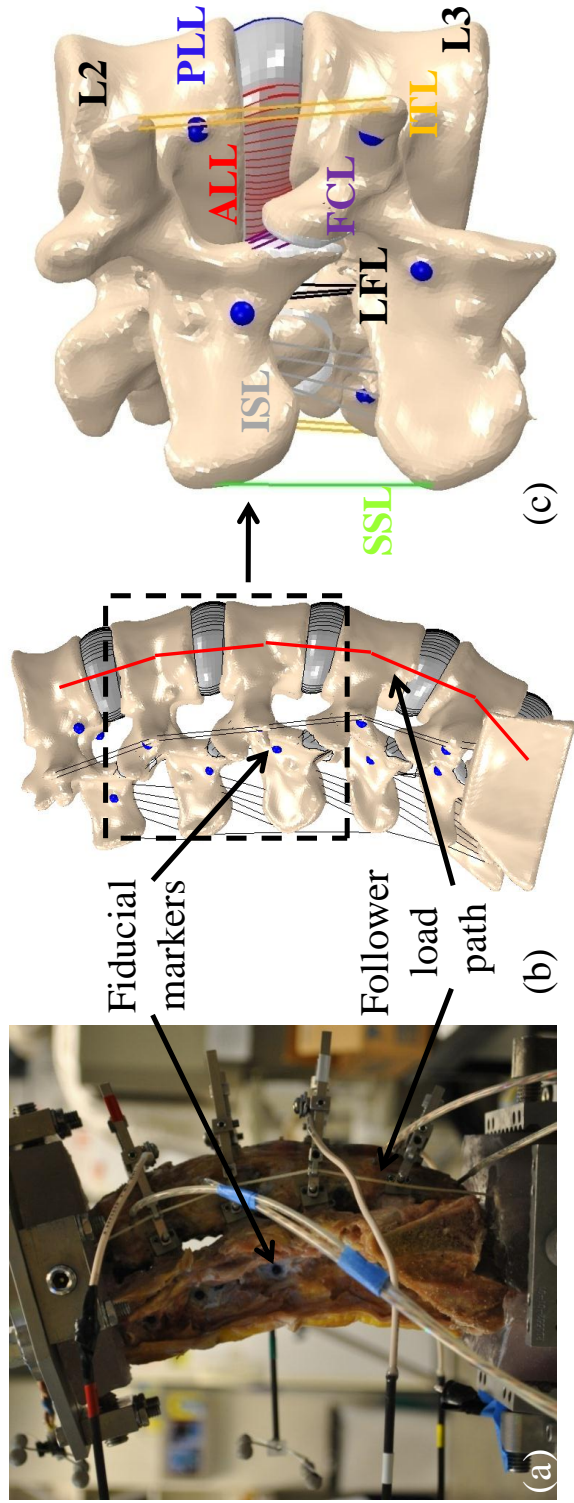
Figure 3.1: (a) Cadaveric setup of *Spine A*. (b) Subject specific finite element model of the lumbosacral spine and (c) Ligamentous representation of FSU L2-L3

52
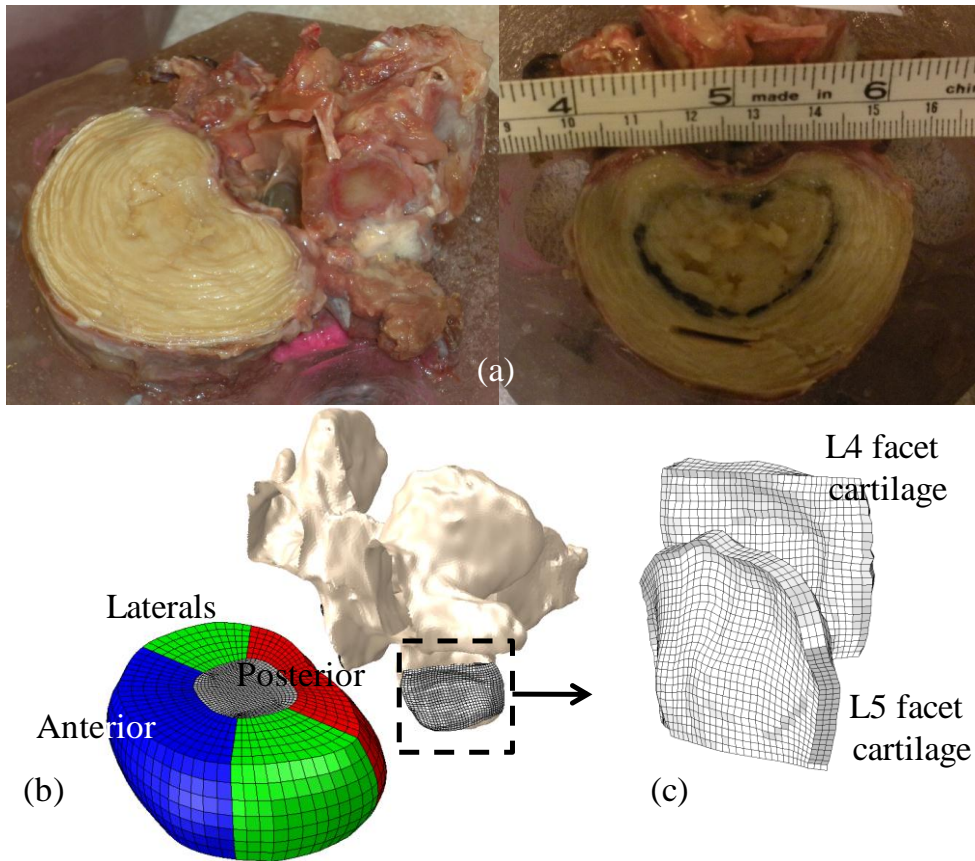
Figure 3.2: (a) Dissection of the IVD and marking of AF-nucleus regions on the

cadaver. (b) Digitization and reconstruction of hex elements representing the AF and its

three regions – anterior, posterior & laterals (c) Hex mesh of articulating facets
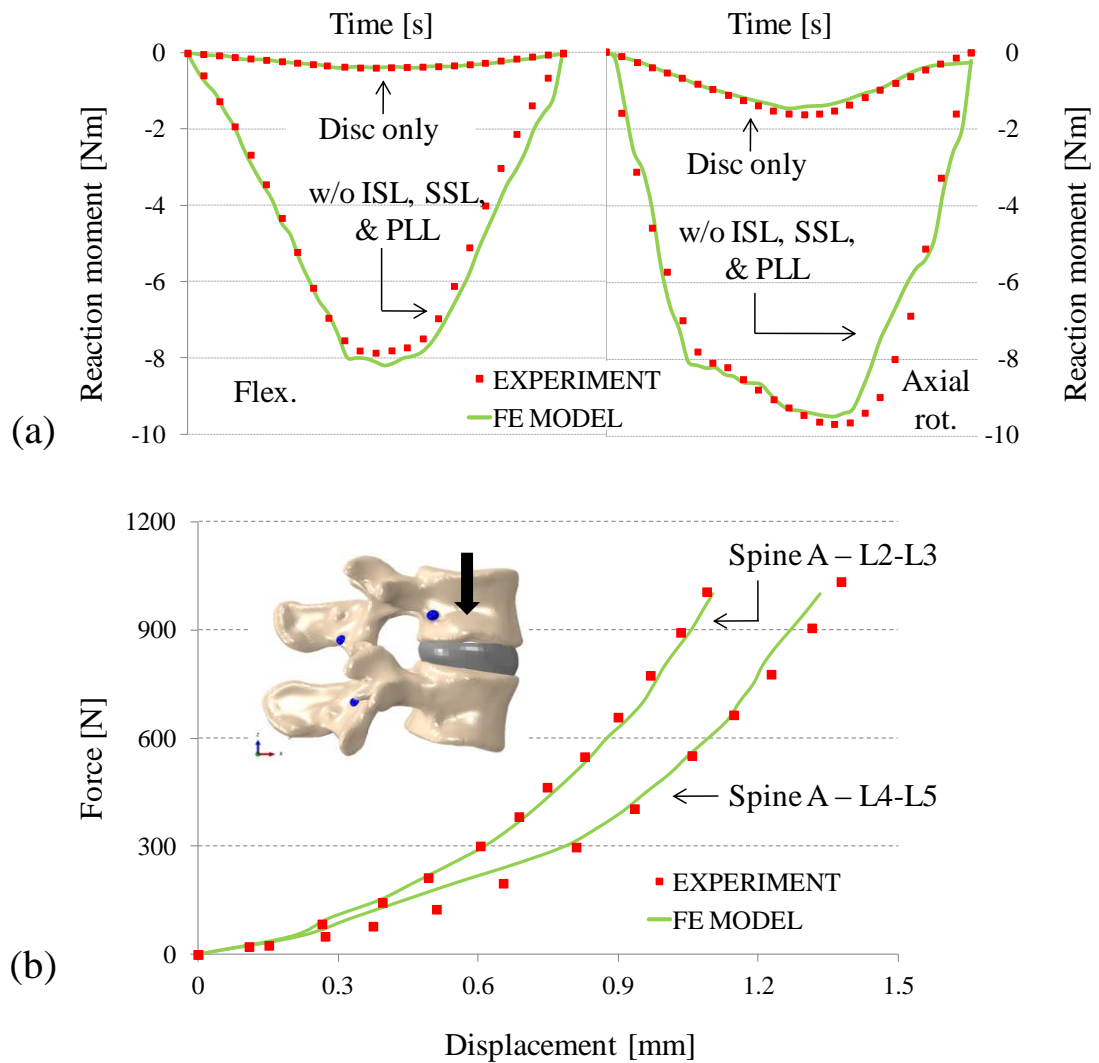
Figure 3.3: (a) Representative reaction moment versus time curves during flexion (left) and axial rotation (right). (b) Experiment and FE model force-displacement response for compression of the intervertebral disc for FSU's L2-L3 & L4-L5

54
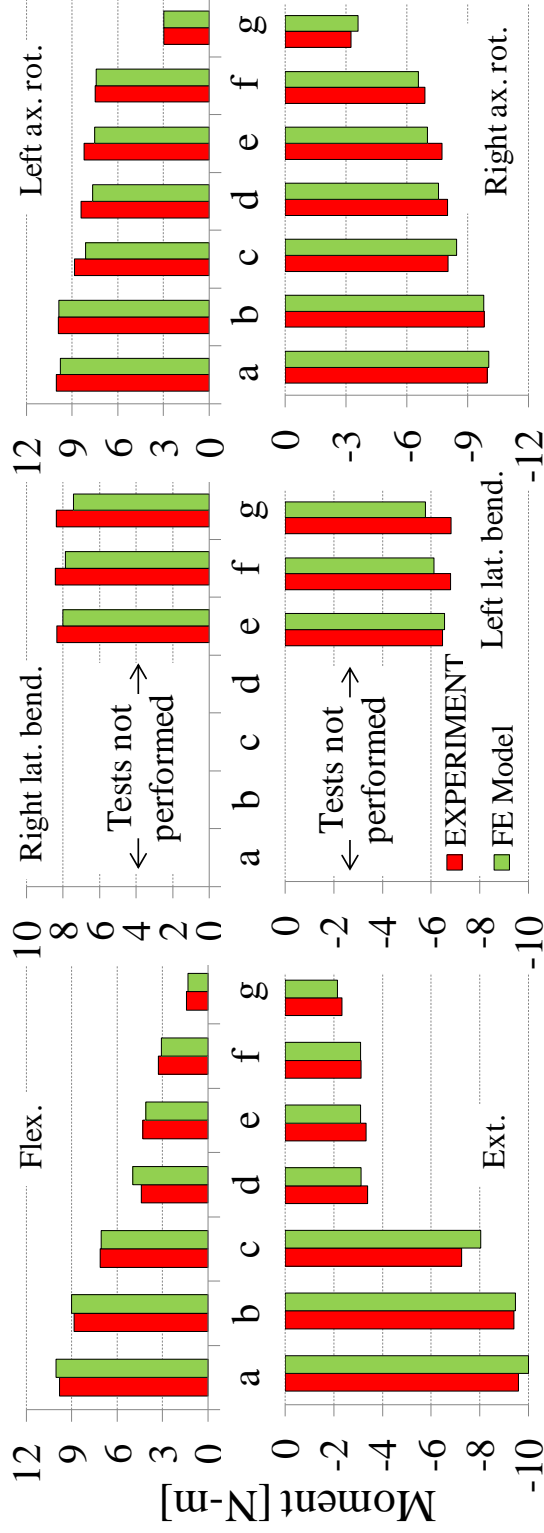
Figure 3.4: Required torque for FSU L2-L3 to achieve the maximum angle limit recorded during the specimen's intact condition during "hybrid" test protocol. Configurations: a. FSU less SSL; b. FSU less SSL & ISL; c. FSU less SSL, ISL, LFL, & PLL; d. FSU less SSL, ISL, LFL, PLL, & ALL; e. FSU less SSL, ISL, LFL, PLL, ALL, & ITL; f. FSU less ligaments; g. FSU less ligaments and facets (disc only)
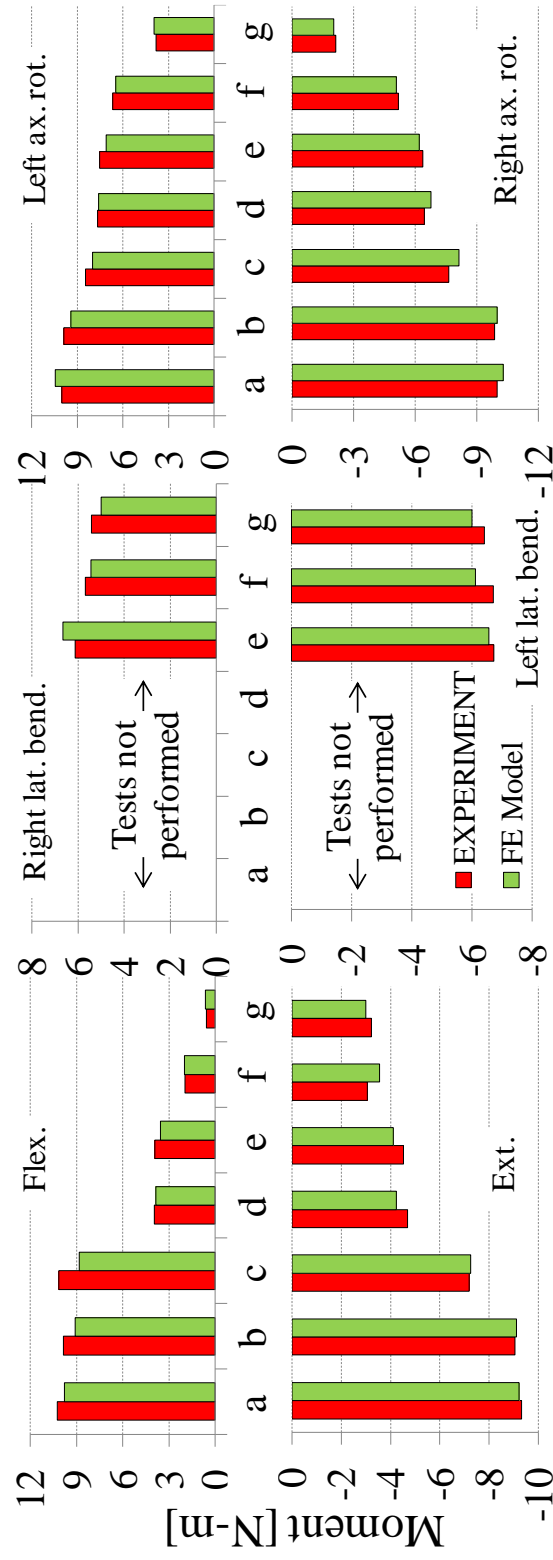
Figure 3.5: Figure 3.5: Required torque for FSU L4-L5 to achieve the maximum angle limit recorded during the specimen's intact condition during "hybrid" test protocol. Configurations: a. FSU less SSL; b. FSU less SSL & ISL; c. FSU less SSL, ISL, LFL, & PLL; d. FSU less SSL, ISL, LFL, PLL, & ALL; e. FSU less SSL, ISL, LFL, PLL, ALL, & ITL; f. FSU less ligaments; g. FSU less ligaments and facets (disc only
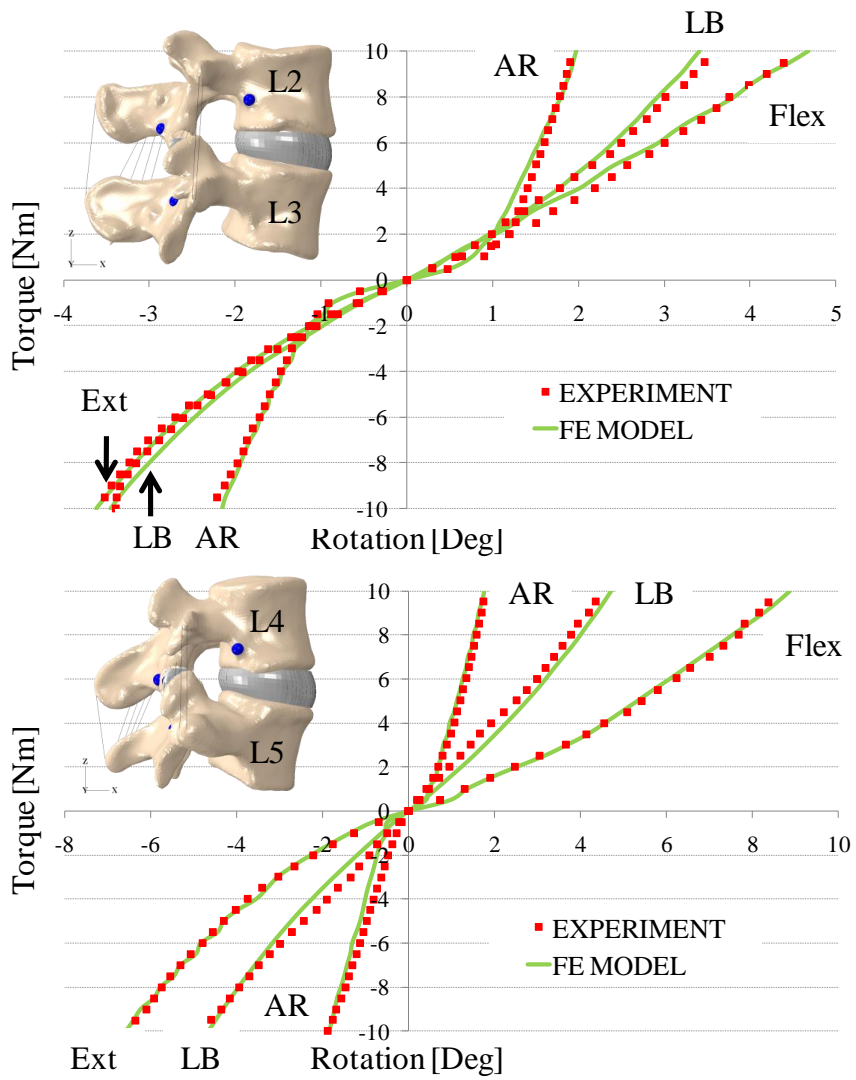
Figure 3.6: Predicted torque-rotation response compared to experiment during flexion-extension, lateral bending, and axial rotation at segments L2-L3 (top) and L4-L5 (bottom)
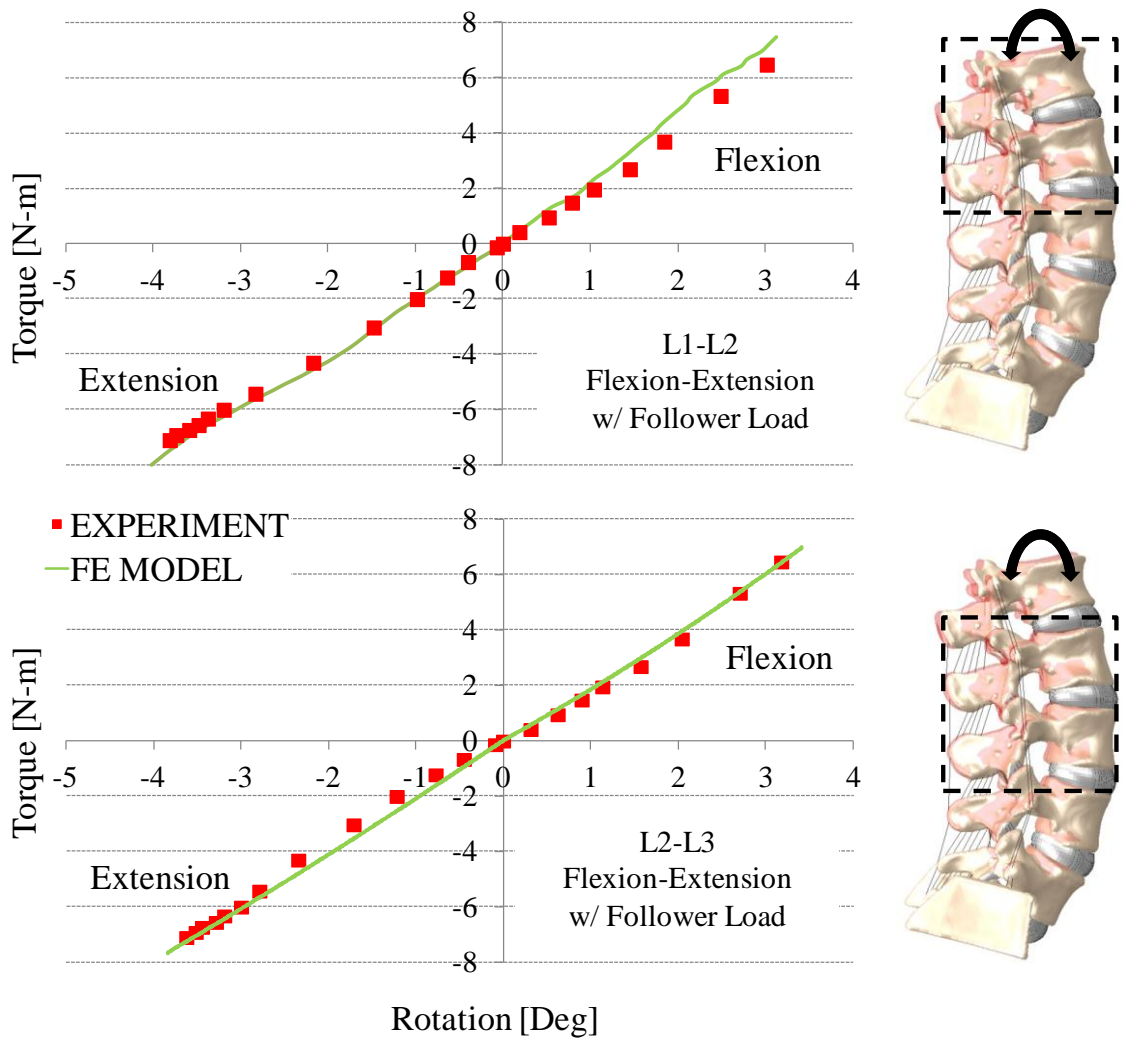
Figure 3.7: Torque-rotation response of intact flexion-extension motion with follower load for at spinal levels L1-L2 and L2-L3
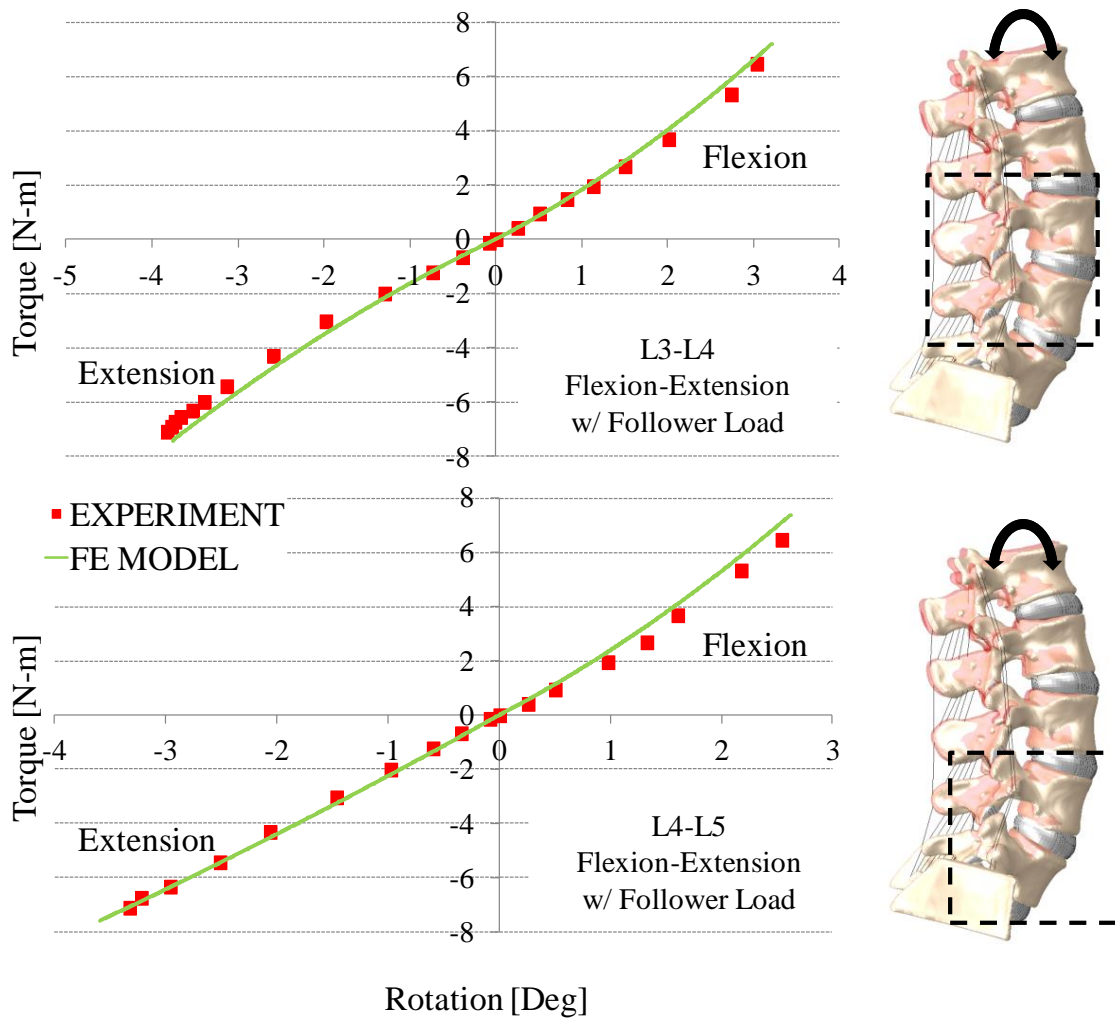
Figure 3.8: Torque-rotation response of intact flexion-extension motion with follower load for at spinal levels L3-L4 and L4-L5
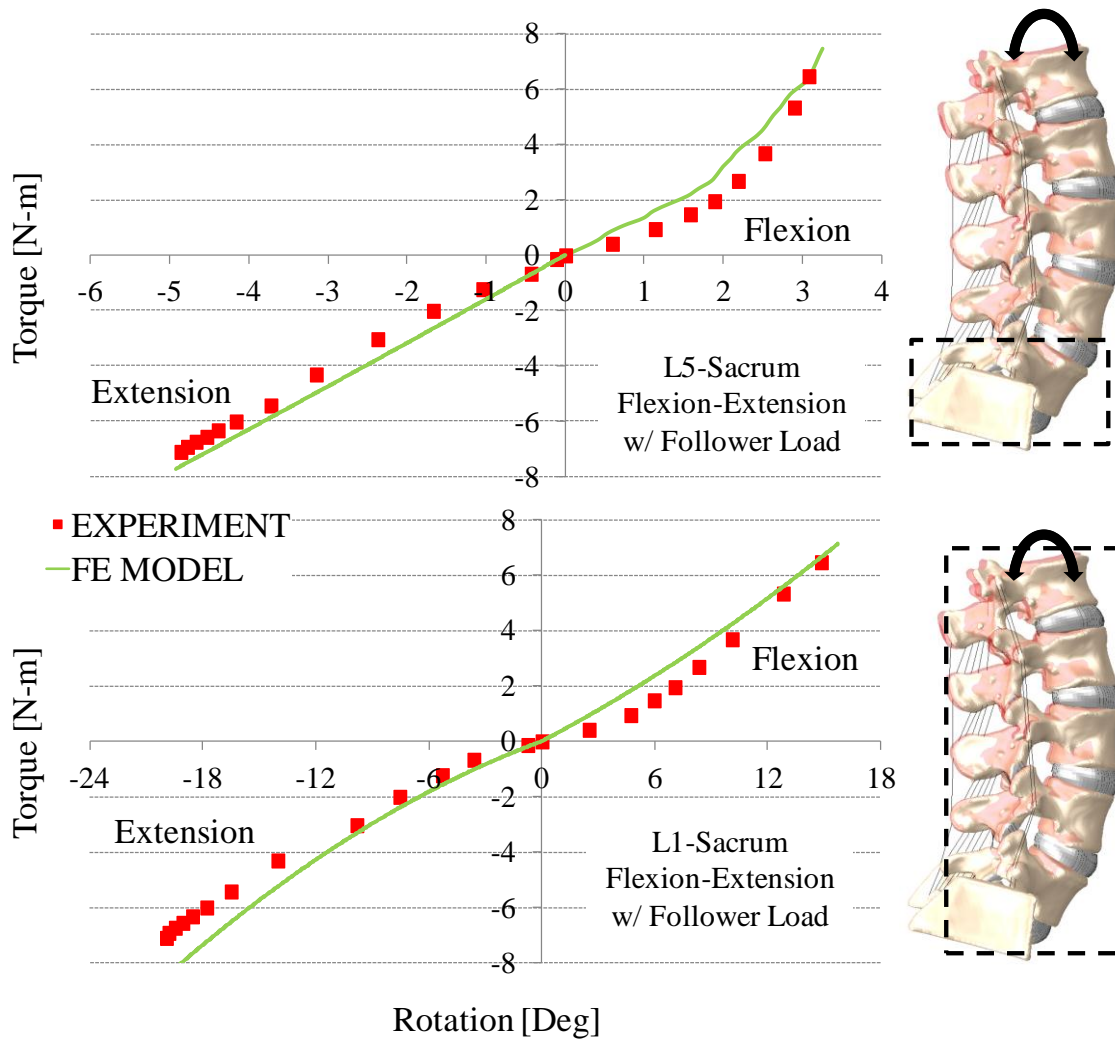
Figure 3.9: Torque-rotation response of intact flexion-extension motion with follower load for at spinal levels L5-Sacrum and L1-Sacrum

.
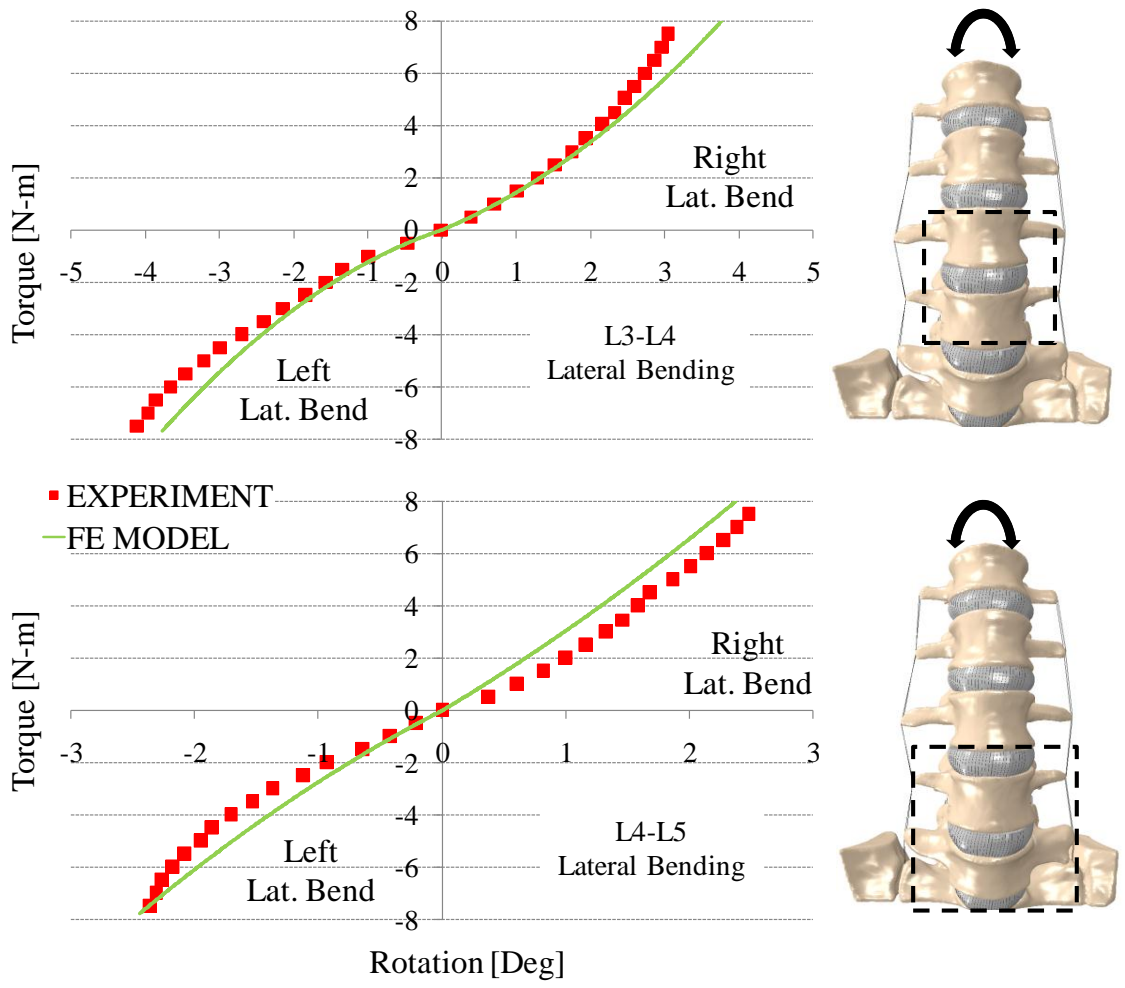
Figure 3.10: Representative torque-rotation response of intact pure moment lateral

bending at spinal levels L3-L4 and L4-L5
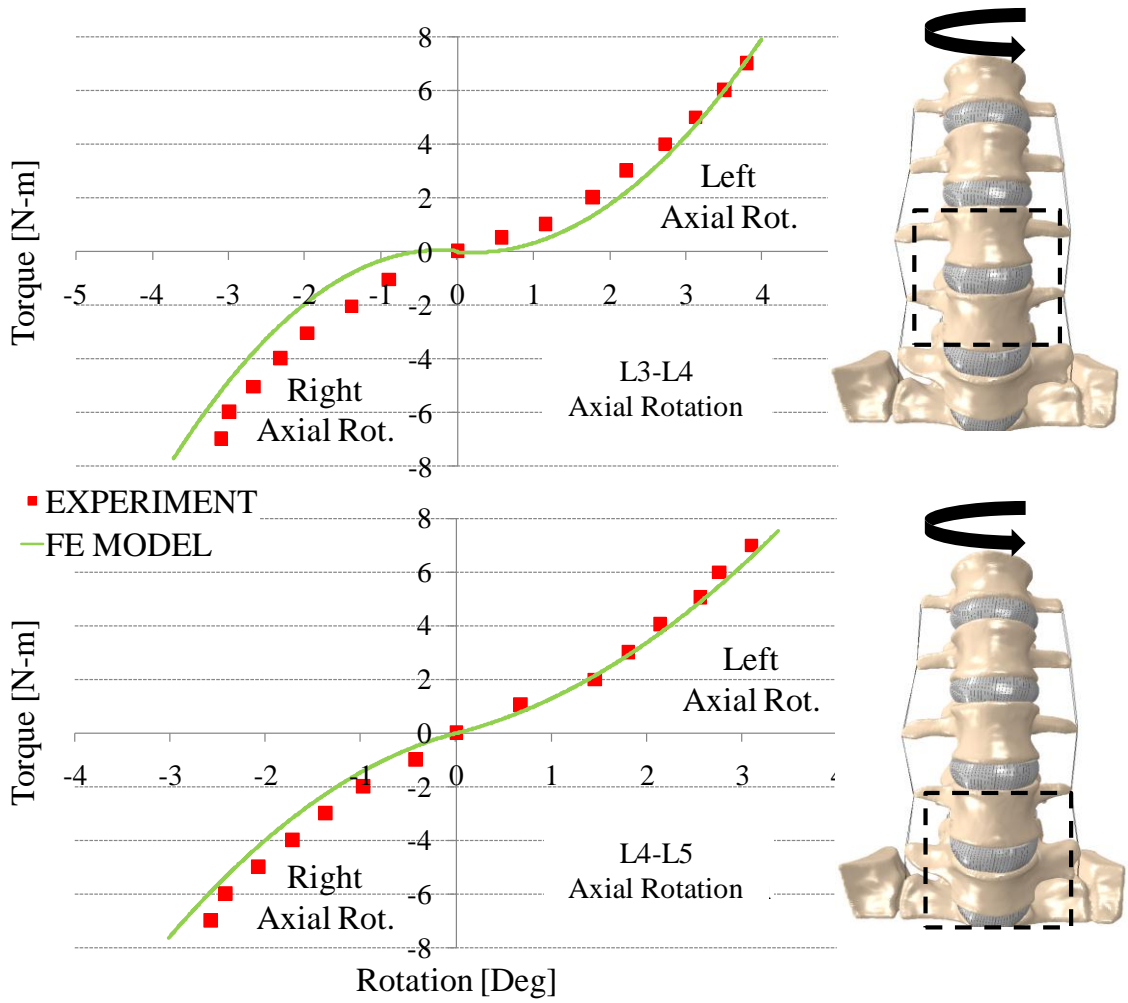
Figure 3.11: Representative torque-rotation response of intact pure moment axial rotation at spinal levels L3-L4 and L4-L5
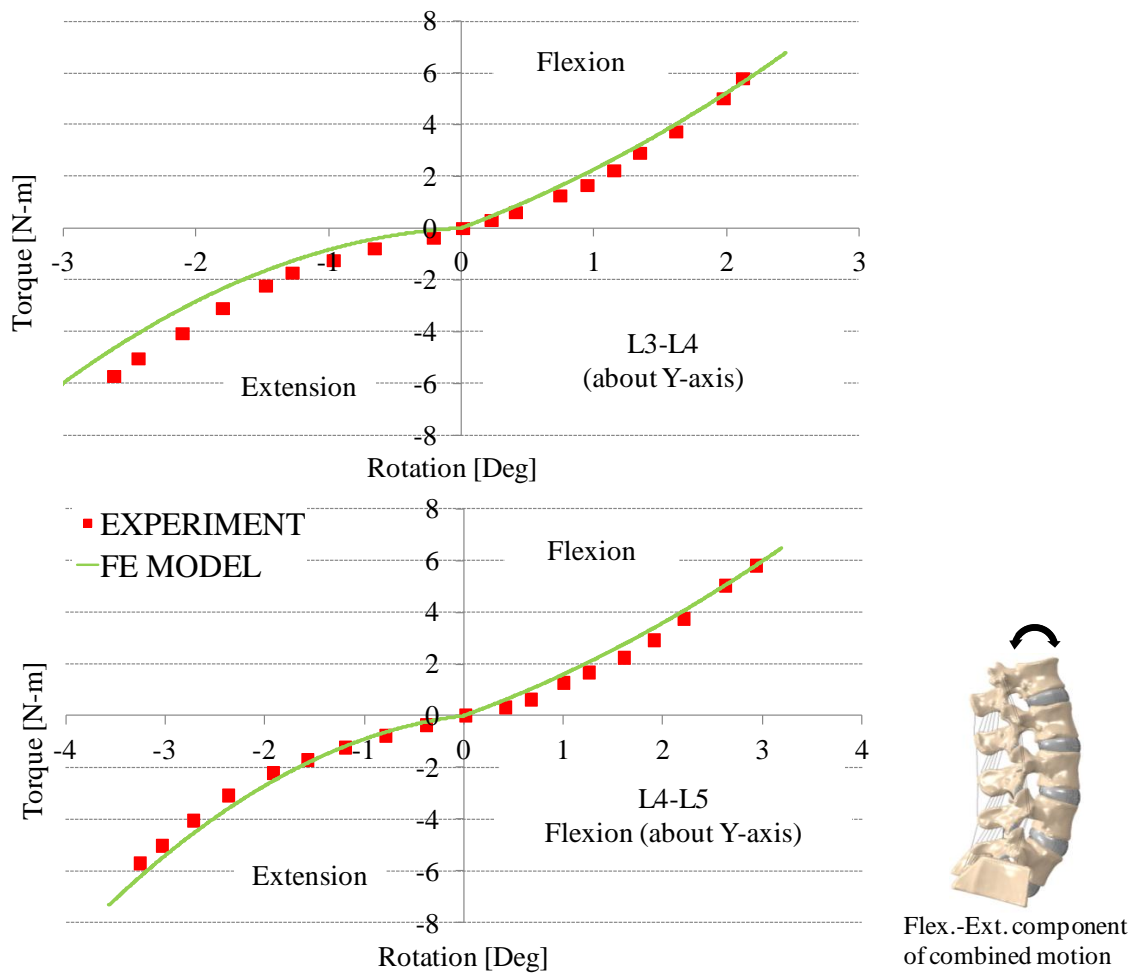
Figure 3.12: Representative torque-rotation response of intact combination motion during flexion and lateral bending at L3-L4 and L4-L5. Plots indicate the flexion and extension components of this motion
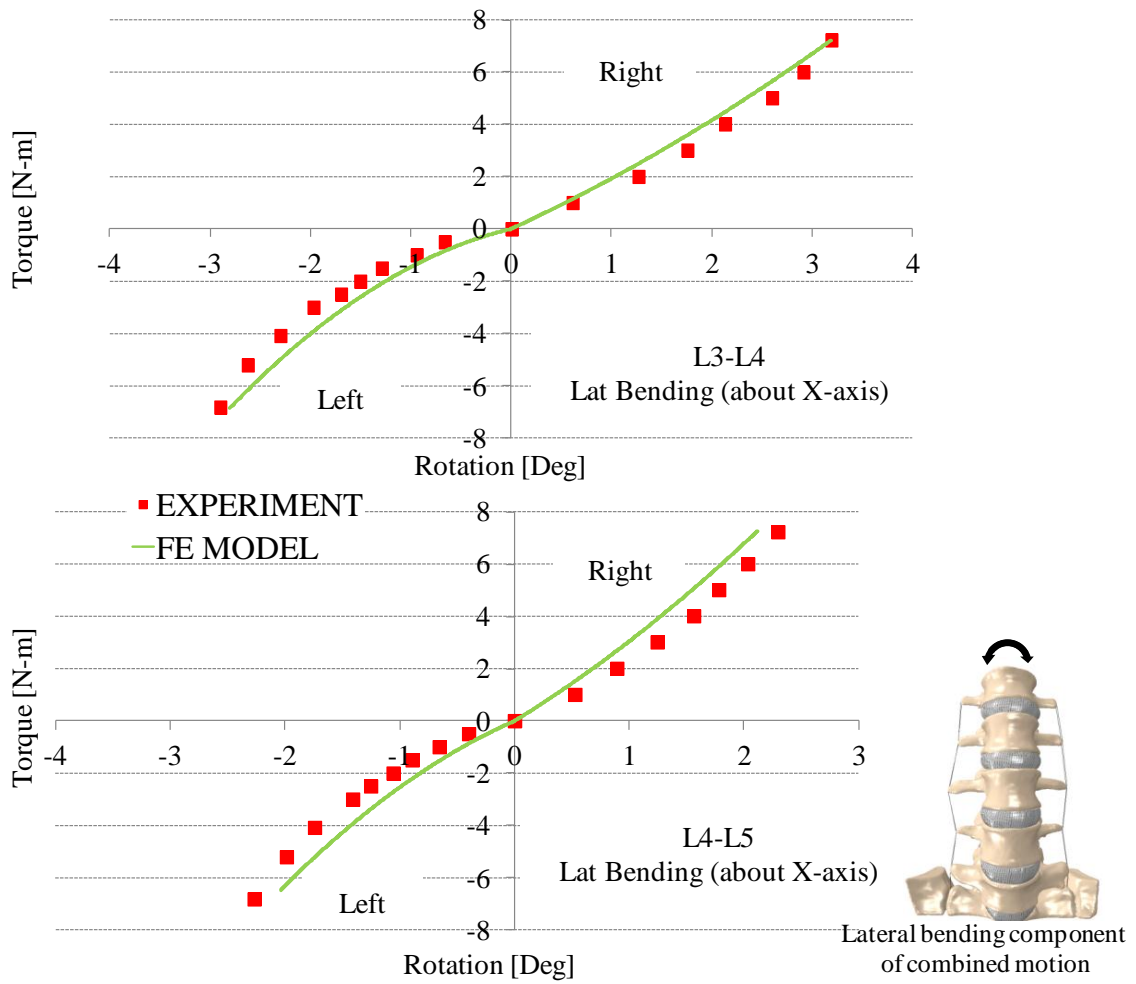
Figure 3.13: Representative torque-rotation response of intact combination motion during flexion and lateral bending at L3-L4 and L4-L5. Plots indicate the lateral bending components of this motion

64
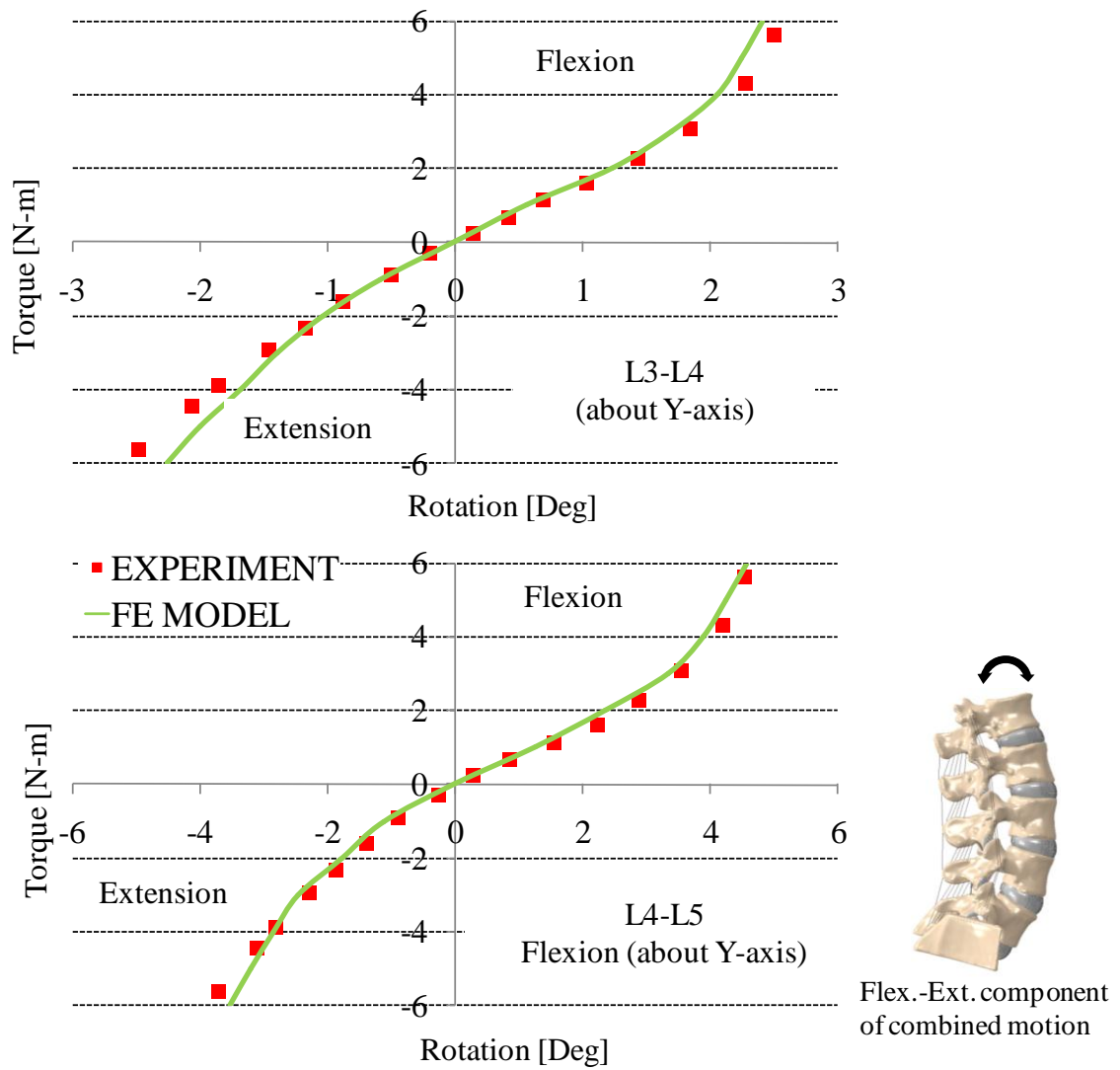
Figure 3.14: Representative torque-rotation response of intact combination motion during flexion and axial rotation at L3-L4 and L4-L5. Plots indicate the flexion and extension components of this motion
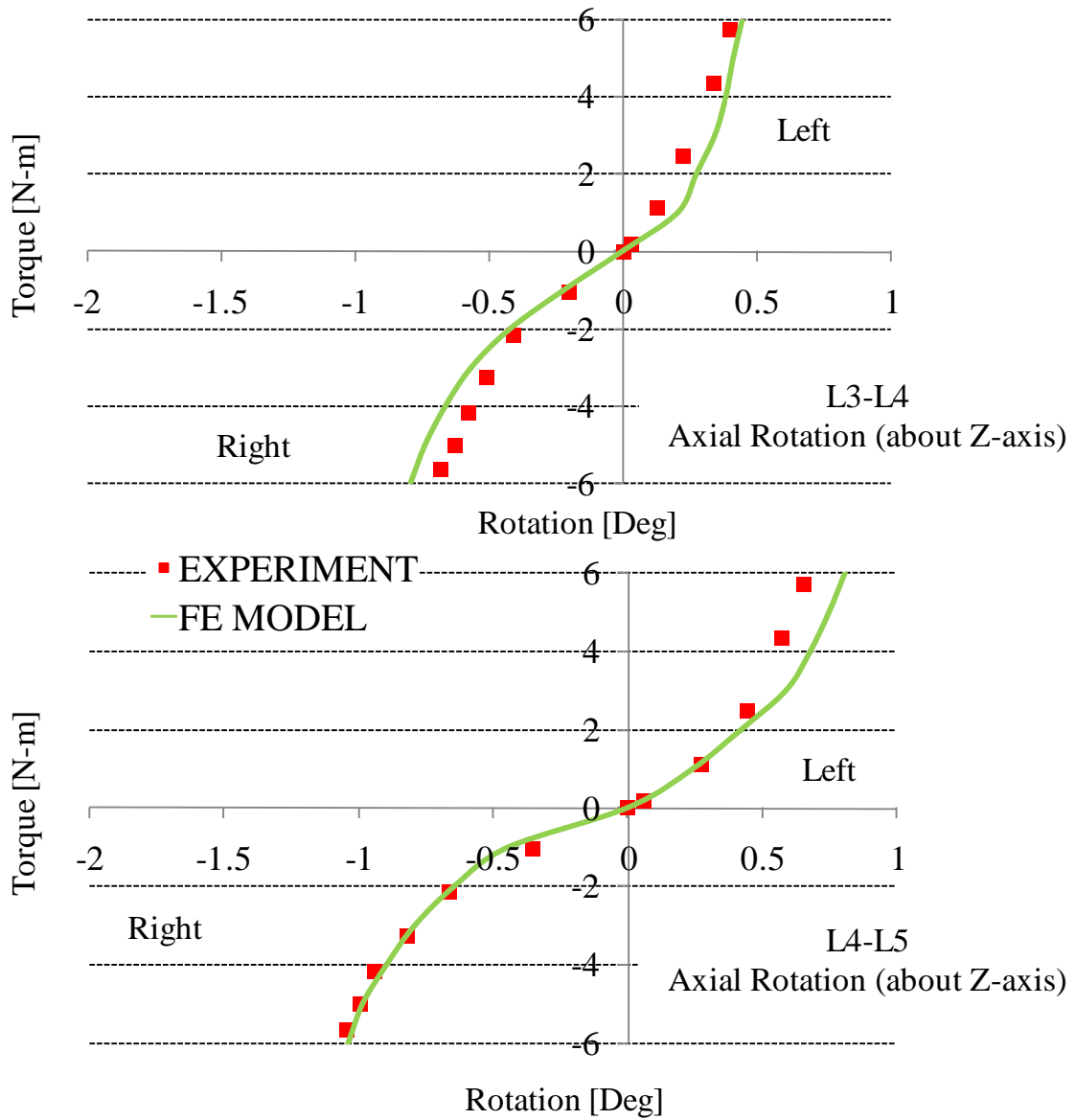
Figure 3.15: Representative torque -rotation response of intact combination motion during flexion and axial rotation at L3-L4 and L4-L5. Plots indicate the axial rotation components of this motion

66

Table 3.1: Sequential sectioning protocol used for FSU testing

Condition	Test Description	Tests performed
	Intact	FE, LB, AR ($\pm$ 10Nm)
a	Section SSL	FE, AR (hybrid to intact ang. disp.)
b	Section ISL	FE, AR (hybrid to intact ang. disp.)
c	Section ALL	FE, AR (hybrid to intact ang. disp.)
d	Section PLL	FE, AR (hybrid to intact ang. disp.)
e	Section ITL	LB, AR (hybrid to intact ang. disp.)
f	Section Facet Capsules	FE, LB, AR (hybrid to intact ang. disp.)
g	Remove Facets (Disc only)	FE, LB, AR (hybrid to intact ang. disp.)

Table 3.2: Comparison of predicted values to measured experimental (Exp.) results at the end of the loading cycle (10Nm). Root Mean Squared Errors (RMSE) for each loading condition

	L2-L3			L4-L5			Avg. RMSE [Deg]
	Exp [Deg]	Model [Deg]	RMSE [Deg]	Exp. [Deg]	Model [Deg]	RMSE [Deg]	
Flexion	4.72	4.68	0.15	8.51	8.87	0.15	0.15
Extension	3.40	3.45	0.10	6.52	6.58	0.08	0.09
Left lateral bending	3.68	3.62	0.05	4.80	4.65	0.22	0.14
Right lateral bending	3.57	3.41	0.10	4.48	4.72	0.25	0.17
Left axial rotation	1.94	1.98	0.10	1.78	1.76	0.08	0.09
Right axial rotation	2.27	2.15	0.05	1.88	1.84	0.18	0.12

Table 3.3: The optimized force-deflection stiffness values for *Spine A* ligaments at level L4-L5

Ligament	FSU L4-L5	
	Force [N]	Deflection [mm]
ALL	500	5.6
PLL	380	5.2
ISL	220	6.2
SSL	250	6.1
ITL	410	3.9
LFL	300	4.3
FCL	500	5.6

Table 3.4: The optimized coefficients for various regions of the AF at level L4-L5. Data represents average values. C_{10}, D, and k_1, are in MPa and k_2 and *kappa* are unitless

	C_{10}	D	K_1	K_2	*kappa*
Anterior	0.4014	0.4603	179.3	421.8	0.0646
Laterals	0.6152	0.2894	18.8	648.0	0.1767
Posterior	1.5715	9.2044	12.2	39.7	0.0763

Chapter 4: Probabilistic Finite Element Modeling to Evaluate Spine Mechanics

4.1 Background and Motivation

The previous chapter described the methods to calibrate, validate and predict the lumbar spine mechanics using subject specific *in vitro* data. This chapter presents an application of probabilistic techniques to assess the effects of material and geometric uncertainty/variability on the mechanics of two functional spinal units (FSU). These findings were then appropriately applied to the entire lumbosacral segment to predict the motion of the entire spine.

4.2 Introduction

Patient-specific finite element (FE) models of the spine can provide assessments of mechanics associated with normal spine function (Eberlein et al., 2004) and degenerative disc disease (DDD) (Schmidt et al., 2007), as well as the impact of fusion, total disc replacement (TDR) and facet arthroplasty treatments (Lee et al., 1991). A functional spinal unit (FSU) is the smallest physiological motion unit of the spine that characterizes properties similar to that of an entire spine. FE model development of the FSU includes the modeling of all its components like the spinal ligaments, intervertebral disc, facet joints, and the vertebral bodies. The primary challenge of modeling this is the

estimation of geometry and the assignment of material properties. The stress-strain or force-deflection relation attributed to the ligaments is usually chosen to reflect the physiological range in which the ligament normally functions but is found to contain significant variability. From the stress-strain curves reported in the literature, the elastic modulus for the ligaments has been in the range of 1MPa to 70MPa (Moracmarco et al., 2010, Sylvestre et al., 2007, De Visser et al., 2007, Lavaste et al., 1992). Chazal et al. obtained data on the geometry and the tensile properties of 43 human spinal ligaments from fresh cadavers with ages between 30 and 80 years (average age 53). A highly inconsistent elongation-load data was measured Chazal et al. (1985). The ground matrix and the collagen fibers in the AF have been represented as either elastic (using Young's modulus and Poissons ratio) or hyperelastic (using material constants) materials. The value of Young's modulus for the ground matrix varied from 1MPa to 8MPa whereas the collagen fiber Young's modulus varied from 7.5MPa to 550MPa (Hato et al., 2007, Sylvestre et al., 2007). A wide range of hyperelastic materials (Yeoh, Mooney–Rivlin, Neo-Hookean material models) have been used with varying constant values (Ayturk et al., 2011, Ezquerro et al., 2011, Schmidt et al., 2007, Rohlmann et al., 2006).

Probabilistic studies based on these deterministic FE formulations are of clinical importance as model input parameters (such as properties of annulus, facets, and ligament stiffness) have been characterized experimentally, but contain substantial variability between subjects. Implant manufacturers are starting to develop products that cater to a population represented in these probabilistic evaluations. Previously, variability in

annulus, nucleus, bone and ligament material properties were included in cervical spine models to predict the distribution of rotation due to an applied flexion-extension moment, sensitivity factors and the risk of injury. Thacker et al. and Ng et al. studied the influence of material moduli uncertainty in cervical spine components on biomechanical responses and disc annulus stress using a 3-D finite element model and Monte Carlo simulation methods (Thacker et al., 2001, Ng et al., 2004). Lee and Teo (2005) used probabilistic sensitivity factors to identify the important bone, disc and ligament material properties affecting sagittal rotation in the FSU L2-L3. Monte Carlo simulation, considered the gold standard, utilizes repeated sampling of the distributions. As accuracy of the probabilistic analysis is proportional to the number of trials, Monte Carlo simulation is computationally expensive, typically requiring thousands of analyses. Most recently, using Monte Carlo simulation and an L3-L5 model, Rohlmann et al. (2009) evaluated the effect of disc replacement alignment, implant radius, facet spacing and scar tissue on intervertebral rotation and facet loading. Recent work has also shown progress in the application of efficient probabilistic techniques, like First-Order Reliability Method (FORM), and Second-order Reliability Method (SORM), as well as reliability techniques and principal component analysis requiring far fewer analyses (Easley et al., 2007, Laz et al., 2007, Fitzpatrick et al., 2011). FORM and SORM are Most Probable Point (MPP) search methods that use an optimization strategy to find the closest point on each constraint to the current design, called the Mean Value Point (MVP). While FORM works primarily on first order analysis, SORM uses a first-order analysis and the

73

principle curvatures of the failure function (second-order analysis) to determine the probability of failure at the MPP.

Accordingly, the objectives of this study were to develop an efficient probabilistic representation of the FSU's L2-L3 and L4-L5 of a 71 years old male specimen using the FORM probabilistic technique, and to compare these efficient representations with the gold standard Monte Carlo approach. With the probabilistic representations, the effects of inherent material uncertainty in ligament stiffness and intervertebral disc as well as the facet joint geometric uncertainties on FSU mechanics were assessed. The range of uncertainty obtained from the FSU analyses were then applied to the lumbosacral spine of the same specimen. The probabilistic framework enabled the prediction of the distribution and bounds of flexion-extension laxity based on experimentally-measured levels of ligament variability and, through the importance factors, the identification of the most important parameters affecting the predicted bounds.

4.3 Methods

4.3.1 FSU L2-L3 and L4-L5 FE Model Development

A 3D explicit finite element lumbar spine FSU L4-L5 model of a 71 years old male subject with mild to moderate disc degeneration was developed in Abaqus/Explicit ((Dassault Systems, Providence, RI, USA) from a series of sagittal computer topography images (in-plane resolution of 0.375 mm/pixel; 512 X 512 pixels; 0.625 mm slice thickness) (Figure 4.1). According to the method used in the previous chapter, the visible

bony structures of the vertebral bodies were manually outlined and exported as 3D surface geometries using ScanIP (Simpleware, Exeter, UK). For computational efficiency, bones and articulating surfaces were considered rigid and represented by triangular shell elements and eight-noded hexahedral elements, respectively. Frictionless contact between articular structures was defined by a pressure-overclosure relationship. Based on the dissected geometry of the IVD (Figure 4.2), the annulus fibrosus (AF) comprised of three major regions (anterior, posterior and laterals) modeled as 8-noded hexahedral elements and a fluid-filled cavity representing the nucleus (Figure 4.2). The AF was represented as anisotropic hyperelastic (Holzapfel) material with C_{10}, D, k_1, k_2 and *kappa* being the material constants.

Seven of the load-bearing soft tissues structures crossing each of the functional spinal unit were represented by non-linear connector elements (Figure 4.1) including the anterior and posterior longitudinal ligament (ALL, PLL), supraspinous and interspinous ligament (SSL, ISL), intertransverse ligament (ITL), facet capsular ligament (FCL) and ligamentum flavum (LFL). The ALL was represented as seven springs in series and 26 springs in parallel. PLL comprised of seven springs in series and 26 springs in parallel. SSL was represented as one spring in series and one spring in parallel. ISL was represented as one spring in series and five springs in parallel. ITL was represented as one spring in series and two springs in parallel. FCL was represented as one spring in series and four springs in parallel. LFL was represented as one spring in series and three springs in parallel (Table 4.1). The ligament attachment sites were primarily based on the

75

dissection performed after testing and confirmed with literature descriptions (Panjabi et al, 1991). Ligament mechanical properties (stiffness and reference strains) were adjusted to match patient-specific experimental torque-rotation response under various loading conditions (flexion, extension, lateral bending and axial rotation). In addition to pure moments, compressive tests were simulated on the FSU where the load was ramped up to 1000 N to obtain a relationship between force-displacement. For this study, pure moment analyses in the principal axes – Flexion-Extension (Flex-Ext), Lateral bending (LB), and axial rotation (AR) were performed force controlled to a moment limit of 10 Nm. In all these analyses, the inferior bone (L3 or L5) was kept fixed and pure moment was applied to the superior bone (L2 or L4). Calibration and validation was performed against subject-specific experimental data using the same technique followed in the previous chapter.

4.3.2 Probabilistic Analysis of the FSU

Probabilistic analyses and sensitivity studies were performed to incorporate the effects of material uncertainty in the ground matrix property, ligament stiffness, ligament reference strain and facet orientation geometric uncertainty using Isight (Dassault Systems, Providence, RI). The probabilistic approach represents input variables as distributions and predicts an output distribution from which the likelihood of a specific level of performance can be determined. In this study, 33 normally distributed input variables were considered: ligament linear stiffness for ALL, PLL, SSL, ISL, ITL, FCL

and LFL (seven inputs), material constants for the AF (twelve inputs), translations (six inputs) and rotations (six inputs) of the facet cartilage for bone L4, and linear pressure-overclosure values (two inputs). Variability in ligament linear stiffness was adopted from controlled experimental studies (Pintar et al., 1992). Force-deflection curves were parametrically defined so that a change in reference strain shifted the curve along the deflection axis and a change in stiffness changed the slope in the linear region. Linear stiffness for all ligament bundles, material constants for the AF, and the linear pressure-overclosure values were normally distributed with mean values based on tuned data and standard deviations equal to 30% of the mean value. Ligament variability came from Pintar et al., 1992 whereas the material constants for AF and linear pressure-overclosure values came from separate uniaxial simulations (Section 3.3.2 and Figure A1.2). These uniaxial test simulations were performed on small strips of the AF in accordance with experiments (Guerin et al., 2006). After performing these simulations on strips from different regions of the AF, the mean values for the material constants were used in the probabilistic analysis. A 0.15 mm and 1.5° standard deviation was used for translations and rotations of the L2 and L4 facet cartilage respectively which at ±2 standard deviations from the mean (5 and 95% probability levels) would represent a total range of 0.6mm and 6° in translations and rotations (based on the physiological allowable space between the facet joints).

Probabilistic analyses were performed with Monte Carlo simulation (500 trials) and computationally efficient reliability method: FORM. The Monte Carlo method uses

repeated trials performed with input values randomly generated according to their distributions to predict a distribution of output. As the accuracy of the Monte Carlo method is dependent on the number of trials, the analysis with 500 trials was used for benchmarking purposes. A convergence study was performed to evaluate the accuracy of using 100 trials, 250 trials and 500 trials. With well-behaved monotonic systems, the FORM method required only the deterministic trial, one trial to perturb each input variable (33 in this study), and one trial to determine the output at specified probability levels. These two probabilistic analysis methods were used to predict distributions of pure moment torque-rotation response, reported as bounds at the 5 and 95% probability levels. Sensitivity plots for a relative ranking of the influence of input parameter variability on output measures were reported in the form of pareto plots. The purpose of the pareto sensitivity plot was to highlight the most important parameters among a (typically large) set of parameters in the analysis. It was based on an algorithm to produce statistically-based acceptance limits (similar to confidence intervals) for each bar in the Pareto plot.

4.3.3 Efficient Lumbosacral Spine FE Model Development

Subject-specific lumbar multi-segment and FSU FE models were developed in Abaqus/Explicit from high-resolution computed tomography scans of the 71 years old male cadaveric spine. The spinal geometry was reconstructed with ScanIP. The FSU included vertebral bodies L4 and L5 and the multi-segment model included vertebral

bodies L1 through sacrum. At each FSU level, 6 DOF connector elements between adjacent vertebrae provided appropriate torque-rotation and force-displacement constraint in the absence of the soft tissue structures. The properties of the connectors were optimized using Isight (Simulia, Providence, RI) to reproduce the measured kinematic-moment data from testing of the FSU in each state of sectioning, from disc-only to intact, under the applied flexion-extension, lateral bending, axial rotation, and axial compression loading. Optimized connector properties from the intact FSU were applied to the multi-segment model and then tuned to level specific kinematic-moment data.

The probabilistic analyses performed on the FSU's L2-L3 and L4-L5, gave the torque-rotation (T-R) response of these FSU's under applied load. The same response was then used as an input in the multi-segmental spine model at these respective levels. For all other levels, the values were extrapolated. The extrapolated value for level L3-L4 was decided by calculating the mean rotation between L2-L3 and L4-L5 at a given torque. The values for levels L1-L2 and L5-Sacrum was computed by subtracting and adding the same magnitude of rotation to the levels L2-L3 and L4-L5 respectively. Flexion and Extension analysis was simulated with these ranges to represent ±2 standard deviations from the mean (5 and 95% probability levels).

4.4 Results

4.4.1 Deterministic Analysis for the FSU

Following the optimization process, the T-R profiles from the FSU L2-L3 and L4-L5 model agreed closely with subject-specific experimental data over the range of load application (Figure 4.3). Average rotational RMSE values were 0.29°, 0.17°, 0.26°, and 0.13°in flexion, extension, left & right lateral bending and left & right axial rotation, respectively.. The optimized values of ligament stiffness, anisotropic hyperelastic disc properties and facet orientations were all within the ranges of values reported in the literature. The combination of non-linear spring elements for ligament representation and rigid material definitions for bony and articular surfaces resulted in model run times of less than 10 min for generation of a single laxity curve.

4.4.2 Probabilistic Analysis for the FSU's

The probabilistic analyses predicted the distribution of flexion-extension laxity, shown as the 5 and 95% laxity bounds with the Monte Carlo and efficient probabilistic technique - FORM (Figure 4.4 and Figure 4.5). Comparing the methods, the rotational RMSE values over the range of loading (entire flexion and extension cycle) were 0.24° and 0.38° for FSU L2-L3 and FSU L4-L5, respectively. Predicting the laxity bounds for a single loading scenario during flexion or extension required less than 50 trials with FORM (approximately 4h) with differences between the methods smaller than the sampling errors associated with the 500-trial Monte Carlo method. The percentage saving

in computation time by using FORM technique over Monte Carlo simulation was approximately 95%.

4.4.3 Predictive Bounds for Lumbosacral Analysis

The 'range' between the upper and lower bound obtained at 2.5, 5, 7.5, and 10Nm for a 5-95% laxity bounds represented 4σ from which the value of 2σ was calculated for all further lumbosacral analysis. This 2σ was in the range of 0.98° to 1.12° for FSU L2-L3. Similarly, for FSU L4-L5, the value of 2σ was in the range of 0.40° to 1.04° (Figure 4.4 and Figure 4.5).Using a 2σ value from the FSU analysis to the lumbosacral model, the upper and lower bounds for the entire spine model were predicted (Figure 4.7 and Figure 4.8)

4.4.4 Pareto Sensitivity Plot

The pareto plots highlighted the most sensitive input parameters in the analysis. From this probabilistic analysis it was seen that the anisotropic hyperelastic constants of the annulus fibrosus were most sensitive to the motion of the FSU followed by the ligaments Figure 4.6. This figure represents the results from the FORM analysis for FSU L4-L5. Similar trends were seen in the FSU L2-L3 sensitivity results. For the FSU L4-L5 at full flexion and full extension, the posterior region of the annulus fibrosus had a normalized sensitivity of 44% and 27% respectively. The fiber orientation in the annlus fibrosus denoted as *kappa* is also sensitive (~3%) to flexion motion of the FSU.

4.5 Discussion

Several groups have analytically created the FSU models by adopting the geometry and material properties from experiments performed on individual components (Goel et al., 1993; Lavaste et al., 1992; Pitzen et al., 2001; Shirazi-Adl, 1991; Zander et al., 2001, 2002). In these models, the complexity of the ligament representation ranged from point to point tension only sets of one-dimensional non-linear springs elements (Zander et al., 2004, Ezquerro et al., 2011) to 'fabric' (two-dimensional) elements (Bowden et al., 2008). A linear elastic material formulation has been used to describe the bulk response of the annulus fibrosus (mainly the annulus ground substance) (Kumaresan et al., 1999); however, the AF behaves nonlinearly and anisotropically under physiological loading (Fujita et al., 1997). The complex articulating facet cartilages have been modeled as tissue representations, gap elements, and frictionless contact elements capable of supporting compression only load normal to its surface (Botolin et al., 2001, Siepe 2010), Goel et al. 1993, Zander et al., 2004, Schmidt et al., 2007). A contact pressure-surface overclosure relationship is generally used in rigid body analysis where manual tuning is performed to estimate the kinematic and contact mechanics from fully deformable cartilage models.

In this study, subject-specific models were developed using geometric dimensions of the discs, ligaments, facet cartilages from CT scan data and dissection during testing of the spines. Probabilistic evaluations were also performed to consider the potential effects

of intersubject variability in the soft tissue mechanical properties on the torque-rotation behavior. The 5-95% bounds using the efficient reliability methods like FORM compared well with the Monte Carlo results. The greatest advantage of the efficient methods over Monte Carlo was the savings in computation time. The efficient methods accurately estimated the results from the Monte Carlo simulation in only 5% of the time. During flexion, the most sensitive parameters were the constants of the annulus fibrosus (in particular the ground matrix and fibers) followed by the posterior ligaments ISL and PLL. During extension, the most sensitive parameters were the ground matrix in the posterior and anterior region of the AF followed by the ligaments ALL and ITL. The importance factors reported by Lee and Teo (2005) were consistent with results seen in this study.

In closing, a probabilistic representation of constraint has been developed with an emphasis on efficiency of the ligament structures and probabilistic method for use in forward driven assessments of joint mechanics and TDR designs. Sensitivity factors provided insight into the parameters (ligament stiffness, disc properties, reference strain) that most affects the kinematics under various loading conditions and flexion-extension angles. The efficient probabilistic representation developed can be used to represent uncertainty for a subject-specific model or, alternatively, may represent the variability present in a population of subjects.
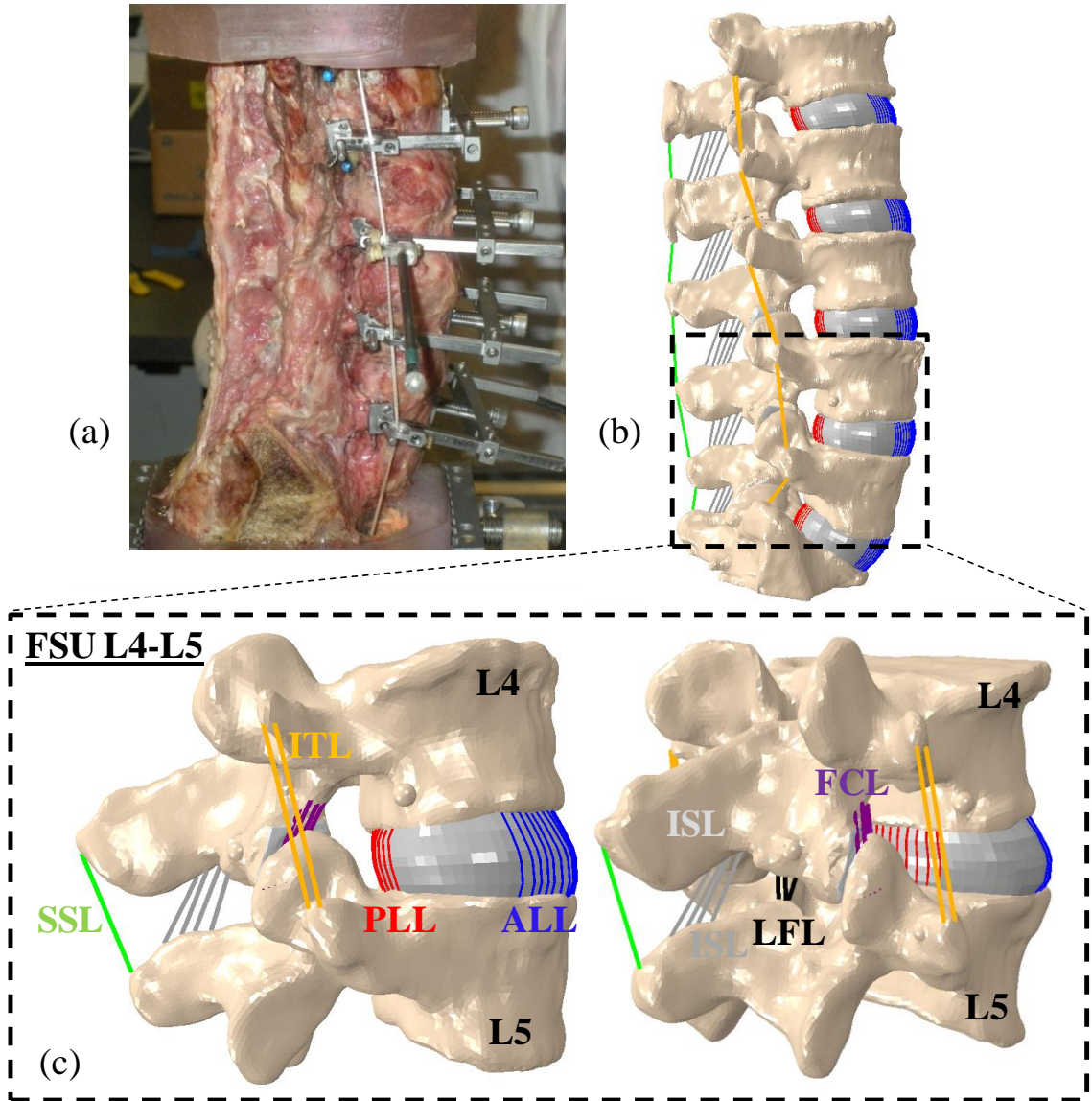
Figure 4.1: (a) Experimental setup of the lumbosacral spine (b) Subject specific finite element model of the lumbosacral spine (c) FSU L4-L5 ligamentous model
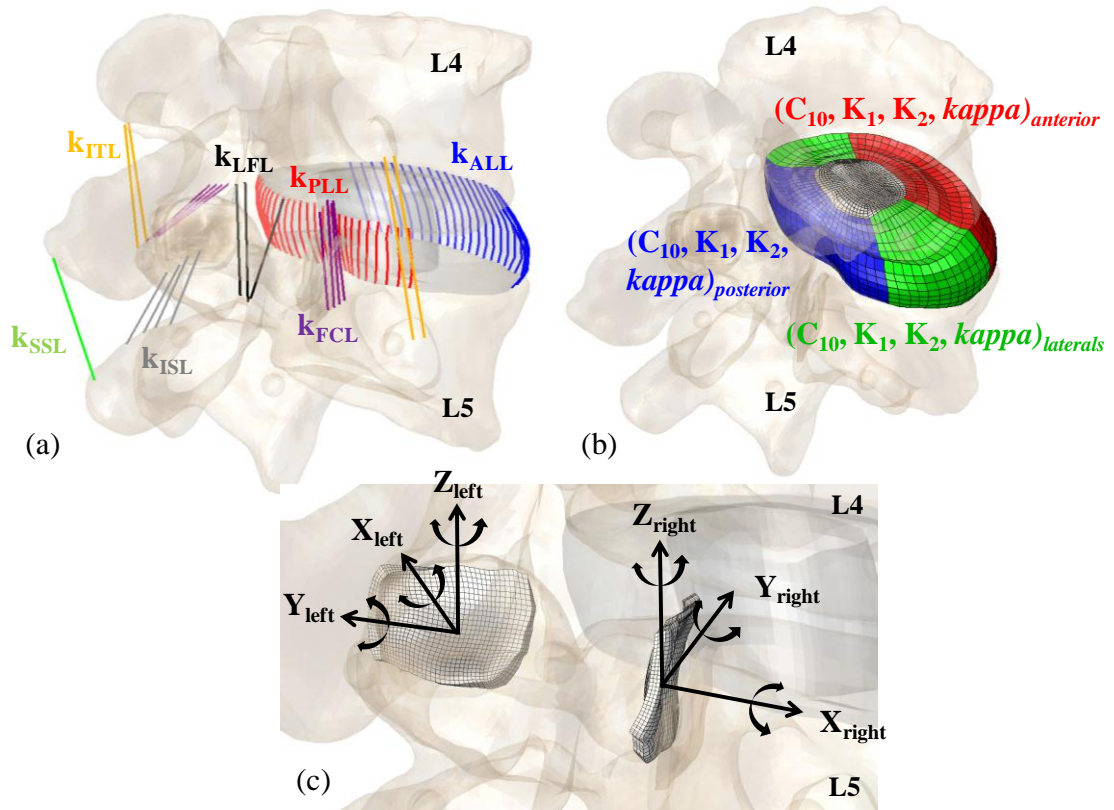
Figure 4.2: Probabilistic input perturbations for (a) ligament stiffness (b) AF disc properties and (c) facet cartilage translations and rotation
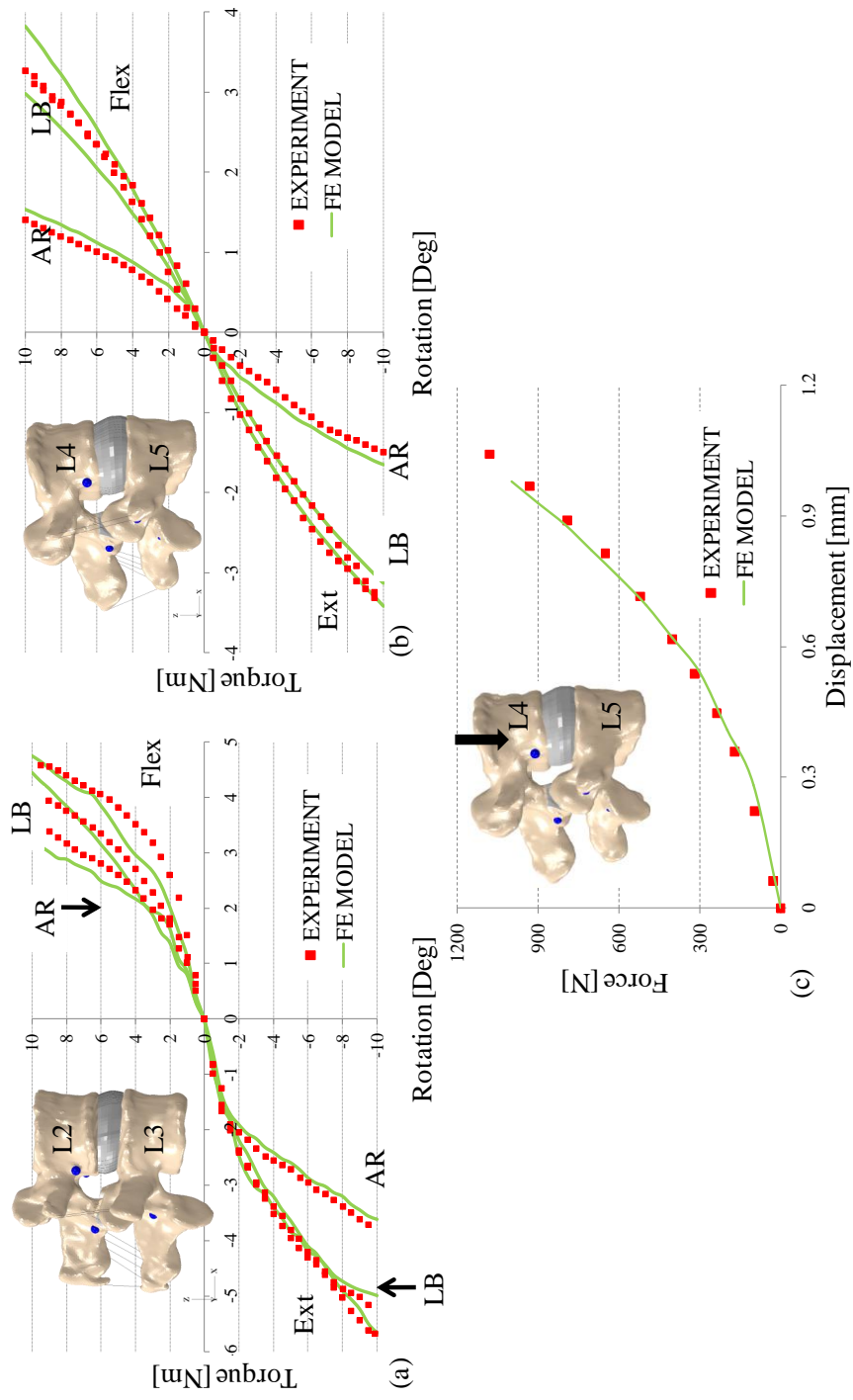
Figure 4.3: (a) Torque-rotation response for intact (a) FSU L2-L3 (b) FSU L4-L5 during flexion (Flex), Extension (Ext)., Lateral Bending (LB) and Axial Rotation (AR). (c) Force-displacement response for axial compression of the disc L4-L5
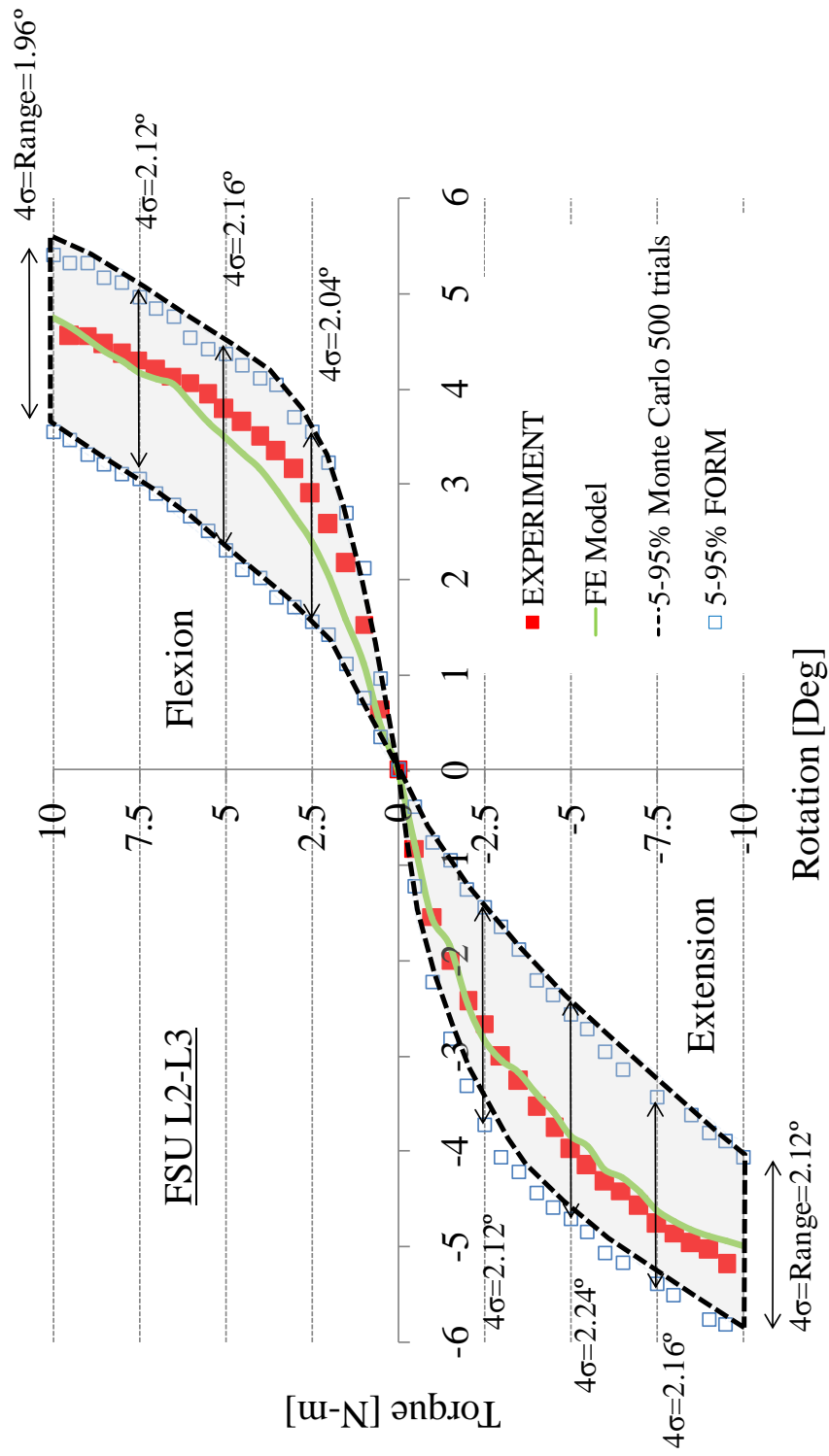
Figure 4.4: Probabilistic torque-rotation behavior for L2-L3 segment comparing MC and efficient reliability technique FORM
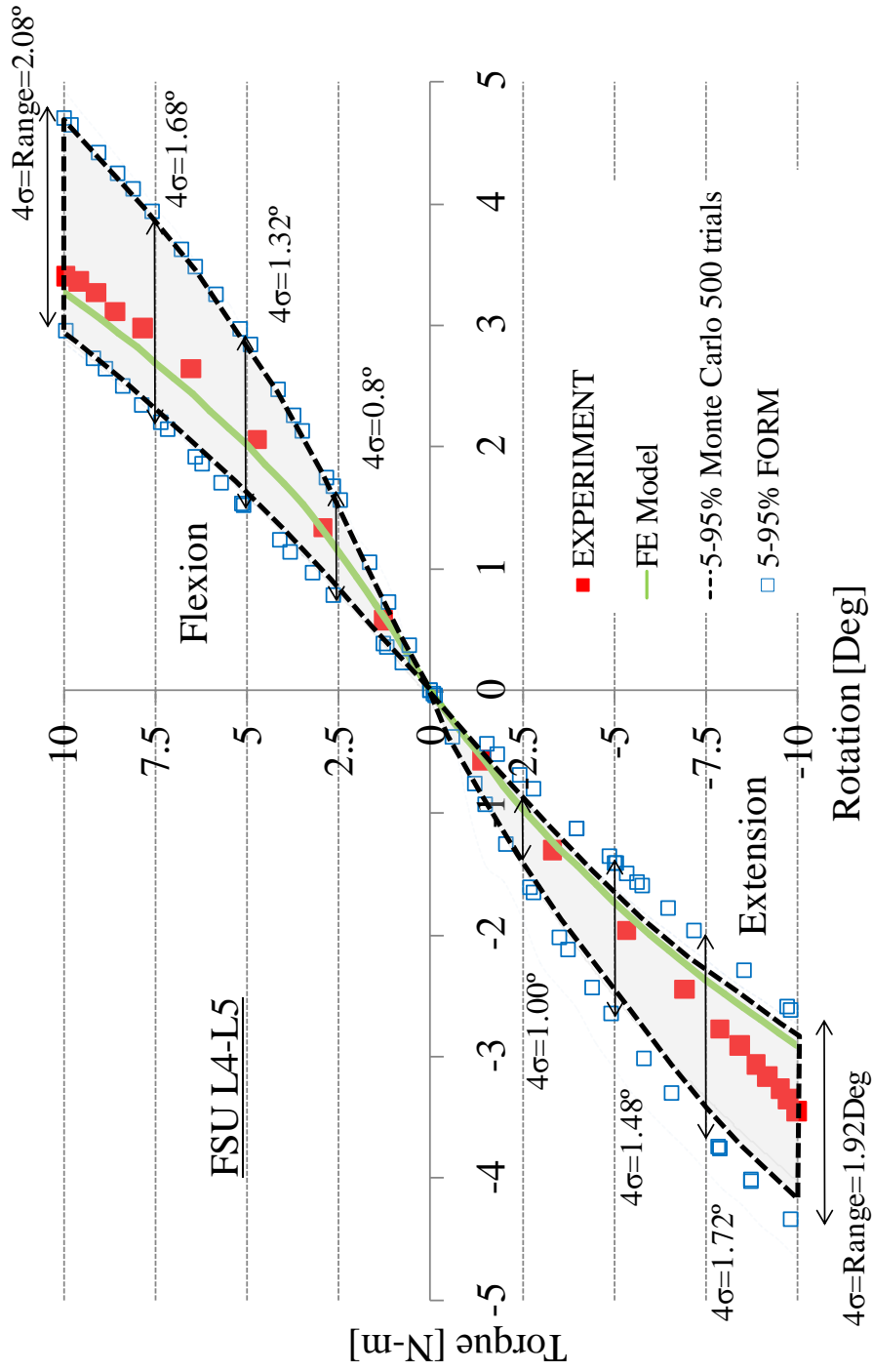
Figure 4.5: Probabilistic torque-rotation behavior for L4-L5 segment comparing MC and efficient reliability technique FORM
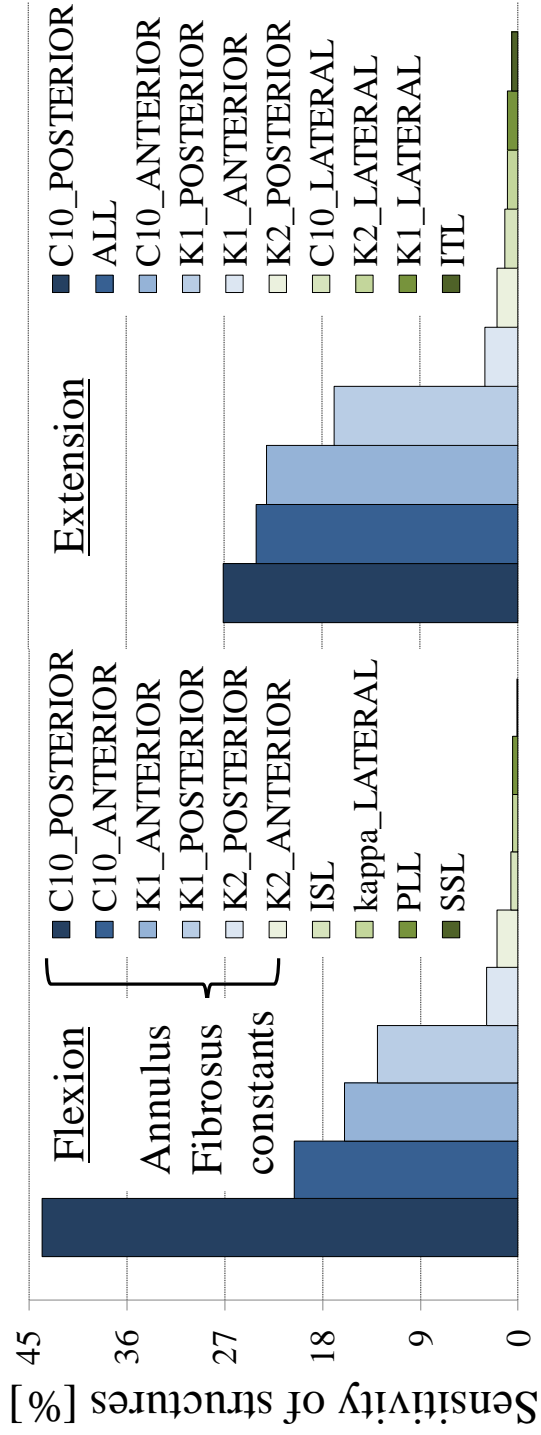
Figure 4.6: Sensitivity factors for probabilistic input parameters affecting torque-rotation behavior during FORM analysis on FSU L4-L5
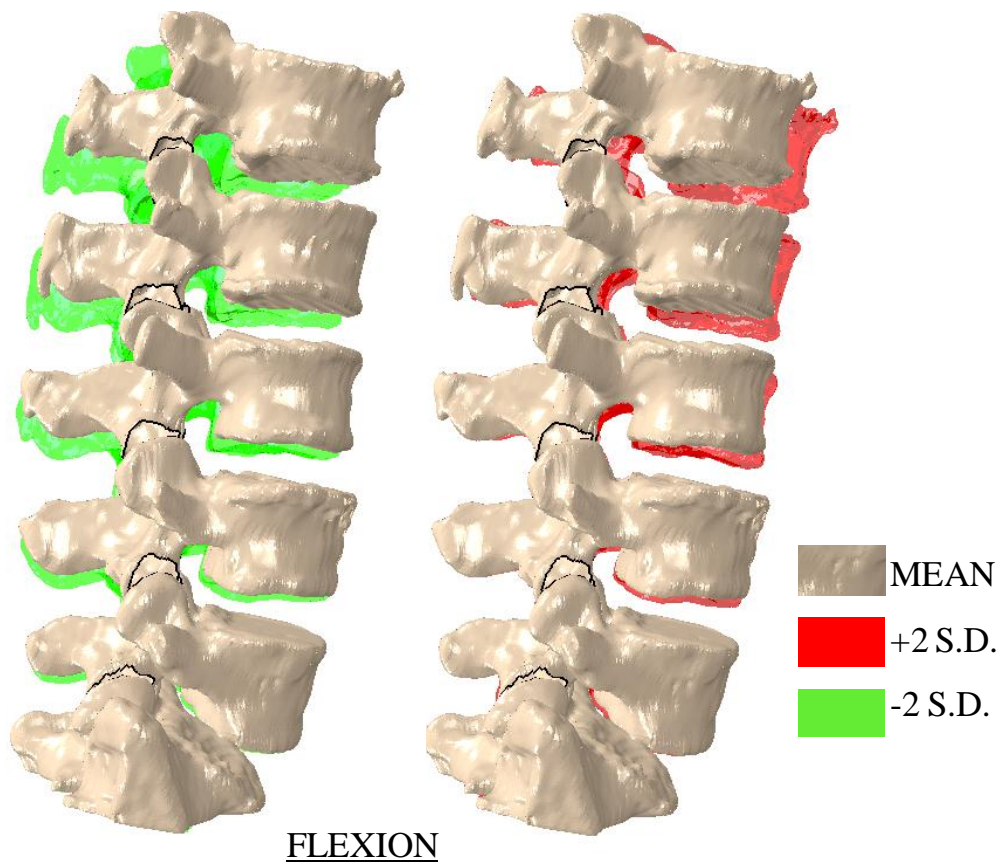
<u>FLEXION</u>

Figure 4.7: ROM of the lumbosacral spine at mean, +2 S.D. (Red) and -2 S.D. (Green) at 10Nm flexion

MEAN
+2 S.D.
-2 S.D.
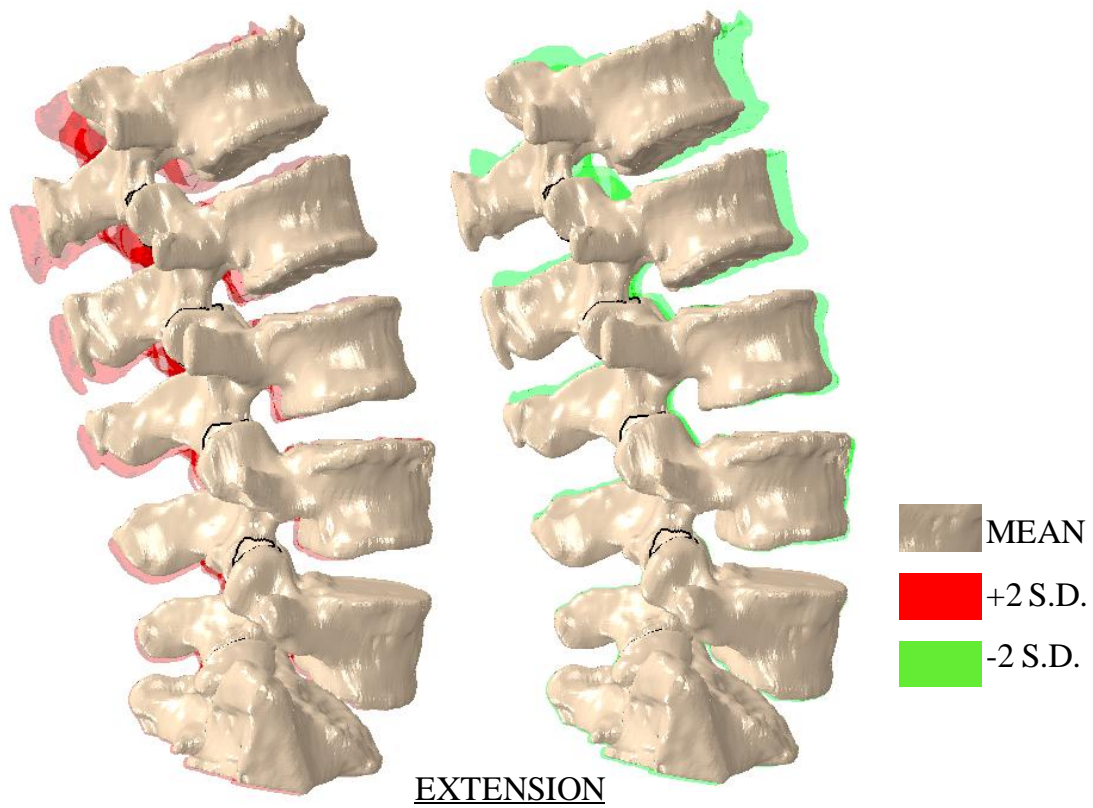
<u>EXTENSION</u>

Figure 4.8: ROM of the lumbosacral spine at mean, +2 S.D. (Red) and -2 S.D. (Green) at 10Nm extension

Table 4.1: Number of connector elements in series in parallel representing the ligaments in the FE model

Ligaments	Ligaments in	
	Series	Parallel
Anterior longitudinal ligament (ALL)	7	26
Posterior longitudinal ligament (ALL)	7	26
Supraspinous Ligament (SSL)	1	1
Interspinous Ligament (ISL)	1	4
Intertransverse Ligament (ITL)	1	2
Facet Capsular Ligament (FCL)	1	4
Ligamentum flavum (LFL)	1	3

Table 4.2: Probabilistic input variables

	Input	Mean μ	Standard Deviation σ	Rationale used / Values from:
Ligament linear stiffness (7 variables)	ALL	Refer Table 3.3	30% of mean value (linear stiffness only)	Pintar et al., 1992
	PLL			
	SSL			
	ISL			
	ITL			
	FCL			
	LFL			
Annulus Fibrosus (AF) (12 variables)	C_{10}	Refer Table 3.4 and Appendix A1.2 for constants	30% of mean value	Uniaxial tensile test simulation on AF specimens similar to experiments (Geurin et al., 2006)
	K_1			
	K_2			
	kappa			
Linear pressure-overclosure values (2 variables)	Left and right facet cartilage	200 MPa	50MPa	Tuned model to experimental data
Left and right facet translation (6 variables)	Along X-, Y- and Z-axis	Intact spine model	0.15	To match physiologically allowable space between the facet
Left and right facet rotation (6 variables)	About X-, Y- and Z-axis	Intact spine model	1.5	To match physiologically allowable space between the facet

Chapter 5: Pre-op Templating for TDR Alignment: Is it Clinically Relevant?

5.1 Background and Motivation

The previous chapters described the fundamental aspects of modeling the human lumbar spine and validating it against subject-specific experimental data. Chapter 4 focused on incorporating inter-subject variability and using statistics/reliability to assess the influence of uncertainties on the mechanics of the spine. This chapter presents an application of the developed FE model to answer clinically relevant questions. Specifically, this chapter focuses on using FE method as a pre-operative templating tool for the alignment of Total Disc Replacements (TDR).

5.2 Introduction

Spinal fusion surgery is one of the conventional approaches to treat pain from degenerative lumbar spine disease. This procedure involves connecting the vertebrae surrounding the painful disc by surgically fusing the bones. Total disc replacement (TDR) is an alternative to interbody fusion as a treatment of disc degenerative diseases in the lumbar spine (Siepe et al., 2003). Unlike spinal fusion, TDR may re-establish functional mobility at the index level and minimize detrimental effects to the adjacent levels (Meyers et al., 2007). It has been shown that clinical outcome (Huang et al, 2005)

94

and the incidence of adjacent level disease (Huang et al. 2006) is linked to the range of motion achieved. The ProDisc-L (Synthes Spine, West Chester, PA) is a semi-constrained implant designed to restore motion. The highly conforming spherical surfaces of the superior endplate and polyethylene inlay prevent the endplates from translating independently. Placement of the spherical center of the device as close as possible to the anatomical axis of rotation of the segment is essential in achieving optimal performance. This placement relates to range of motion (ROM), the distribution of soft tissue loading and facet joint anatomy and forces.

Pre-operative templating is considered an important step prior to orthopedic surgeries It has been shown to be a reliable and accurate way to determine the position and the size of surgical components (Descamps et al. 2012). In the past, digital templating has been performed for hip arthroplasty in order to anticipate problems and prevent complications (Schmidutz et al., 2012). Acetate templating has been widely used in predicted knee implants selection accurately (Specht et al., 2007). Also, a surgeon-friendly spine surgery simulator that predicts the correction of a scoliotic spine as a function of the patient characteristics and instrumentation variables has also been developed (Aubin et al., 2003).

Patient-specific finite element (FE) models of the spine can provide assessments of mechanics associated with normal spine function and degenerative disc disease (DDD) (Schmidt et al., 2007), as well as the impact of fusion (Yan et al., 2011), total disc replacement (TDR) (Rundell et al., 2008) and facet arthroplasty treatments (Lee et al.,

1991). An explicit FE formulation of the lumbosacral level as well as the functional spinal unit (FSU) is useful in performing parametric evaluations of various properties and treatments due to its efficiency in handling complex, changing contact conditions and the ability to evaluate either rigid or deformable body contact. This FE modeling technique also helps evaluate the bone-on-bone impingement or implant impingement. The strain computation at the bone interface is possible using FE modeling tehcnique. Accordingly, the objective of the present study was to pre-operatively assess the mechanical compatibility of the ProDisc-L TDR to the anatomy of the indexed motion segment of several patients using a patient-specific finite element model. To achieve this, multiple FE models were developed ranging from a healthy spine (with no history of spine related problems) to spines of patients who underwent total disc replacement surgery (Table 5.1). Specifically, the objectives were (a) to evaluate the effect of anterior-posterior (A-P) and medial-lateral (M-L) positional variation of the Prodisc-L implanted in a FE model of a 24 years old female FSU L4-L5 on ROM during flexion-extension, lateral bending, and axial rotation; (b) to evaluate the significance of A-P position of the superior bone relative to the inferior bone of a 24 years old female FSU L4-L5, which leads to anterior or retro-listhesis of one vertebra relative to the other; (c) to evaluate the amount of distraction required for a 42 years old male FSU L4-L5 to achieve maximum flexion in the process of deciding whether spinal fusion is required.

5.3 Methods

5.3.1 *In Vitro* Testing, Calibration and Validation of a FE Model

A series of *in vitro* tests were conducted on a fresh-frozen intact lumbosacral spine. The spine was identified as *Spine A* (33 years old male subject in healthy spine condition). To prepare the spine for computed tomographic (CT) scanning, the specimen underwent gross dissection to remove unnecessary spinal levels, residual rib attachments, and soft tissues structures. Pure-moment, combined motion, and compressive tests were performed. Pure-moment (flexion-extension, lateral bending, axial rotation) and combined motions testing was performed according to the developed testing protocol using a custom multi-axis spine motion simulator (Figure 5.1) in tandem with a Vicon 3-D motion analysis 4-camera system to track segmental spinal motions. Specifically, for the FSU testing, a sequential sectioning protocol was performed to remove spinal structures while repeating tests to evaluate the contribution of the sectioned structures to the overall mechanical stability of the motion segment.

Three-dimensional explicit FE model of *Spine A* was developed in Abaqus/Explicit ((Dassault Systems, Providence, RI, USA) from a series of coronal CT images (in-plane resolution of 0.375 mm/pixel; 512 X 512 pixels; 0.625mm slice thickness). The visible bony structures of the vertebral bodies were manually segmented and exported as 3D surface geometries using ScanIP (Simpleware, Exeter, UK). Seven of the load-bearing ligamentous structures crossing each of the FSU were represented by connector elements (Figure 5.1) including the anterior and posterior longitudinal ligament

97

(ALL, PLL), supraspinous and intraspinous ligament (SSL, ISL), intertransverse ligament (ITL), facet capsular ligament (FCL) and ligamentum flavum (LFL). These ligaments were modeled by multiple nonlinear, tension only connector elements in series and parallel. Most of the ligament attachment sites were based of the dissection performed after testing. Few attachment sites were adopted from literature based descriptions (Panjabi et al., 1991). Based on the dissected geometry of the intervertebral disc (IVD), the annulus fibrosus (AF) comprised of three major regions (anterior, posterior and laterals) modeled as 8-noded hexahedral elements and a fluid-filled cavity representing the nucleus pulposus. To validate the FSU model, Abaqus/Explicit analyses were performed using a stepwise addition of structures approach starting with the most basic configuration of the bones separated by the IDV. The facet cartilages were then added in the model followed by the facet capsules (FCL), ITL, ALL, PLL, LFL, ISL, and SSL. Pure moment analysis in the principal axis – Flexion-Extension (Flex-Ext), Lateral bending (LB), and axial rotation (AR) were performed force controlled to either a moment limit of 10Nm (in the intact FSU configuration) or, in the case of a "hybrid" analysis, to the maximum angle limit recorded during the specimen's intact configuration. Except for the intact configuration analysis, the inferior bone was kept fixed and displacement was applied to the fiducial markers modeled on superior bone to reproduce the hybrid tests. The finite element analysis was repeated after the addition of each spinal structure to evaluate the contribution of the sectioned structures to the overall stability of the segment. Reaction moment (RM) from the analysis was compared to the

98

moment measured during the testing. At the end of this validation, a set of material properties for the IVD, ligaments and facets were obtained that were used for all FSU models in this study.

5.3.2. FE Model Development of Instrumented Spine with Prodisc-L

For each patient plan, the ProDisc-L (Synthes Spine) was virtually implanted using an anterior approach, which involved removal of the entire ALL, PLL and the anterior and posterior annulus including the entire nucleus pulposus. The lateral regions of the annulus remained intact. The ProDisc-L was aligned in the intervertebral space to maximize ROM ('neutral' position). The location of ProDisc-L was varied in the A-P and M-L direction in the midline in 1 mm increments (Figure 5.2c) on a 24 years old female subject. ROM was determined based on impingement of the facet joints or implant. Both available implant endplate angles and different implant sizes were evaluated to determine both the appropriate implant and associated optimal position. In addition, for the same subject, the relative A-P positioning of the implant endplates was evaluated by moving the superior endplate relative to the inferior endplate 1 mm in each direction, creating a relative anterior or retro-listhesis. After moving the superior bone relative to the inferior bone, the ProDisc-L position was varied in the A-P direction in increments of 0.5 mm.

Different implant sizes were then trialed using FE modeling on a 42 years old male subject to identify the optimal implant geometry matching the anatomy of the patient. Lastly, in order to decide if fusion or TDR is the preferred method of treating

back pain, the posterior disc height and amount of distraction required to achieve the optimal range of motion was assessed on a 27 years old female.

5.4 Results

5.4.1 Intact FSU Kinematics

For the intact case, *Spine A* (33 years old male), material property optimization of L2-L3 and L4-L5 FSU's were performed using the torque-rotation behavior in flexion-extension, lateral bending and axial rotation using the procedure described in Chapter 3. These analyses were performed force controlled with applied torques of 10 N-m. Torque-rotation response comparison of the model with the experiment for FSU L2-L3 and L4-L5 is shown in Figure 5.3 top and bottom respectively. The non-linearity of the FSU was excellently represented by the FE model. The root mean squared errors (RMSE) were computed over the torque-rotation curves for each loading degree of freedom. RMSE for all loading cases was between 0.05 and 0.25° with the average being in the range of 0.09 to 0.17°.

5.4.2 A-P and M-L Translations

As observed clinically, the disc anterior-posterior (A-P) positioning in the 24 years old female subject had a linear relationship with resulting flexion-extension ROM and facet loading. Posterior positioning increased flexion ROM and facet contact force, while anterior positioning decreased these measures (Figure 5.4a). Because of the

spherical design of the ProDisc-L and the physiological presence of the facet joints, influence of positioning on the ROM during axial rotation was extremely small (less than 1deg) compared to other degrees of freedom (Figure 5.4b). Facet contact limited the flexion motion, while impingement of the device limited extension (Figure 5.4c). For the specific geometry used, facet contact also limited lateral bending and axial rotation (Figure 5.5). Relative AP positioning of the implant endplates also showed substantial changes to ROM. Higher ROM (almost twice) was seen when L4 was positioned posterior relative to L5 by 1mm (Figure 5.6) causing anterior and retro-listhesis.

5.4.3 Implant Selection and Sensitivity

Altering the implant size selection, which has an effect on how far posteriorly the axis of rotation can be located, influenced the potential range of motion that can be achieved. The use of a medium size ProDisc-L over large size in the 42 years old male subject resulted in increased ROM. Figure 5.7 shows the increased ROM obtained when the bones were distracted from 12.6 mm to 14.3 mm on the anterior side and from 6.8 mm to 10 mm on the posterior side. The percentage increase was in the range of 3.2 to 5.2 % during flexion and extension at different A-P positions on the midline. Generally, the smaller anatomy with the same implant was more sensitive to alignment and showed greater change in resulting ROM as a function of position.

5.4.4 Distraction – TDR or Fusion

The 27 years old female subject shown in Figure 5.8 had small anatomy and a narrow disc. Virtual implantation resulted in a distraction of about 7 mm resulting in near dislocation of the facet joints. However, this patient showed a substantial increase in the ROM (9.9 Deg in flexion and 5.9 Deg in extension) as no facet impingement could occur. Hence, in this case where the distraction of the segment considered is excessive, fusion was preferred.

5.5 Discussion

ROM results are consistent with current clinical practice for posterior placement; however the most posterior placement did limit extension. Understanding the influence of TDR placement on range of motion and facet loading can improve functional outcomes of this procedure. Evaluating the influence of placement to optimize ROM may be even more important with asymmetric patient anatomy. Anterior-posterior position of the superior relative to the inferior endplate, which leads to anterior or retro-listhesis of one vertebra relative to the other, plays a significant role in the motion achievable at the indexed segment. In patients where less than 5 degrees of motion was achievable due to mismatch between the patient's anatomy and the implant geometry, fusion is recommended. Ultimately preservation of motion is the clinical objective; however where this can only be achieved through excessive distraction of the motion segment, fusion is preferred. Pre-op templating through simulation is beneficial in deciding if the patient is

suitable for TDR. Overall, careful patient selection and understanding the influence of TDR alignment on ROM, facet loading, and ligament elongation can improve functional outcomes of this procedure. Clinical correlation of patients undergoing this form of pre-op templating continues.

In closing, a technique for pre-op templating is suggested using FE modeling. This technique can act as a guide in the process of implant selection, fusion or TDR procedure selection. If used in conjunction with clinical practices, FE can be clinically relavent as a pre-op templating tool in TDR alignment.
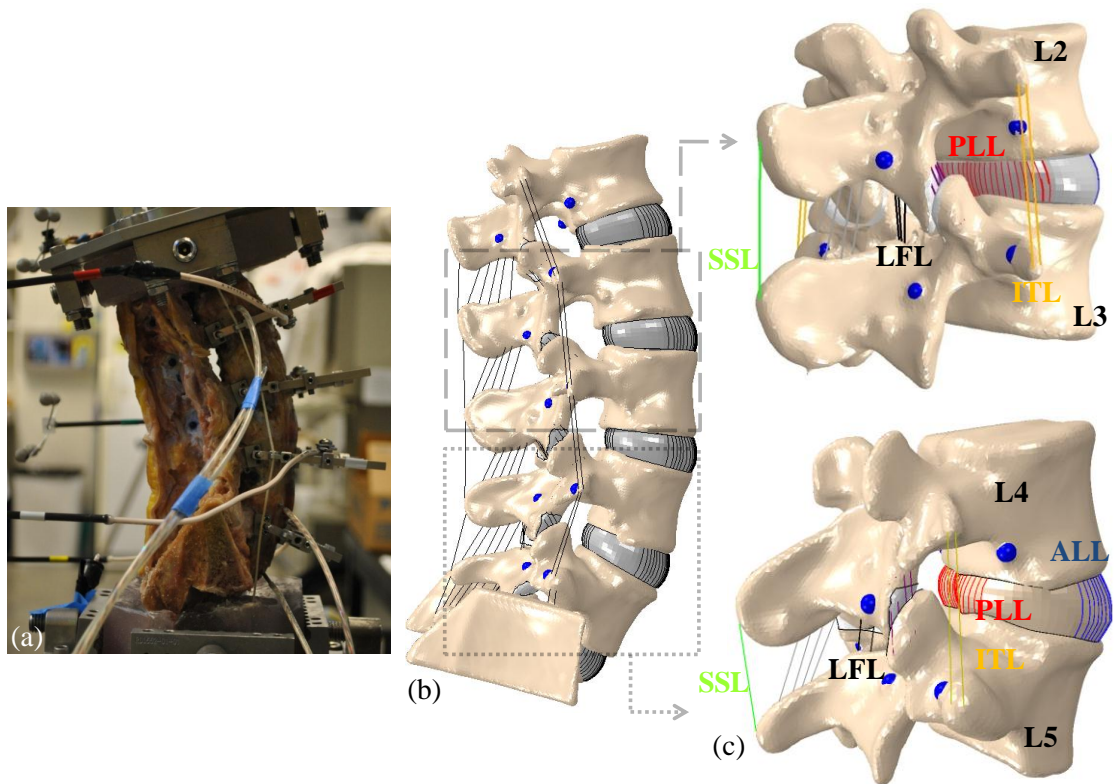
Figure 5.1: (a) Cadaveric setup of *Spine A*. (b) Subject specific finite element model of the lumbosacral spine and (c) Ligamentous representation of FSU L2-L3 (top) and FSU L4-L5 (bottom)
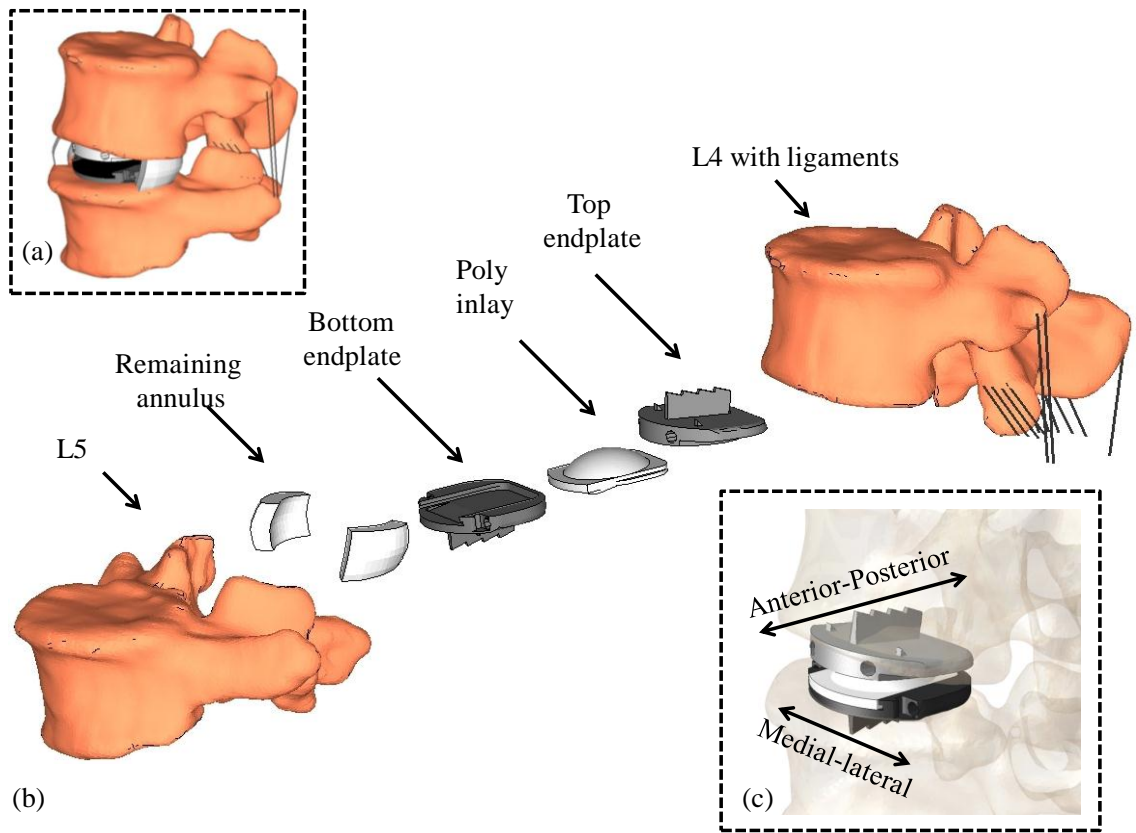
Figure 5.2: (a) FSU L4-L5 with the ProDisc-L, (b) exploded view of the FSU with Prodisc-L components, and (c) positional variation of the Prodisc-L in the Anterior-Posterior (AP) and Medial-Lateral (ML) position
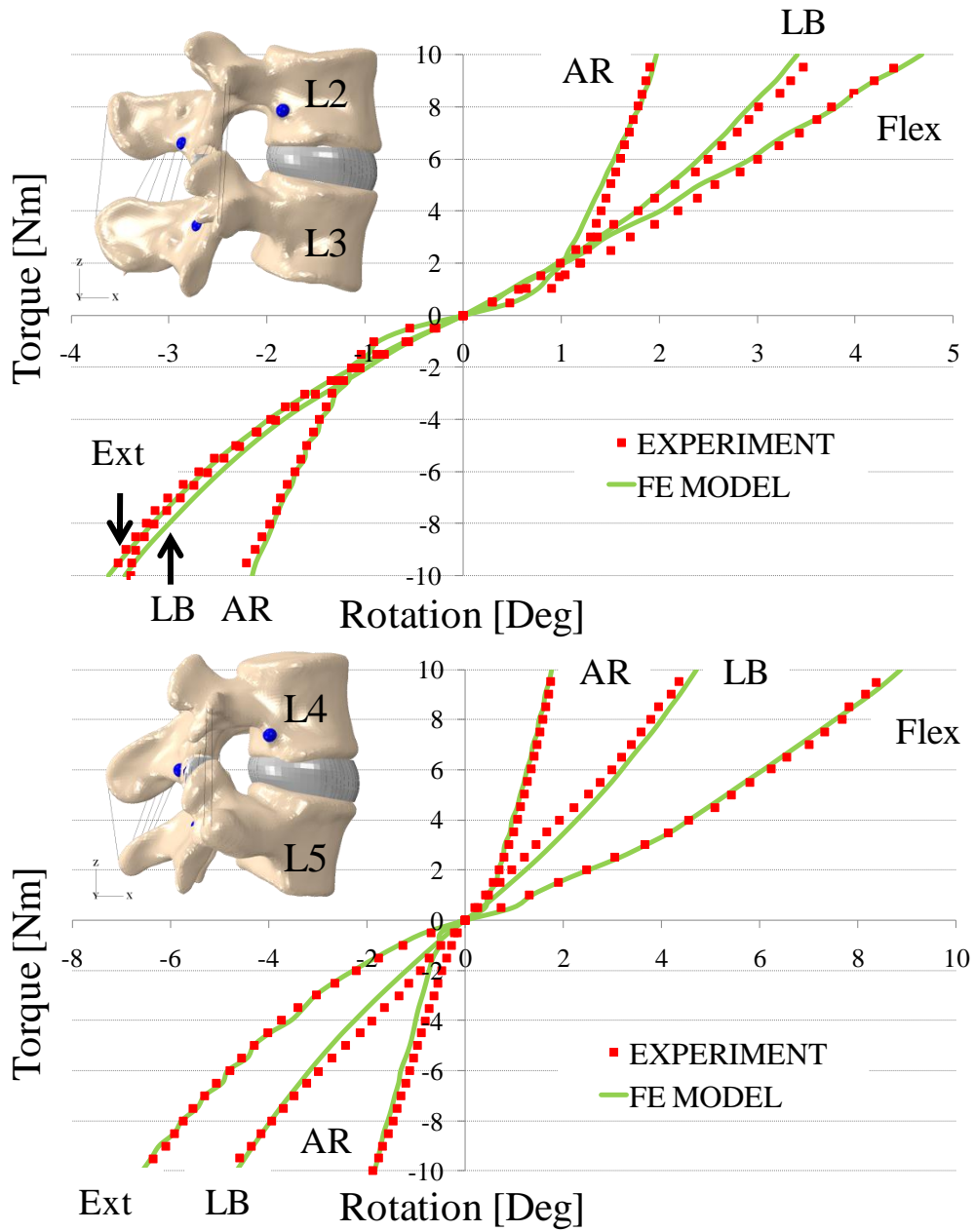
Figure 5.3: Predicted torque-rotation response compared to experiment during flexion-extension, lateral bending, and axial rotation at levels L2-L3 (top) and L4-L5 (bottom)
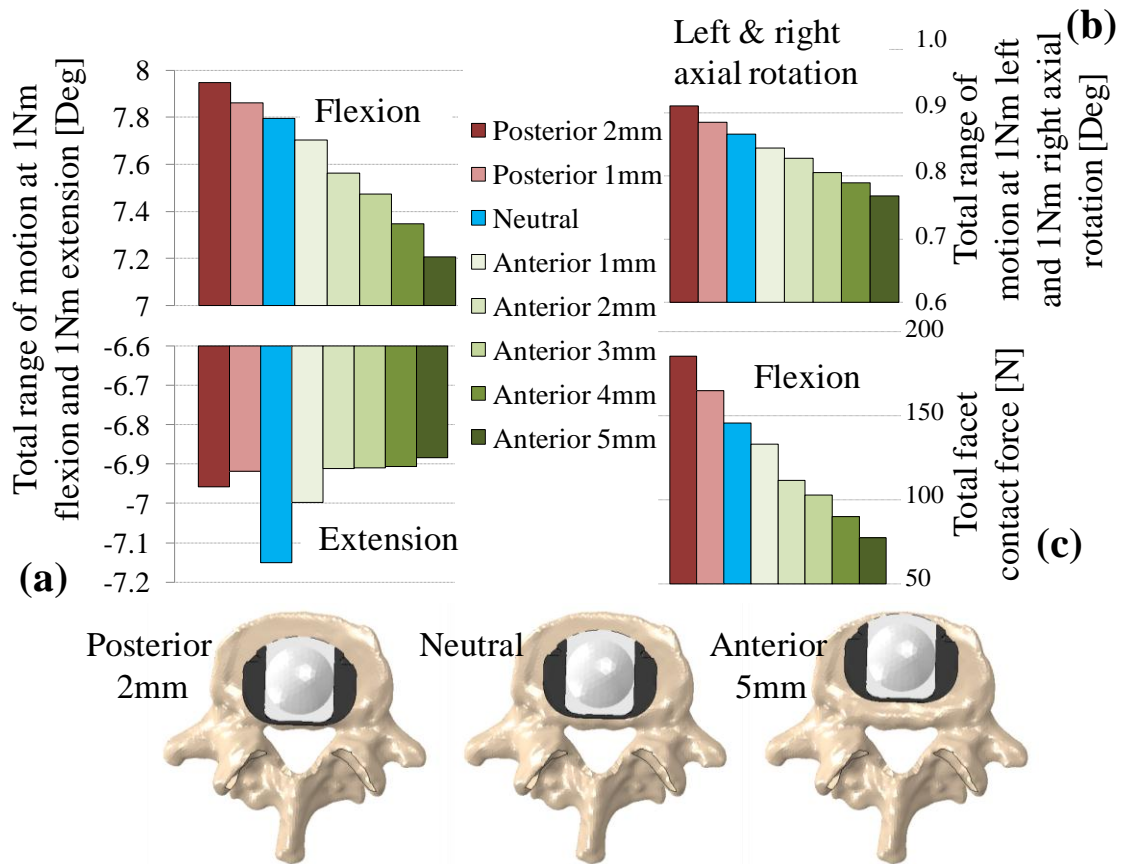
Figure 5.4: Range of motion with the ProDisc-L during (a) flexion-extension, (b)

axial rotation, and (c) facet contact force with anterior-posterior position variation
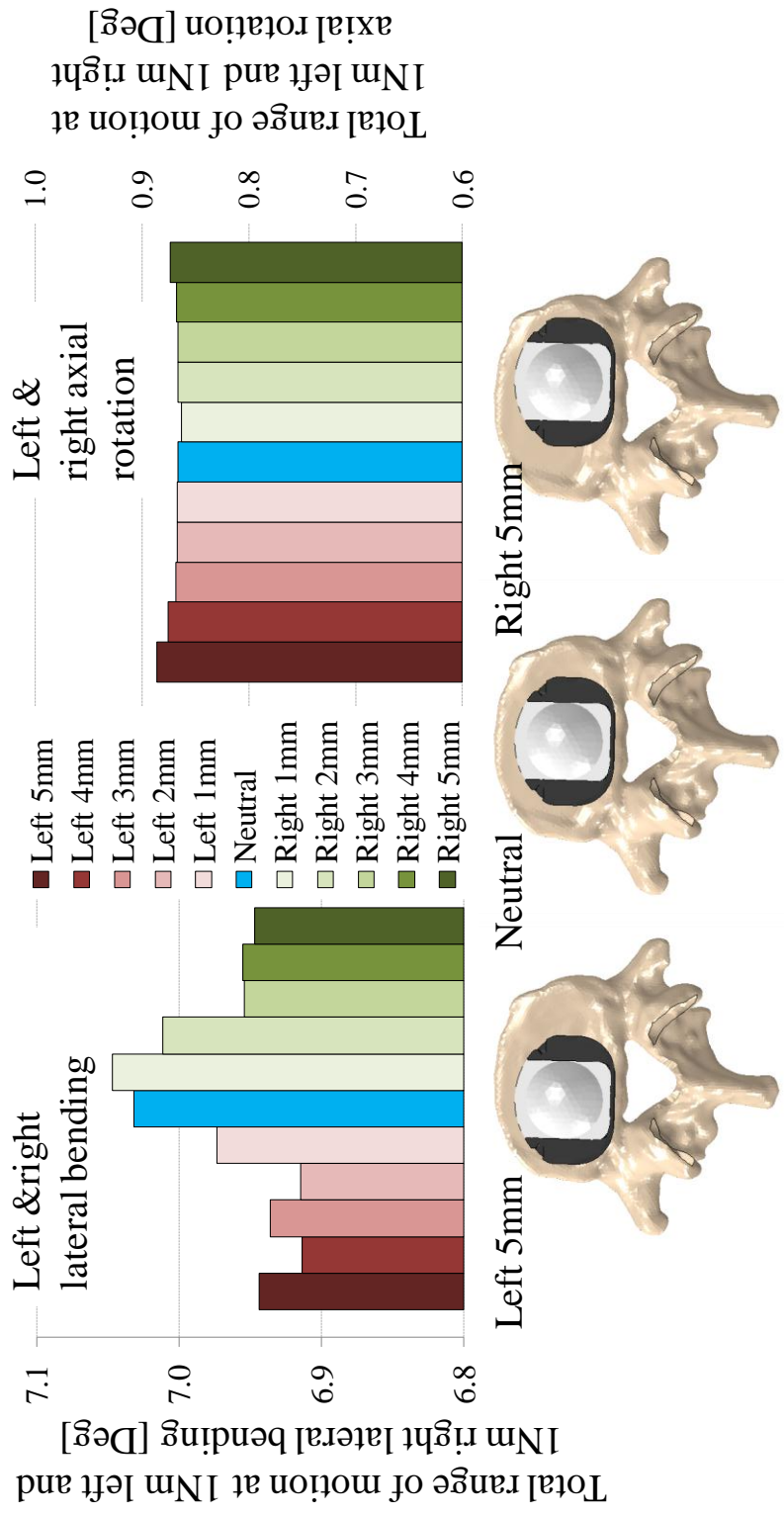
Figure 5.5: Total range of motion with the ProDisc-L during (a) lateral bending and (b) axial rotation with M-L position variation
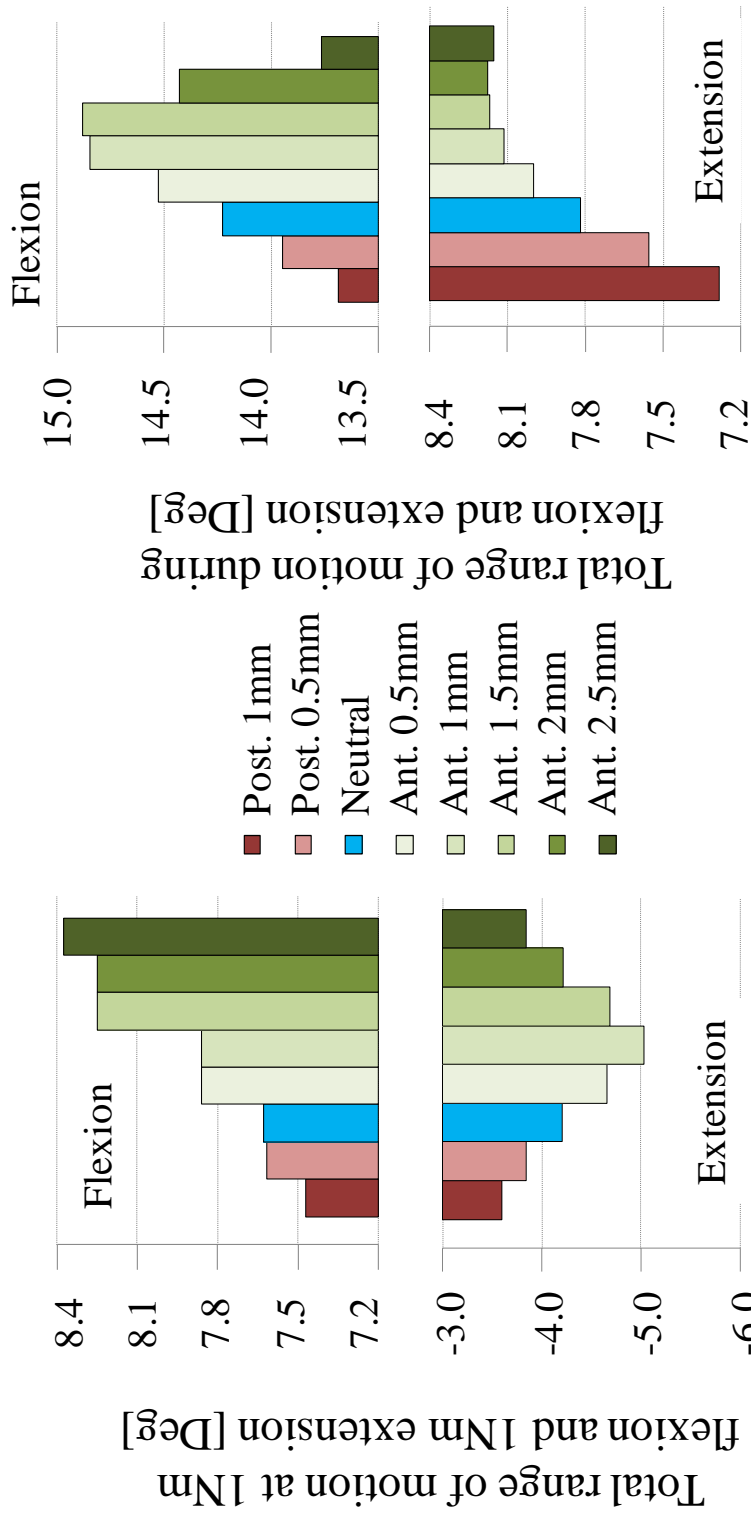
Figure 5.6: ROM due to anterior (a) or posterior (b) displacement of the superior endplate
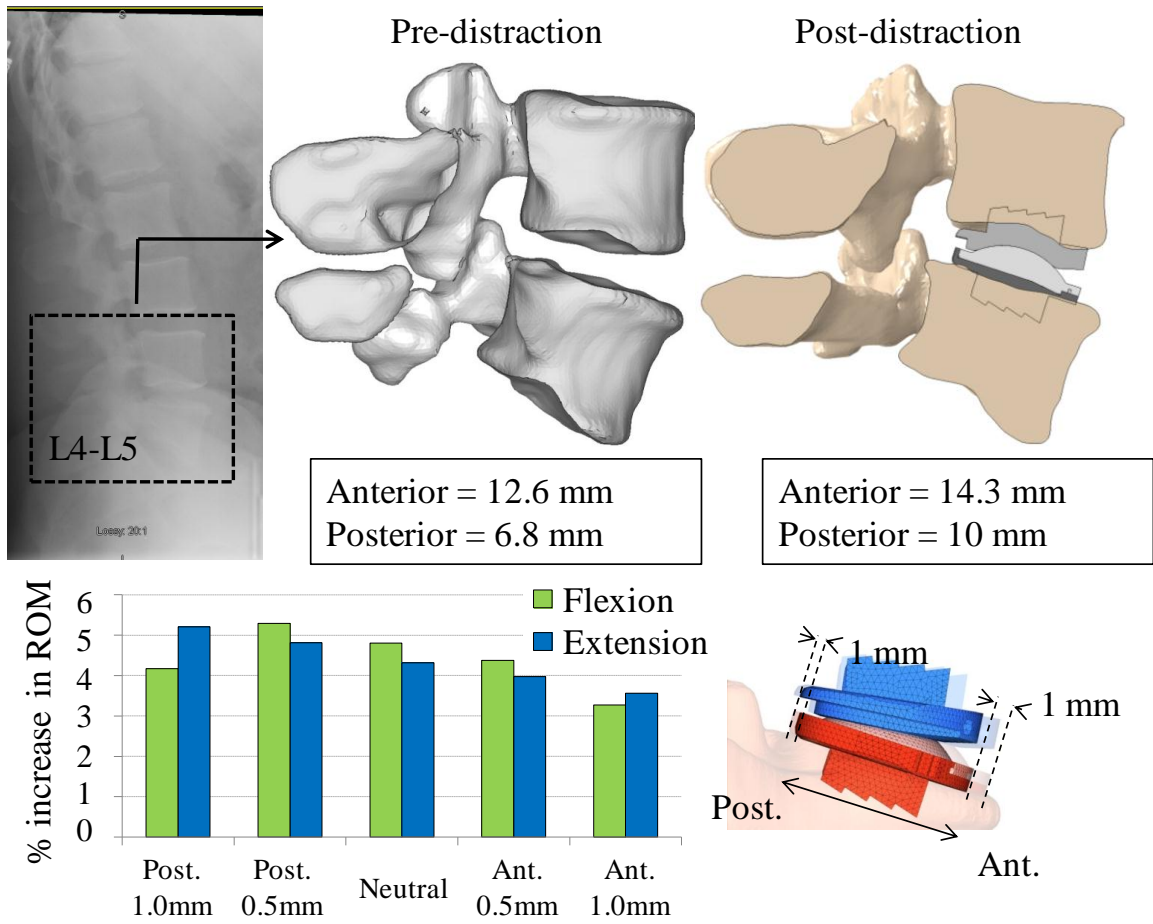
Figure 5.7: Increased ROM evident in a 42 years old large male when a medium

implant was modeled compared to a large implant
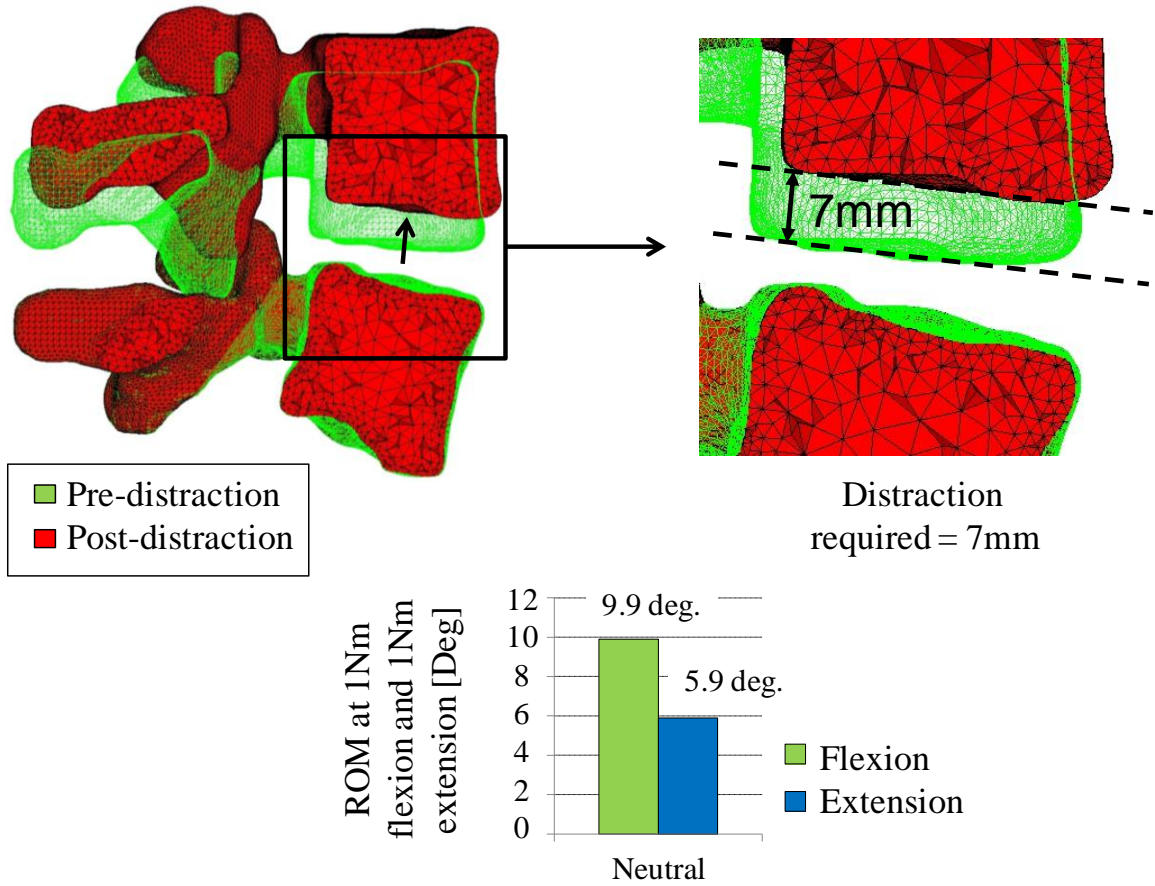
Figure 5.8: 27 yr old female showing an excellent ROM, but the smallest implant available resulted in over distraction of the segment

Table 5.1: Patient selection and information

Sr. No.	Patient	FE model used for investigating	Results
1	33 years male	Intact spine	Section 5.4.1
2	24 years female	A-P and M-L translation of ProDisc-L	Section 5.4.2
3	42 years male	Implant selection and sensitivity	Section 5.4.3
4	27 years female	TDR or Fusion required?	Section 5.4.4

Chapter 6: Conclusions and Recommendations

6.1 Conclusion

Creating subject-specific FE biomechanical models of the spine is challenging due to the difficulty in anatomicaly accurate geometry creation and accurate representation of biological materials. However, once calibrated against subject-specific *in vitro* data, the relative ease in modifying loads and/or boundary conditions, mechanical and material property assignment, or conducting sensitivity or probabilistic studies can provide valuable information about the mechanics that would otherwise be impossible or cost-prohibitive to obtain using conventional measurements and testing. Accordingly, the studies in this dissertation present a progression of work in the field of lumbar spine modeling, calibrating, validating and using these validated spines for making predictions to use them for surgical judgments. Greater focus of this work has been on explicit finite element modeling. Special emphasis was placed on model predictions against subject specific *in vitro* data. Higher prediction accuracy was achieved because of the subject-specific model tuning. This dissertation also focused on using some of the established probabilistic techniques and reliability methods to better represent a population taking into account some of the biological uncertainties inherent in the human spine. In application to implant placement study, this dissertation represents development of a pre-

113

op template using FE modeling to assist surgeons in making pre-op recommendations. These recommendations can be in terms of implant selection, optimum positioning of implant, or deciding if TDR is recommended over a conventional spinal fusion.

Chapter 3 described the uniqueness of modeling the AF and calibrating the anisotropic hyperelastic parameters. This modeling technique using anisotropic hyperelastic material model for the ground matrix, fibers and the nucleus plays a crucial role in understanding the role of each structure of the intervertebral disc. The probabilistic model of the spine described in Chapter 4 represents a novel application of well-established probabilistic techniques and reliability methods. These techniques successfully identified the important aspects of soft tissue constraints as well as geometric features like the facet joints. These investigations help understanding the variability and the clinical outcome of a population sample. For example, the results from the sensitivity analysis showed that the properties of the disc were most sensitive followed by few of the recruited ligaments. These may be used in future optimization endeavors by focusing on some of the most important parameters as compared to the unimportant parameters where the load transfer might be negligible. The agreement between predicted laxity bounds using the FORM technique and the gold standard Monte Carlo methods demonstrate the computational advantage of using the FORM technique to generate results similar to the Monte Carlo method at a reduced computational cost (~95% savings in computation time). Chapter 4 also discusses the possibility of running the probabilistic analysis on the FSU level and extrapolating the findings to look at the uncertainty anticipated in the lumbosacral spine.

The work in Chapter 5 demonstrated that pre-op templating using FE modeling is technically feasible and clinically relevant to assist surgeons in their preoperative planning. It was also seen how understanding the influence of TDR placement on range of motion and facet loading can improve functional outcomes of this procedure. Although, the choice of the actual surgical procedure (fusion or TDR) is dependent on the surgeon's own preference based on past experience. However, this chapter discusses how the surgeon can use the FE model to assist him in this decision making process.

6.2 Future Work

The spinal ligaments in the current FE model were represented as axial type one-dimensional connector elements. The material representation was based on a non-linear force versus displacement relation that was primarily a tension only spring-like elastic behavior. These ligaments were spread over a finite width to represent anatomically equivalent band like structures. A two-dimensional (membrane or fiber-reinforced membranes) or three-dimensional (solid hexahedral or tetrahedral elements) ligamentous representation would be advantageous in this model because of the finding that ligaments support complex loading patterns with non-uniform plane stress distributions rather than simple axial stresses (Dickey et al., 1996). As a proof-of-concept, one FSU was modeled with two-dimensional fiber reinforced membrane elements (Appendix A1.15). Also, it has been reported that the ligaments of the lumbar spine are in a state of pre-stress (Tkaczuk, 1968).In this model, the ligaments were geometrically created in an unloaded

115

state which meant that the ligaments were in a stress-free state in the neutral (unloaded) position. This approach is beneficial in eliminating the complexity of geometric and material modeling. However, to properly assess the wrapping behavior, especially the ALL and PLL around the intervertebral disc and the facet capsule, it will be beneficial to understand the state of the two-dimensional ligaments in comparison with point-to-point one-dimensional ligaments. Also, during optimization, the linear region of the ligament force versus displacement curve was perturbed. This approach was sufficient to calibrate the overall behavior of the model in this study, but perturbing the toe-in region of this force versus displacement curve can be useful in calibrating the model more appropriately. Finally, the modeling of the FE model was carried out with the application of follower load. This was in line with the *in vitro* testing performed on the cadavers. However, as the next step in improving this FE model, simulation of muscle forces as represented by Wilke 1995, Zander 2001, Calisse 1999, Arjmand 2009 will be more appropriate.

Few studies have reported the ratio of the annulus fibrosus to nucleus volume in the human intervertebral disc (Ezquerro., 2011). In the current model, during calibration, this ratio was not a variable. Perturbing this ratio, i.e., changing the volume of nucleus present inside the disc may mimic the intervertebral disc mechanics more appropriately. However, based on the dissected spine measurements, the annulus fibrosus region and nucleus pulposus regions were approximately created in this model.

The effect of mechanically simulated muscle forces on lumbar spine specimens was first examined by Panjabi et al., (1989). In their work, only one single force vector simulating a group of intrinsic muscles was acting on intact and injured human lumbar spine segments. Since then, numerous *in vitro* and modeling studies have looked at the effect of muscle force magnitudes and attachment sites (Wilke 1995, Zander 2001, Calisse 1999, Arjmand 2009). In the current FE model, the muscle forces were not simulated. The absence of muscle forces was compensated by simulating user specified loading and boundary condition in the form of follower load (Patwardhan et al, 1999)

To summarize this dissertation, the techniques described here represent advancements in FE modeling of the lumbar spine by creating, calibrating and analyzing more complex multi-axial loading conditions of the spine. Future work should attempt to apply these techniques to more challenging natural as well as implanted state of the lumbar spine. Additionally, clinical correlation of patients undergoing spinal implantation and this form of pre-operative templating should be continued.

Works Cited

Acaroglu, E.R., Iatridis, J.C., Setton, L.A., Foster, R.J., Mow, V.C., Weidenbaum, M., 1995. Degeneration and aging affect the tensile behavior of human lumbar anulus fibrosus. Spine (Phila Pa 1976) 20, 2690-2701.

Adams, M.A., Dolan, P., Biomechanics of vertebral compression fractures and clinical application. Arch Orthop Trauma Surg 131, 1703-1710.

Adams, M.A., Hutton, W.C., 1983. The mechanical function of the lumbar apophyseal joints. Spine (Phila Pa 1976) 8, 327-330.

Ahmed, A.M., Duncan, N.A., Burke, D.L., 1990. The effect of facet geometry on the axial torque-rotation response of lumbar motion segments. Spine (Phila Pa 1976) 15, 391-401.

Anderson, D.D., Goldsworthy, J.K., Li, W., James Rudert, M., Tochigi, Y., Brown, T.D., 2007. Physical validation of a patient-specific contact finite element model of the ankle. J Biomech 40, 1662-1669.

Arjmand, N., Gagnon, D., Plamondon, A., Shirazi-Adl, A., Lariviere, C., 2009. Comparison of trunk muscle forces and spinal loads estimated by two biomechanical models. Clin Biomech (Bristol, Avon) 24, 533-541.

Ayturk, U.M., Puttlitz, C.M., Parametric convergence sensitivity and validation of a finite element model of the human lumbar spine. Comput Methods Biomech Biomed Engin 14, 695-705.

Aubin, C.E., Petit, Y., Stokes, I.A., Poulin, F., Gardner-Morse, M., Labelle, H., 2003. Biomechanical modeling of posterior instrumentation of the scoliotic spine. Comput Methods Biomech Biomed Engin 6, 27-32.

Bass, E.C., Ashford, F.A., Segal, M.R., Lotz, J.C., 2004. Biaxial testing of human annulus fibrosus and its implications for a constitutive formulation. Ann Biomed Eng 32, 1231-1242.

Bellini, C.M., Galbusera, F., Raimondi, M.T., Mineo, G.V., Brayda-Bruno, M., 2007. Biomechanics of the lumbar spine after dynamic stabilization. J Spinal Disord Tech 20, 423-429.

Best, B.A., Guilak, F., Setton, L.A., Zhu, W., Saed-Nejad, F., Ratcliffe, A., Weidenbaum, M., Mow, V.C., 1994. Compressive mechanical properties of the human anulus fibrosus and their relationship to biochemical composition. Spine (Phila Pa 1976) 19, 212-221.

Botolin, S., Puttlitz, C., Baldini, T., Petrella, A., Burger, E., Abjornson, C., Patel, V., Facet joint biomechanics at the treated and adjacent levels after total disc replacement. Spine (Phila Pa 1976) 36, E27-32.

Bowden, A.E., Guerin, H.L., Villarraga, M.L., Patwardhan, A.G., Ochoa, J.A., 2008. Quality of motion considerations in numerical analysis of motion restoring implants of the spine. Clin Biomech (Bristol, Avon) 23, 536-544.

Brolin, K., Halldin, P., 2004. Development of a finite element model of the upper cervical spine and a parameter study of ligament characteristics. Spine (Phila Pa 1976) 29, 376-385.

Brown, T., Hansen, R.J., Yorra, A.J., 1957. Some mechanical tests on the lumbosacral spine with particular reference to the intervertebral discs; a preliminary report. J Bone Joint Surg Am 39-A, 1135-1164.

Calisse, J., Rohlmann, A., Bergmann, G., 1999. Estimation of trunk muscle forces using the finite element method and in vivo loads measured by telemeterized internal spinal fixation devices. J Biomech 32, 727-731.

Cassidy, J.J., Hiltner, A., Baer, E., 1989. Hierarchical structure of the intervertebral disc. Connect Tissue Res 23, 75-88.

Chazal, J., Tanguy, A., Bourges, M., Gaurel, G., Escande, G., Guillot, M., Vanneuville, G., 1985. Biomechanical properties of spinal ligaments and a histological study of the supraspinal ligament in traction. J Biomech 18, 167-176.

de Visser, H., Adam, C.J., Crozier, S., Pearcy, M.J., 2007. The role of quadratus lumborum asymmetry in the occurrence of lesions in the lumbar vertebrae of cricket fast bowlers. Med Eng Phys 29, 877-885.

Descamps, S., Livesey, C., Learmonth, I.D., Determination of digitised radiograph magnification factors for pre-operative templating in hip prosthesis surgery. Skeletal Radiol 39, 273-277.

Dickey, J.P., Bednar, D.A., Dumas, G.A., 1996. New insight into the mechanics of the lumbar interspinous ligament. Spine (Phila Pa 1976) 21, 2720-2727.

119

el-Bohy, A.A., Yang, K.H., King, A.I., 1989. Experimental verification of facet load transmission by direct measurement of facet lamina contact pressure. J Biomech 22, 931-941.

Elliott, D.M., Setton, L.A., 2000. A linear material model for fiber-induced anisotropy of the anulus fibrosus. J Biomech Eng 122, 173-179.

Elliott, D.M., Setton, L.A., 2001. Anisotropic and inhomogeneous tensile behavior of the human anulus fibrosus: experimental measurement and material model predictions. J Biomech Eng 123, 256-263.

Eyre, D.R., Muir, H., 1976. Types I and II collagens in intervertebral disc. Interchanging radial distributions in annulus fibrosus. Biochem J 157, 267-270.

Ezquerro, F., Garcia Vacas, F., Postigo, S., Prado, M., Simon, A., 2011. Calibration of the finite element model of a lumbar functional spinal unit using an optimization technique based on differential evolution. Med Eng Phys 33, 89-95.

Ezquerro, F., Simon, A., Prado, M., Perez, A., 2004. Combination of finite element modeling and optimization for the study of lumbar spine biomechanics considering the 3D thorax-pelvis orientation. Med Eng Phys 26, 11-22.

Fujita, Y., Duncan, N.A., Lotz, J.C., 1997. Radial tensile properties of the lumbar annulus fibrosus are site and degeneration dependent. J Orthop Res 15, 814-819.

Gedet, P., Thistlethwaite, P.A., Ferguson, S.J., 2007. Minimizing errors during in vitro testing of multisegmental spine specimens: considerations for component selection and kinematic measurement. J Biomech 40, 1881-1885.

Goel, V.K., Kong, W., Han, J.S., Weinstein, J.N., Gilbertson, L.G., 1993. A combined finite element and optimization investigation of lumbar spine mechanics with and without muscles. Spine (Phila Pa 1976) 18, 1531-1541.

Goel, V.K., Monroe, B.T., Gilbertson, L.G., Brinckmann, P., 1995. Interlaminar shear stresses and laminae separation in a disc. Finite element analysis of the L3-L4 motion segment subjected to axial compressive loads. Spine (Phila Pa 1976) 20, 689-698.

Goel, V.K., Nye, T.A., Clark, C.R., Nishiyama, K., Weinstein, J.N., 1987. A technique to evaluate an internal spinal device by use of the Selspot system: an application to Luque closed loop. Spine (Phila Pa 1976) 12, 150-159.

Gornet, M.F., Chan, F.W., Coleman, J.C., Murrell, B., Nockels, R.P., Taylor, B.A., Lanman, T.H., Ochoa, J.A., Biomechanical assessment of a PEEK rod system for semi-rigid fixation of lumbar fusion constructs. J Biomech Eng 133, 081009.

Guerin, H.A., Elliott, D.M., 2006. Degeneration affects the fiber reorientation of human annulus fibrosus under tensile load. J Biomech 39, 1410-1418.

Haldar, A., Mahadevan, S., 2000. Reliability and Statistical Methods in Engineering Design. Wiley, New York.

Halloran, J.P., Petrella, A.J., Rullkoetter, P.J., 2005. Explicit finite element modeling of total knee replacement mechanics. J Biomech 38, 323-331.

Hato, T., Kawahara, N., Tomita, K., Murakami, H., Akamaru, T., Tawara, D., Sakamoto, J., Oda, J., Tanaka, S., 2007. Finite-element analysis on closing-opening correction osteotomy for angular kyphosis of osteoporotic vertebral fractures. J Orthop Sci 12, 354-360.

Heuer, F., Schmidt, H., Klezl, Z., Claes, L., Wilke, H.J., 2007. Stepwise reduction of functional spinal structures increase range of motion and change lordosis angle. J Biomech 40, 271-280.

Holzapfel, G.A., Gasser, T.C., Ogden, R.W., 2004. Comparison of a multi-layer structural model for arterial walls with a fung-type model, and issues of material stability. J Biomech Eng 126, 264-275.

Horton, W.G., 1958. Further observations on the elastic mechanism of the intervertebral disc. J Bone Joint Surg Br 40-B, 552-557.

Kalichman, L., Hunter, D.J., 2007. Lumbar facet joint osteoarthritis: a review. Semin Arthritis Rheum 37, 69-80.

Kim, Y., 2007. Finite element analysis of anterior lumbar interbody fusion: threaded cylindrical cage and pedicle screw fixation. Spine (Phila Pa 1976) 32, 2558-2568.

Kumaresan, S., Yoganandan, N., Pintar, F.A., 1998. Finite element modeling approaches of human cervical spine facet joint capsule. J Biomech 31, 371-376.

Kumaresan, S., Yoganandan, N., Pintar, F.A., Maiman, D.J., 1999. Finite element modeling of the cervical spine: role of intervertebral disc under axial and eccentric loads. Med Eng Phys 21, 689-700.

Kurowski, P., Kubo, A., 1986. The relationship of degeneration of the intervertebral disc to mechanical loading conditions on lumbar vertebrae. Spine (Phila Pa 1976) 11, 726-731.

Lavaste, F., Skalli, W., Robin, S., Roy-Camille, R., Mazel, C., 1992. Three-dimensional geometrical and mechanical modelling of the lumbar spine. J Biomech 25, 1153-1164.

Laz, P.J., Pal, S., Fields, A., Petrella, A.J., Rullkoetter, P.J., 2006. Effects of knee simulator loading and alignment variability on predicted implant mechanics: a probabilistic study. J Orthop Res 24, 2212-2221.

Lee, K.K., Teo, E.C., 2005. Material sensitivity study on lumbar motion segment (L2-L3) under sagittal plane loadings using probabilistic method. J Spinal Disord Tech 18, 163-170.

Lee, M.J., Bransford, R.J., Bellabarba, C., Chapman, J.R., Cohen, A.M., Harrington, R.M., Ching, R.P., The effect of bilateral laminotomy versus laminectomy on the motion and stiffness of the human lumbar spine: a biomechanical comparison. Spine (Phila Pa 1976) 35, 1789-1793.

Lee, C.K., Langrana, N.A., Parsons, J.R., Zimmerman, M.C., 1991. Development of a prosthetic intervertebral disc. Spine (Phila Pa 1976) 16, S253-255.

Lu, Y.M., Hutton, W.C., Gharpuray, V.M., 1996. Do bending, twisting, and diurnal fluid changes in the disc affect the propensity to prolapse? A viscoelastic finite element model. Spine (Phila Pa 1976) 21, 2570-2579.

Markolf, K.L., 1972. Deformation of the thoracolumbar intervertebral joints in response to external loads: a biomechanical study using autopsy material. J Bone Joint Surg Am 54, 511-533.

McBroom, R.J., Hayes, W.C., Edwards, W.T., Goldberg, R.P., White, A.A., 3rd, 1985. Prediction of vertebral body compressive fracture using quantitative computed tomography. J Bone Joint Surg Am 67, 1206-1214.

McNally, D.S., Arridge, R.G., 1995. An analytical model of intervertebral disc mechanics. J Biomech 28, 53-68.

Moramarco, V., Perez del Palomar, A., Pappalettere, C., Doblare, M., An accurate validation of a computational model of a human lumbosacral segment. J Biomech 43, 334-342.

Natali, A., Meroi, E., 1990. Nonlinear analysis of intervertebral disk under dynamic load. J Biomech Eng 112, 358-363.

Natarajan, R.N., Ke, J.H., Andersson, G.B., 1994. A model to study the disc degeneration process. Spine (Phila Pa 1976) 19, 259-265.

Oreskes, N., Shrader-Frechette, K., Belitz, K., 1994. Verification, validation, and confirmation of numerical models in the Earth sciences. Science 263, 641-646.

Osti, O.L., Vernon-Roberts, B., Fraser, R.D., 1990. 1990 Volvo Award in experimental studies. Anulus tears and intervertebral disc degeneration. An experimental study using an animal model. Spine (Phila Pa 1976) 15, 762-767.

Oxland, T.R., Panjabi, M.M., Southern, E.P., Duranceau, J.S., 1991. An anatomic basis for spinal instability: a porcine trauma model. J Orthop Res 9, 452-462.

Panjabi, M., Abumi, K., Duranceau, J., Oxland, T., 1989. Spinal stability and intersegmental muscle forces. A biomechanical model. Spine (Phila Pa 1976) 14, 194-200.

Panjabi, M.M., 1991. [Three-dimensional testing of the stability of spinal implants]. Orthopade 20, 106-111.

Panjabi, M.M., Greenstein, G., Duranceau, J., Nolte, L.P., 1991. Three-dimensional quantitative morphology of lumbar spinal ligaments. J Spinal Disord 4, 54-62.

Panjabi, M.M., White, A.A., 3rd, Johnson, R.M., 1975. Cervical spine mechanics as a function of transection of components. J Biomech 8, 327-336.

Patwardhan, A.G., Havey, R.M., Meade, K.P., Lee, B., Dunlap, B., 1999. A follower load increases the load-carrying capacity of the lumbar spine in compression. Spine (Phila Pa 1976) 24, 1003-1009.

Pintar, F.A., Yoganandan, N., Myers, T., Elhagediab, A., Sances, A., Jr., 1992. Biomechanical properties of human lumbar spine ligaments. J Biomech 25, 1351-1356.

Pitzen, T., Matthis, D., Steudel, W.I., 2001. [A validated finite element model of the human spine--description of the model and initial application]. Z Orthop Ihre Grenzgeb 139, 40-44.

Polga, D.J., Beaubien, B.P., Kallemeier, P.M., Schellhas, K.P., Lew, W.D., Buttermann, G.R., Wood, K.B., 2004. Measurement of in vivo intradiscal pressure in healthy thoracic intervertebral discs. Spine (Phila Pa 1976) 29, 1320-1324.

Roberts, S., Menage, J., Urban, J.P., 1989. Biochemical and structural properties of the cartilage end-plate and its relation to the intervertebral disc. Spine (Phila Pa 1976) 14, 166-174.

Rohlmann, A., Bauer, L., Zander, T., Bergmann, G., Wilke, H.J., 2006. Determination of trunk muscle forces for flexion and extension by using a validated finite element model of the lumbar spine and measured in vivo data. J Biomech 39, 981-989.

Rohlmann, A., Neller, S., Bergmann, G., Graichen, F., Claes, L., Wilke, H.J., 2001. Effect of an internal fixator and a bone graft on intersegmental spinal motion and intradiscal pressure in the adjacent regions. Eur Spine J 10, 301-308.

Rundell, S.A., Auerbach, J.D., Balderston, R.A., Kurtz, S.M., 2008. Total disc replacement positioning affects facet contact forces and vertebral body strains. Spine (Phila Pa 1976) 33, 2510-2517.

Schmidt, H., Heuer, F., Simon, U., Kettler, A., Rohlmann, A., Claes, L., Wilke, H.J., 2006. Application of a new calibration method for a three-dimensional finite element model of a human lumbar annulus fibrosus. Clin Biomech (Bristol, Avon) 21, 337-344.

Schmidt, H., Kettler, A., Heuer, F., Simon, U., Claes, L., Wilke, H.J., 2007. Intradiscal pressure, shear strain, and fiber strain in the intervertebral disc under combined loading. Spine (Phila Pa 1976) 32, 748-755.

Schmidutz, F., Steinbruck, A., Wanke-Jellinek, L., Pietschmann, M., Jansson, V., Fottner, A., The accuracy of digital templating: a comparison of short-stem total hip arthroplasty and conventional total hip arthroplasty. Int Orthop.

Sharma, M., Langrana, N.A., Rodriguez, J., 1995. Role of ligaments and facets in lumbar spinal stability. Spine (Phila Pa 1976) 20, 887-900.

Shirazi-Adl, A., 1991. Finite-element evaluation of contact loads on facets of an L2-L3 lumbar segment in complex loads. Spine (Phila Pa 1976) 16, 533-541.

Shirazi-Adl, S.A., Shrivastava, S.C., Ahmed, A.M., 1984. Stress analysis of the lumbar disc-body unit in compression. A three-dimensional nonlinear finite element study. Spine (Phila Pa 1976) 9, 120-134.

Shirazi-Adl, A., 1994. Biomechanics of the lumbar spine in sagittal/lateral moments. Spine (Phila Pa 1976) 19, 2407-2414.

Shirazi-Adl, A., Ahmed, A.M., Shrivastava, S.C., 1986. Mechanical response of a lumbar motion segment in axial torque alone and combined with compression. Spine (Phila Pa 1976) 11, 914-927.

Siepe, C.J., Zelenkov, P., Sauri-Barraza, J.C., Szeimies, U., Grubinger, T., Tepass, A., Stabler, A., Mayer, M.H., The fate of facet joint and adjacent level disc degeneration following total lumbar disc replacement: a prospective clinical, X-ray, and magnetic resonance imaging investigation. Spine (Phila Pa 1976) 35, 1991-2003

Specht, L.M., Levitz, S., Iorio, R., Healy, W.L., Tilzey, J.F., 2007. A comparison of acetate and digital templating for total knee arthroplasty. Clin Orthop Relat Res 464, 179-183.

Stokes, I.A., Gardner-Morse, M., 2001. Lumbar spinal muscle activation synergies predicted by multi-criteria cost function. J Biomech 34, 733-740.

Sylvestre, P.L., Villemure, I., Aubin, C.E., 2007. Finite element modeling of the growth plate in a detailed spine model. Med Biol Eng Comput 45, 977-988.

Thompson, R.E., Pearcy, M.J., Downing, K.J., Manthey, B.A., Parkinson, I.H., Fazzalari, N.L., 2000. Disc lesions and the mechanics of the intervertebral joint complex. Spine (Phila Pa 1976) 25, 3026-3035.

Tkaczuk, H., 1968. Tensile properties of human lumbar longitudinal ligaments. Acta Orthop Scand, Suppl 115:111+.

Ueno, K., Liu, Y.K., 1987. A three-dimensional nonlinear finite element model of lumbar intervertebral joint in torsion. J Biomech Eng 109, 200-209.

Viceconti, M., Olsen, S., Nolte, L.P., Burton, K., 2005. Extracting clinically relevant data from finite element simulations. Clin Biomech (Bristol, Avon) 20, 451-454.

Wagner, D.R., Lotz, J.C., 2004. Theoretical model and experimental results for the nonlinear elastic behavior of human annulus fibrosus. J Orthop Res 22, 901-909.

Weiss, J.A., Gardiner, J.C., Ellis, B.J., Lujan, T.J., Phatak, N.S., 2005. Three-dimensional finite element modeling of ligaments: technical aspects. Med Eng Phys 27, 845-861.

Wen, N., Lavaste, F., Santin, J.J., Lassau, J.P., 1993. Three-dimensional biomechanical properties of the human cervical spine in vitro. I. Analysis of normal motion. Eur Spine J 2, 2-11.

White, A.A., 3rd, Panjabi, M.M., 1978. The basic kinematics of the human spine. A review of past and current knowledge. Spine (Phila Pa 1976) 3, 12-20.

White AA, P.M., 1980. Clinical biomechanics of the spine.

Wilke, H.J., Wolf, S., Claes, L.E., Arand, M., Wiesend, A., 1995. Stability increase of the lumbar spine with different muscle groups. A biomechanical in vitro study. Spine (Phila Pa 1976) 20, 192-198.

Wilke, H.J., Claes, L., Schmitt, H., Wolf, S., 1994. A universal spine tester for in vitro experiments with muscle force simulation. Eur Spine J 3, 91-97.

Wilke, H.J., Wolf, S., Claes, L.E., Arand, M., Wiesend, A., 1996. Influence of varying muscle forces on lumbar intradiscal pressure: an in vitro study. J Biomech 29, 549-555.

Williams, J.R., Natarajan, R.N., Andersson, G.B., 2007. Inclusion of regional poroelastic material properties better predicts biomechanical behavior of lumbar discs subjected to dynamic loading. J Biomech 40, 1981-1987.

Wilson, D.C., Niosi, C.A., Zhu, Q.A., Oxland, T.R., Wilson, D.R., 2006. Accuracy and repeatability of a new method for measuring facet loads in the lumbar spine. J Biomech 39, 348-353.

Womack, W., Ayturk, U.M., Puttlitz, C.M., Cartilage thickness distribution affects computational model predictions of cervical spine facet contact parameters. J Biomech Eng 133, 011009.

Wu, Y.T., Millwater, H.R., Cruse, T.A., 1990. Advanced Probabilistic Structural-Analysis Method for Implicit Performance Functions. Aiaa Journal 28, 1663-1669.

Yan, J.Z., Qiu, G.X., Wu, Z.H., Wang, X.S., Xing, Z.J., Finite element analysis in adjacent segment degeneration after lumbar fusion. Int J Med Robot 7, 96-100.

Yoganandan, N., Knowles, S.A., Maiman, D.J., Pintar, F.A., 2003. Anatomic study of the morphology of human cervical facet joint. Spine (Phila Pa 1976) 28, 2317-2323.

Zander, T., Rohlmann, A., Bergmann, G., 2004. Influence of ligament stiffness on the mechanical behavior of a functional spinal unit. J Biomech 37, 1107-1111.

Zander, T., Rohlmann, A., Calisse, J., Bergmann, G., 2001. Estimation of muscle forces in the lumbar spine during upper-body inclination. Clin Biomech (Bristol, Avon) 16 Suppl 1, S73-80.
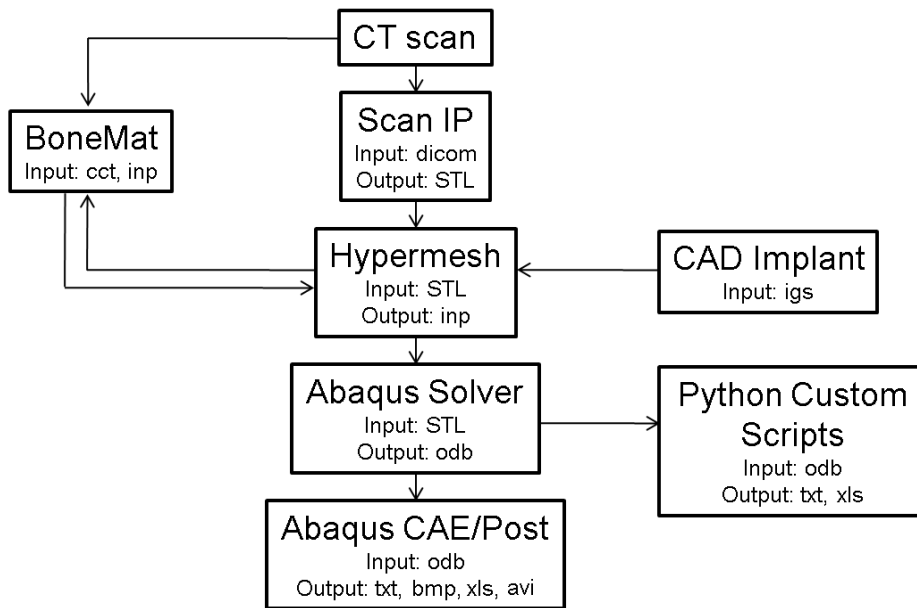
Figure A1.1. Model development workflow
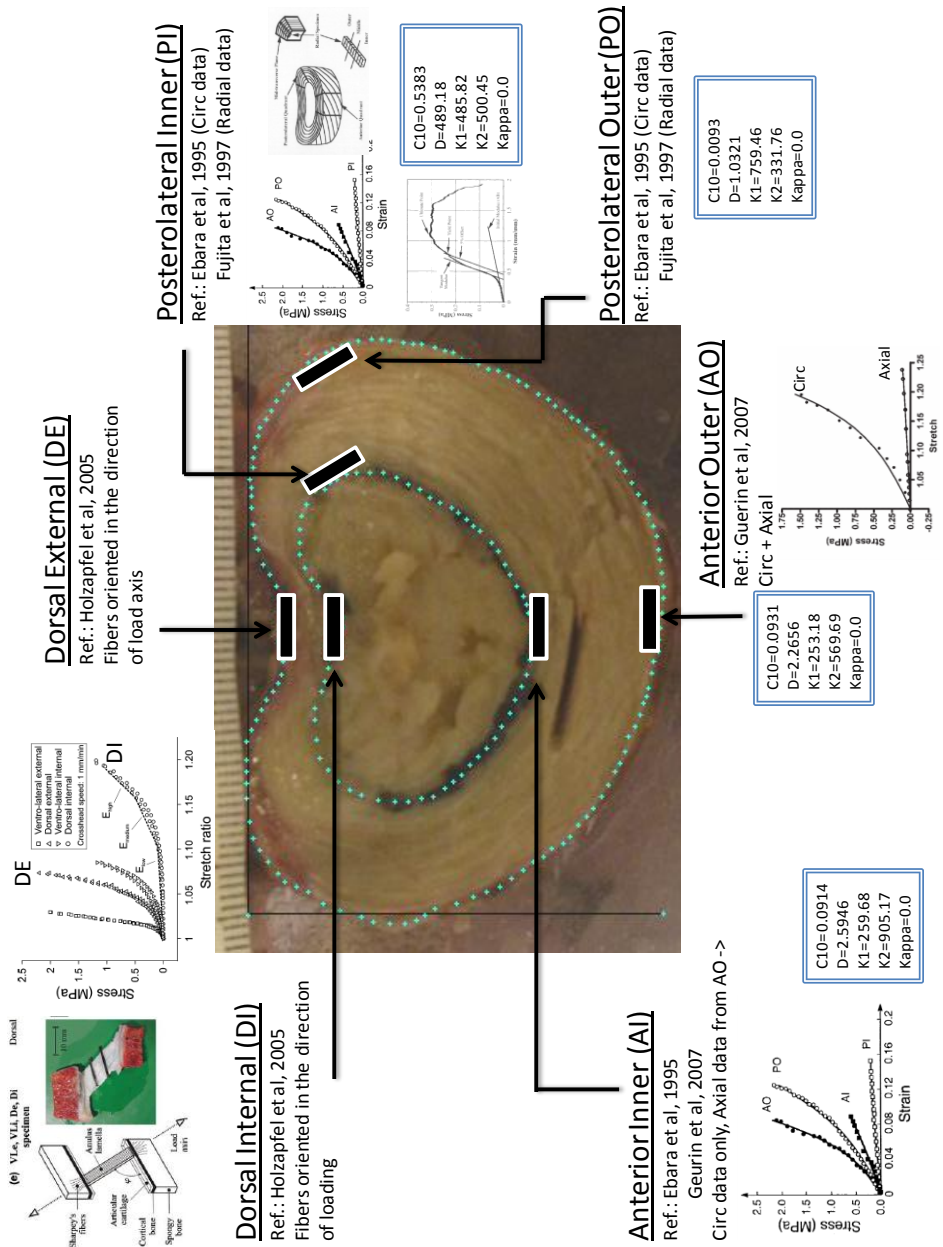
Figure A1.2. Optimized material constants for location specific AF uniaxial tensile test simulation to match the force-deflection curves
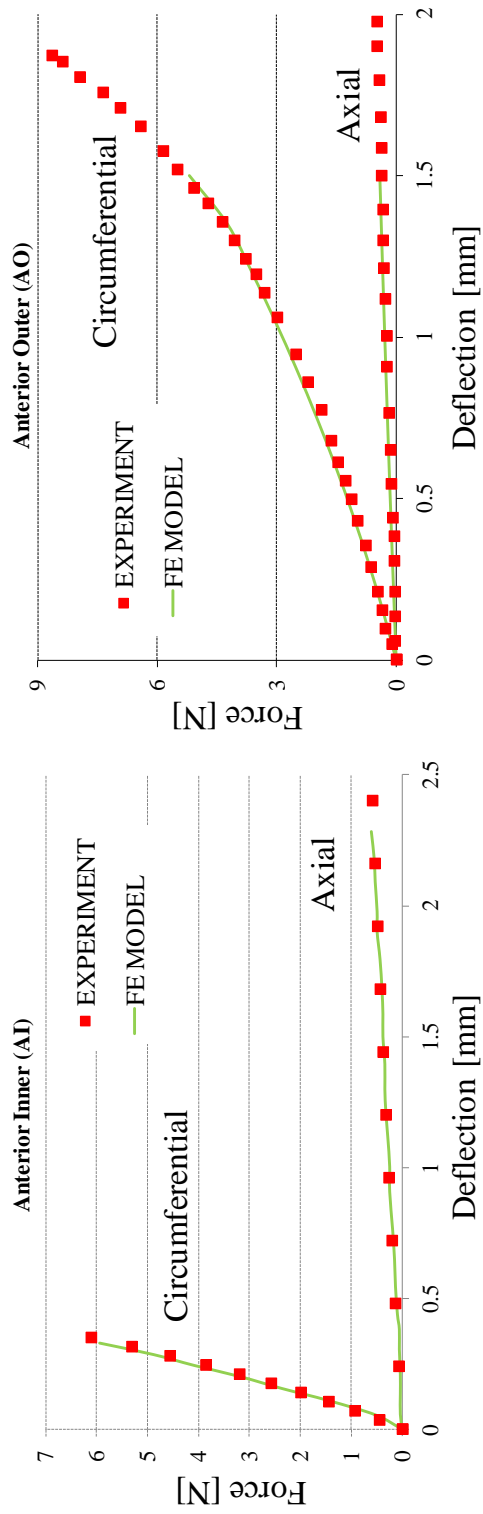
Figure A1.3. Force-deflection curves for location specific AF unaxial tensile test simulation – AI and AO

locations

130
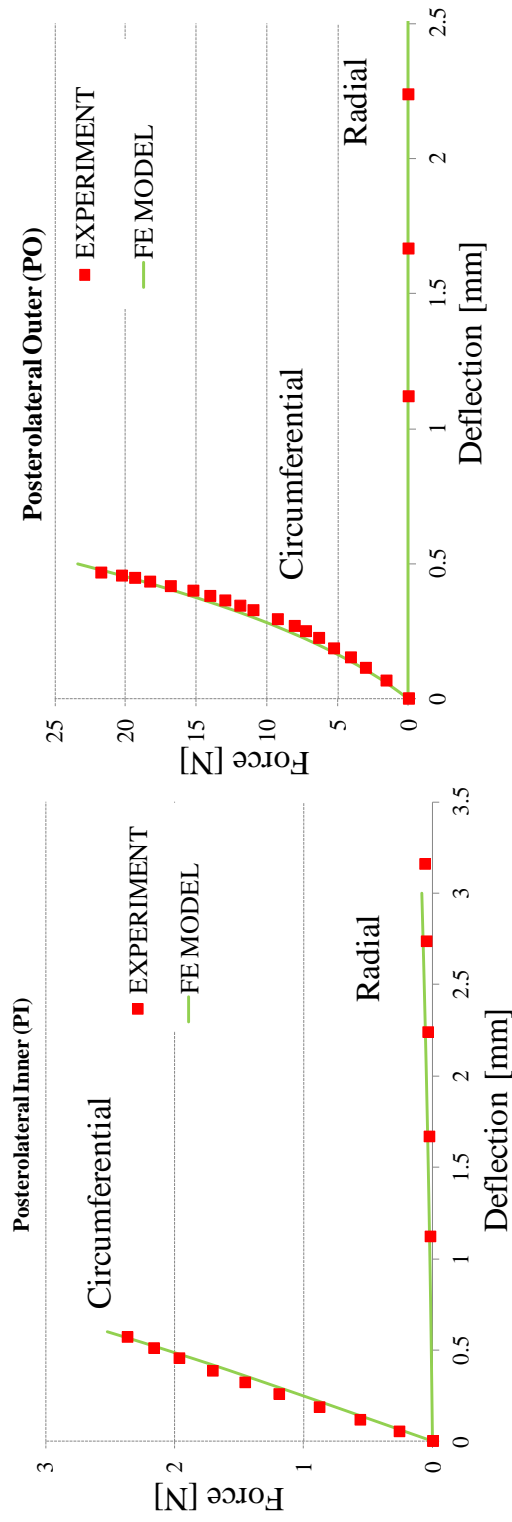
Figure A1.4. Force-deflection curves for location specific AF unaxial tensile test simulation – PI and PO locations
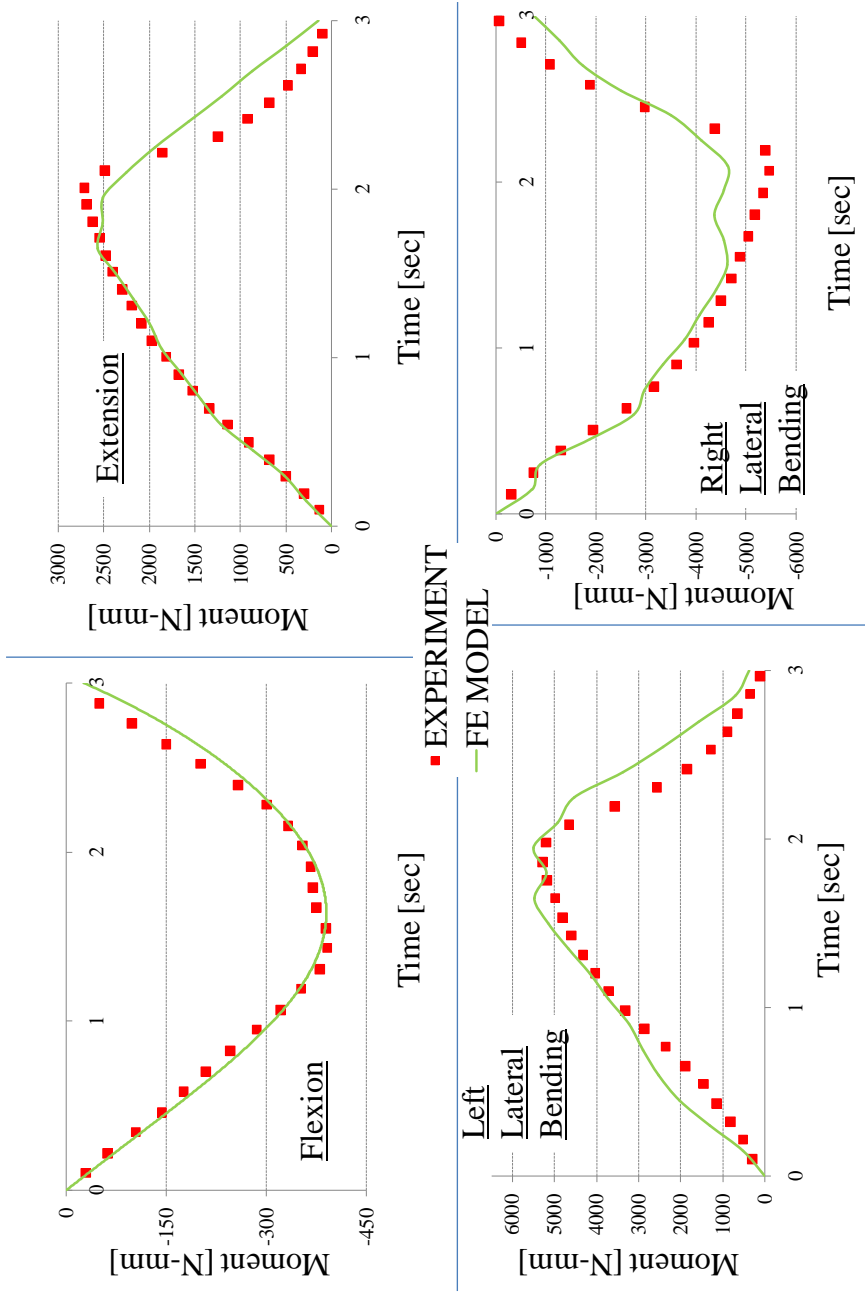
Figure A1.5. Reaction moment versus time for test 47 and 48 during flex-ext and lateral bending
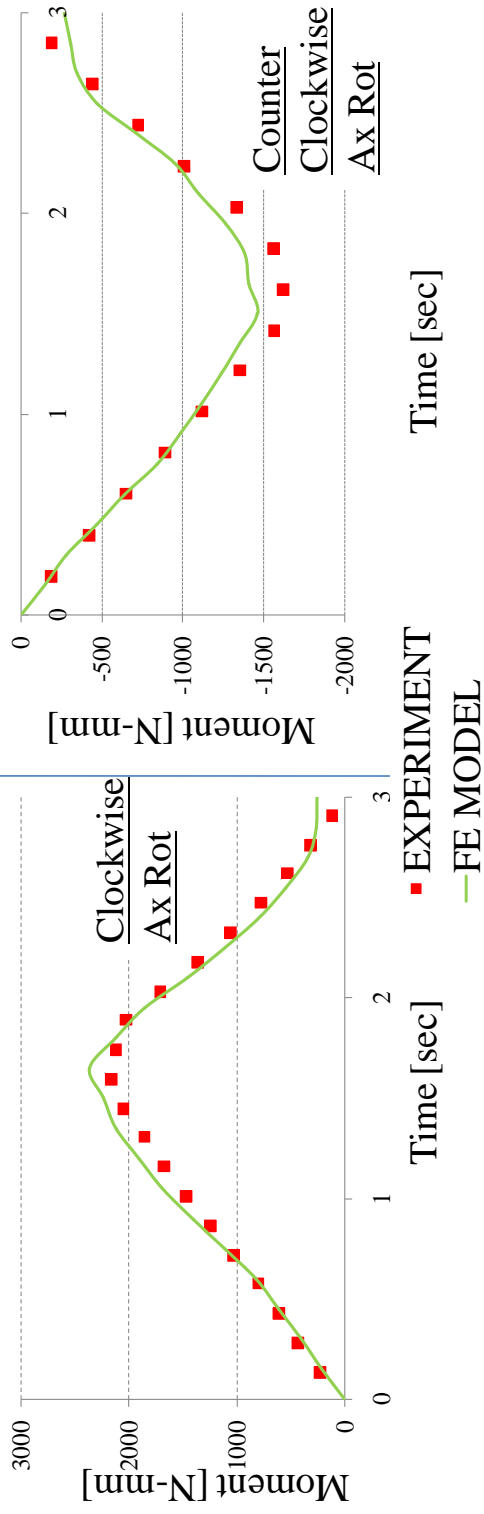
Figure A1.6. Reaction moment versus time for test 49 during axial rotation
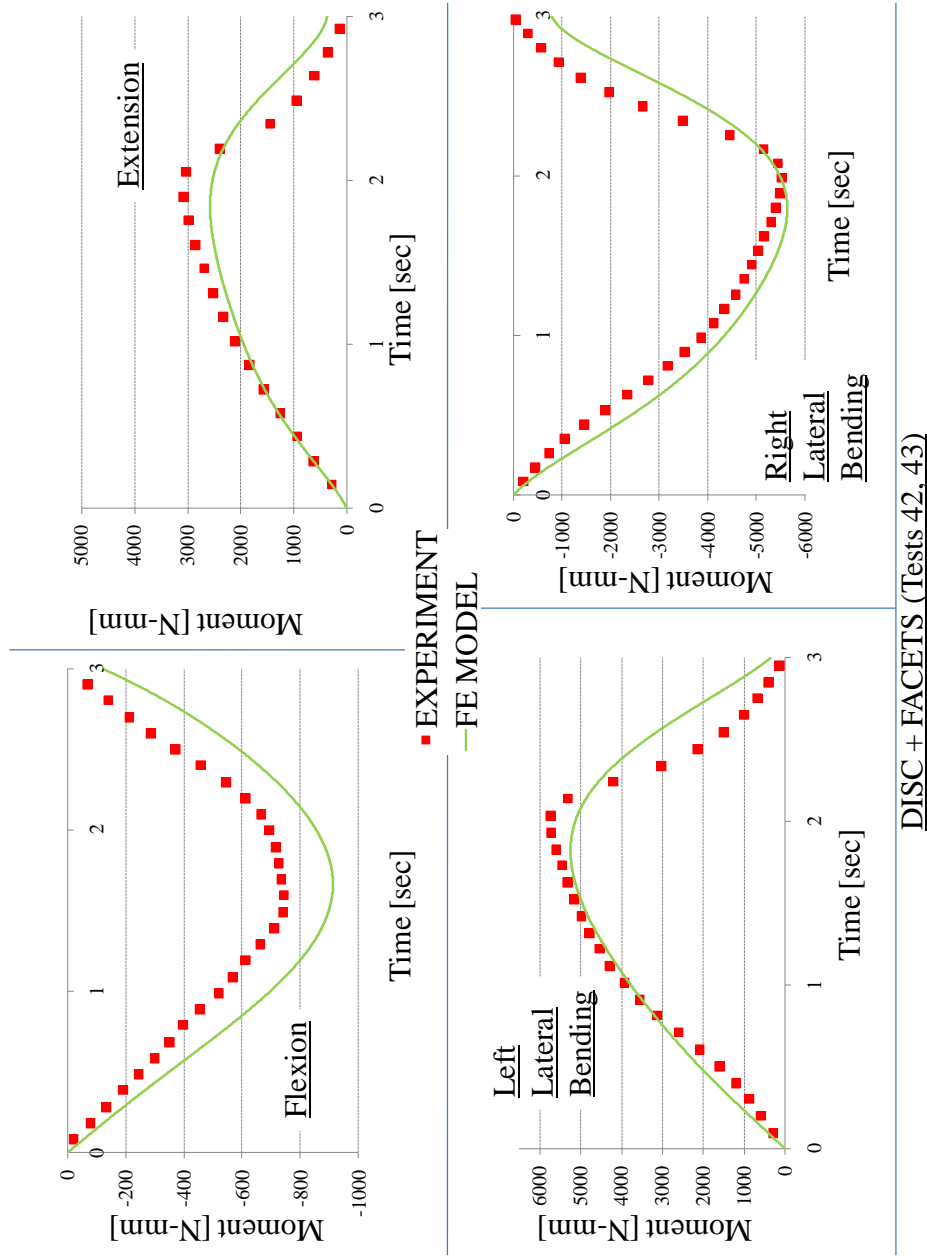
Figure A1.7. Reaction moment versus time for test 42 and 43during flex-ext and lateral
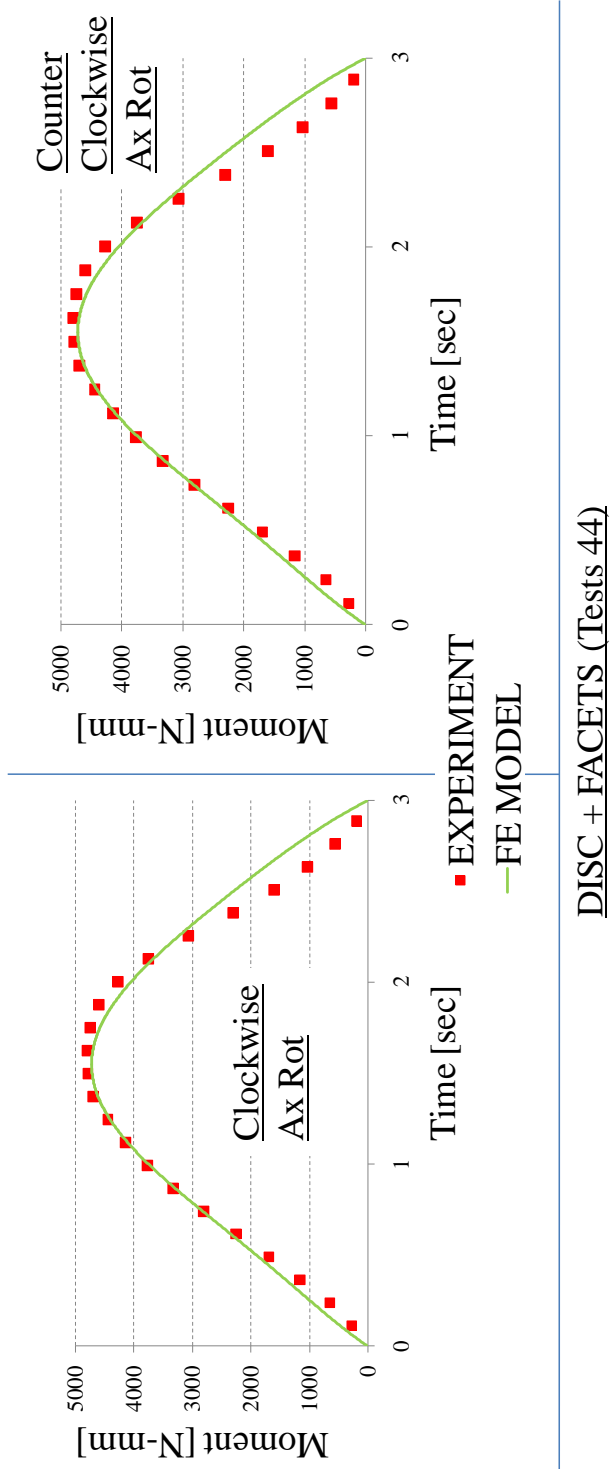
Figure A1.8. Reaction moment versus time for test 44 during axial rotation
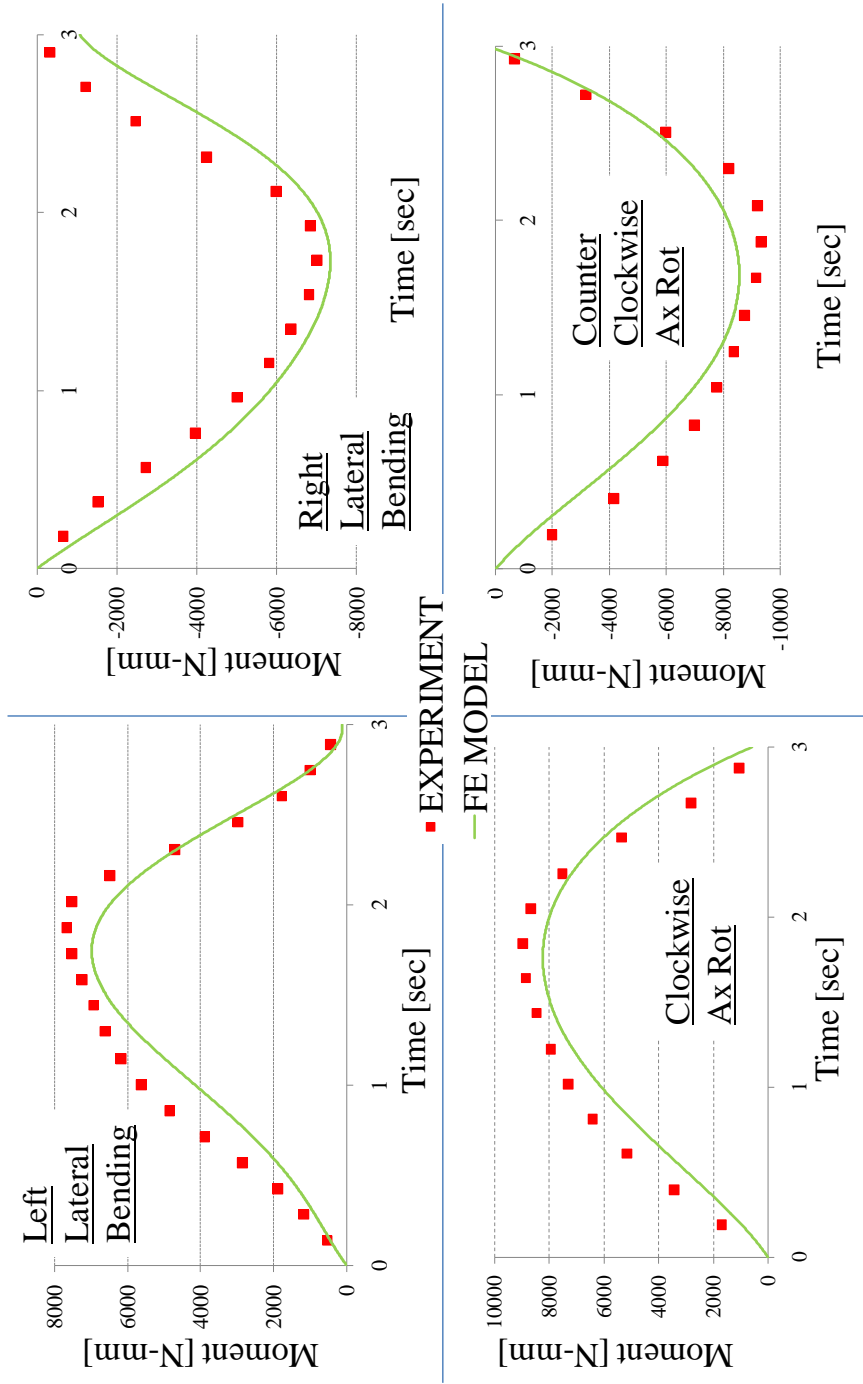
Figure A1.9. Reaction moment versus time for test 33 and 34 during flex-ext and axial rotation
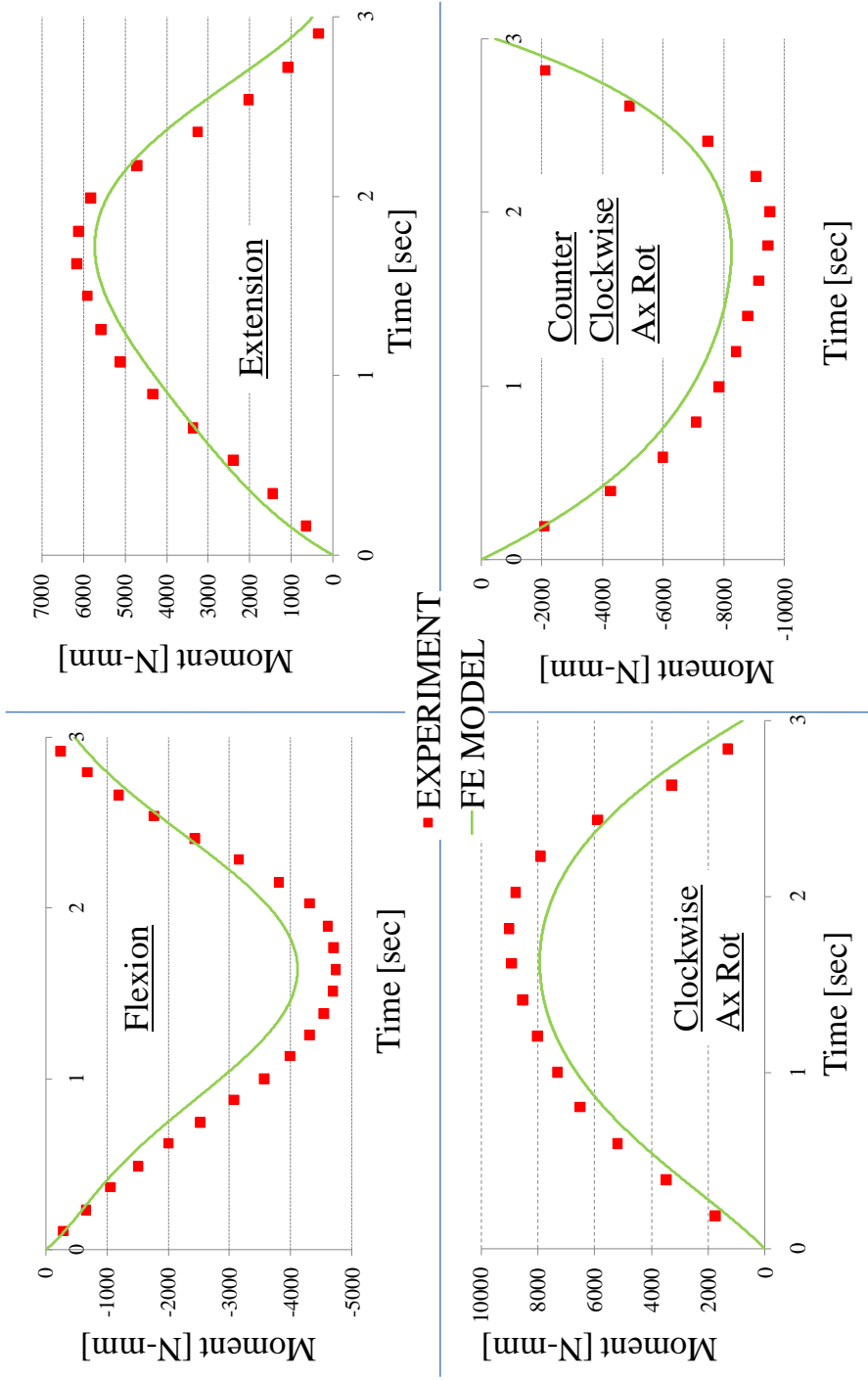
Figure A1.10. Reaction moment versus time for test 29 and 30 during flex-ext and axial rotation

137
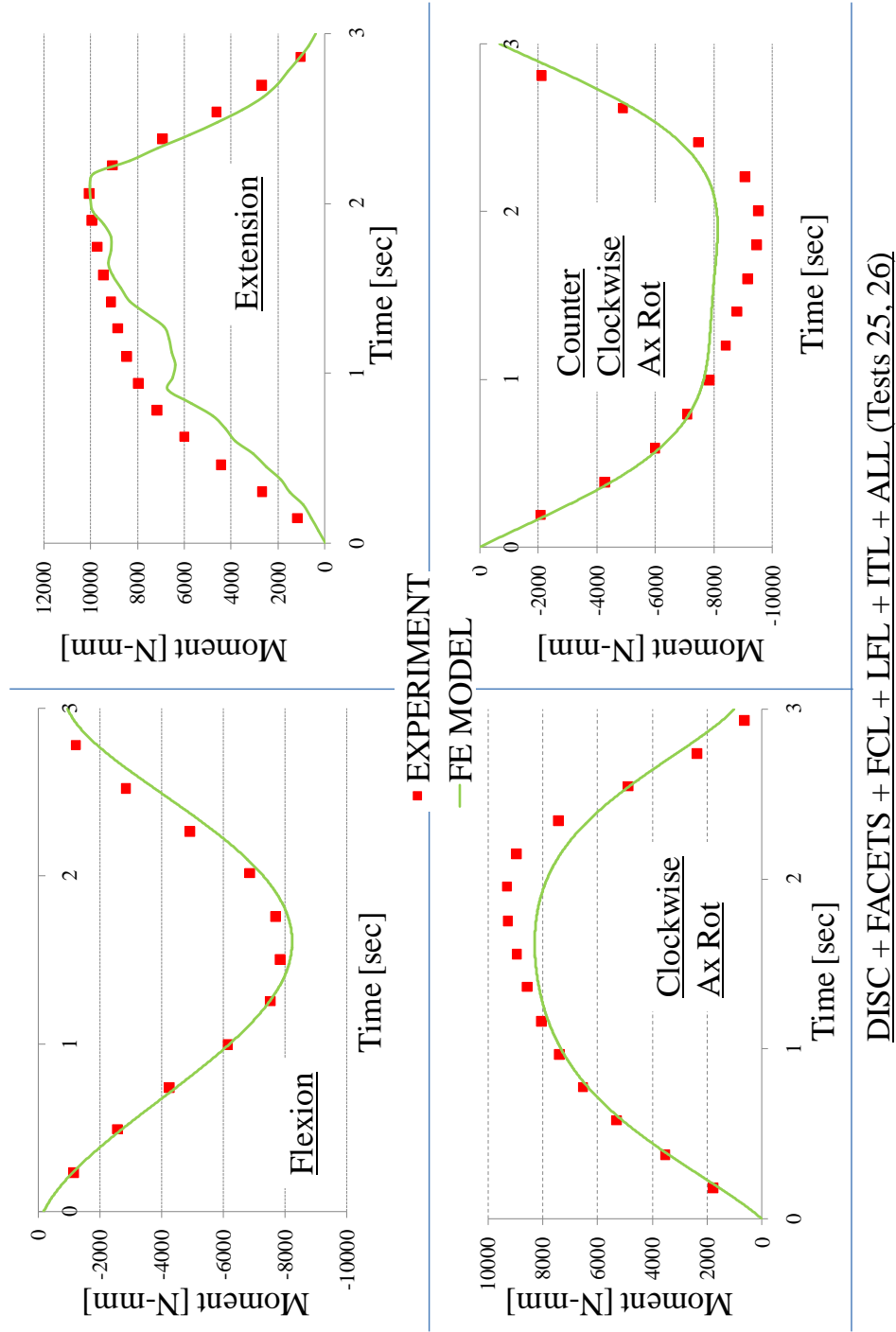
Figure A1.11. Reaction moment versus time for test 25 and 26 during flex-ext and lateral bending
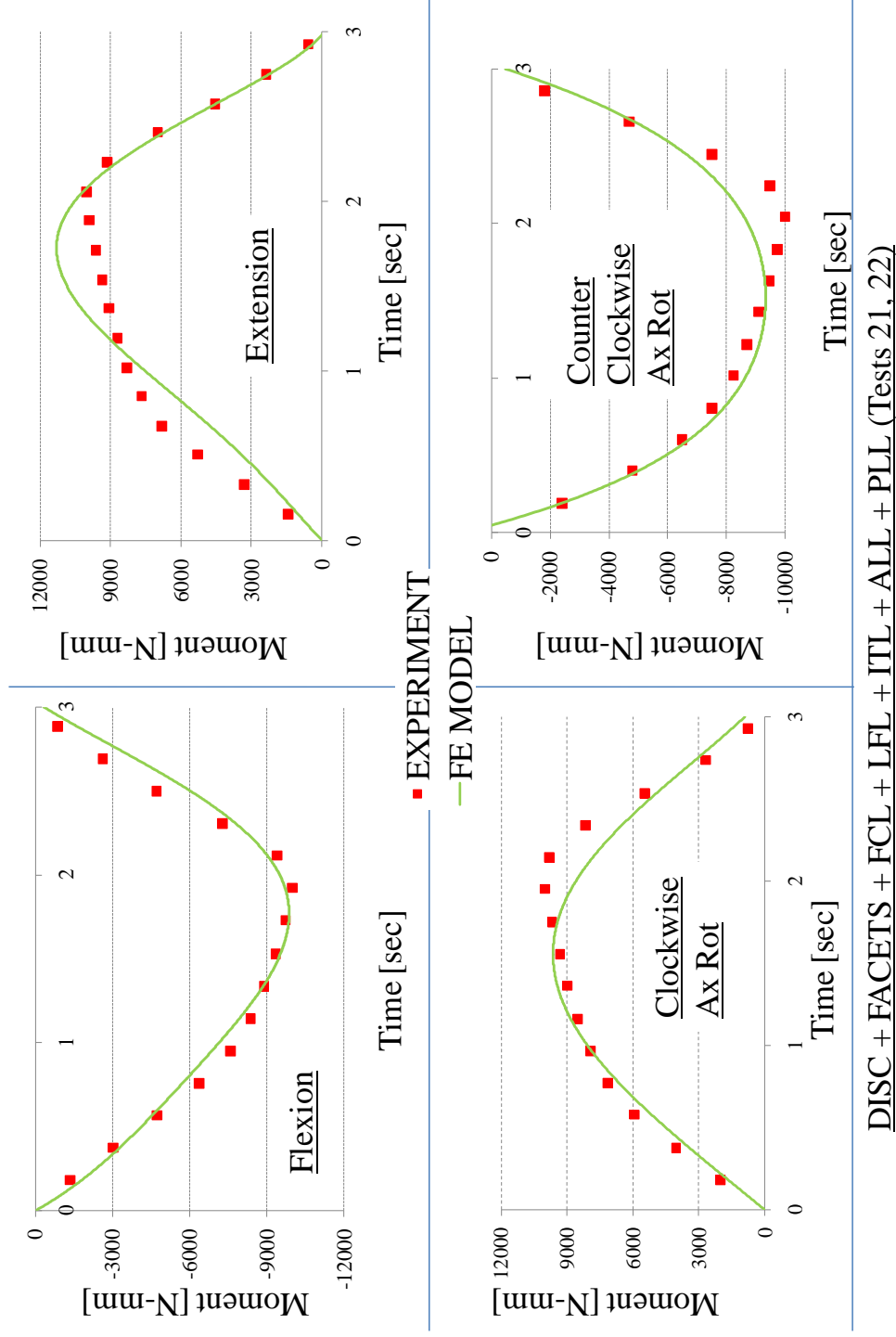
Figure A1.12. Reaction moment versus time for test 21 and 22 during flex-ext and lateral bending

139
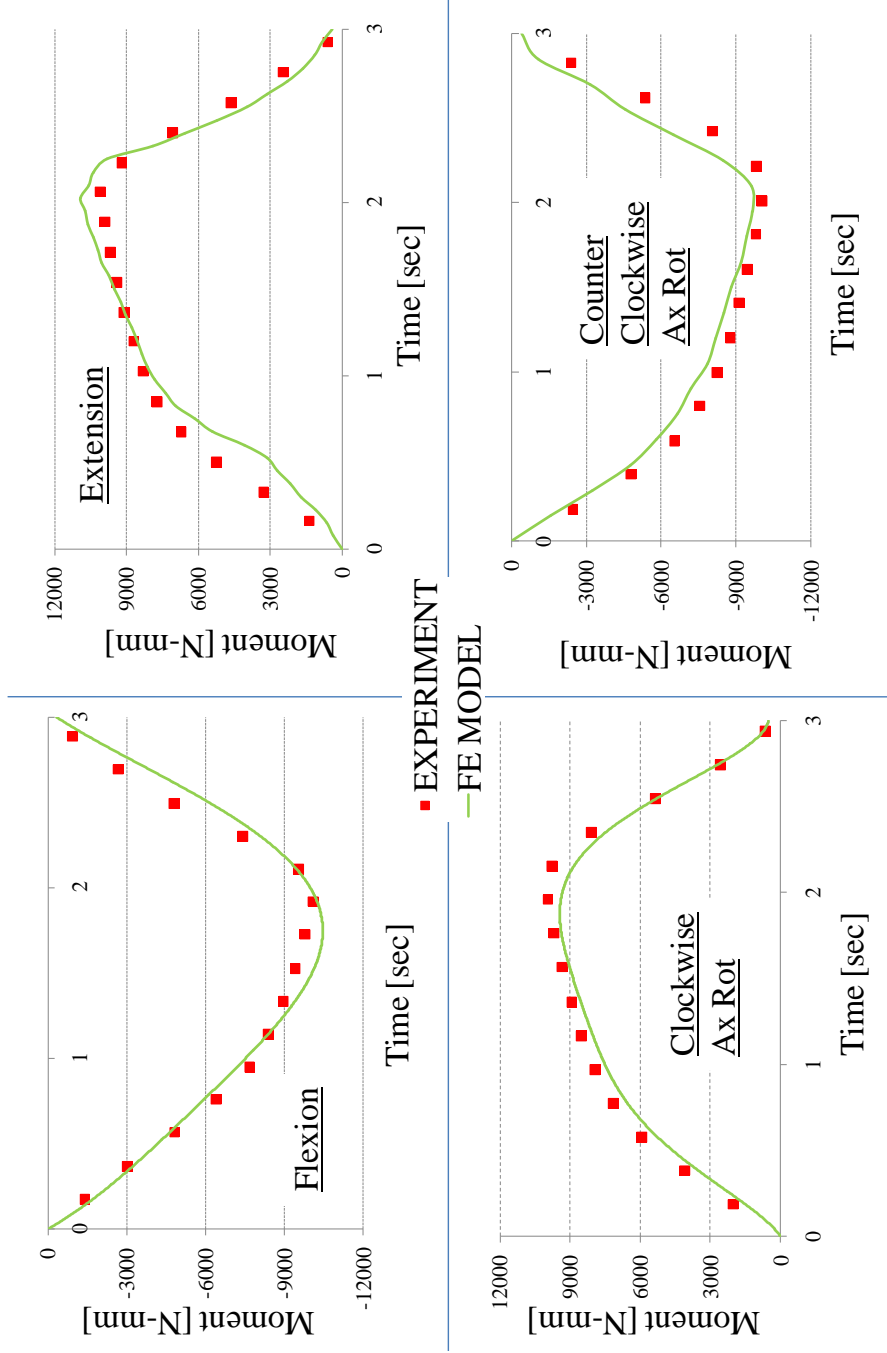
Figure A1.13. Reaction moment versus time for test 17 and 18 during flex-ext and lateral bending

140

Left lateral bending

Right axial rotation

Extension

Left axial rotation

Flexion

Right lateral bending

LE, Min. Principal
(Avg: 75%)

0.00000
-0.01250
-0.02500
-0.03750
-0.05000
-0.06250
-0.07500
-0.08750
-0.10000
-0.11250
-0.12500
-0.13750
-0.15000
-0.26569
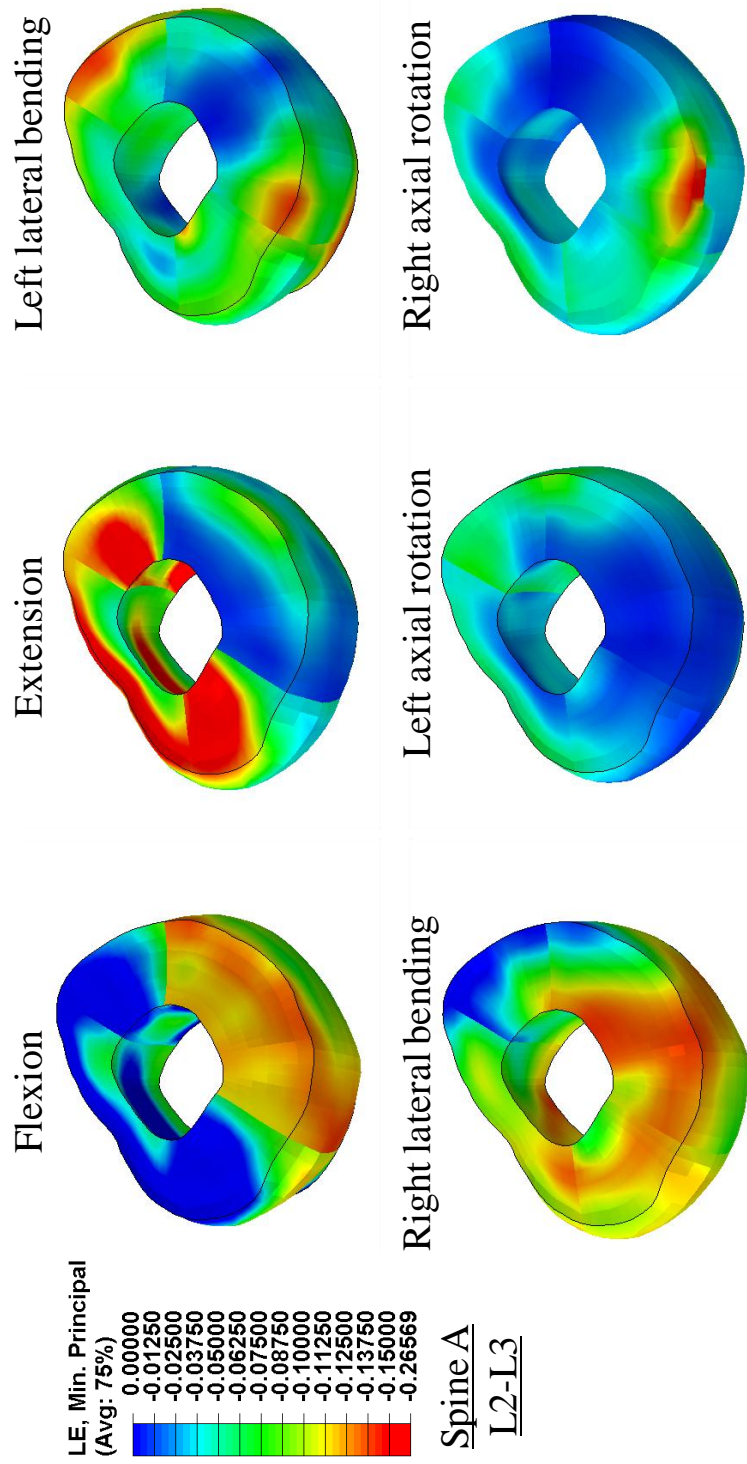
Spine A
L2-L3

Figure A1.14. Representative compressive strains in the annulus for *Spine A* - L2-L3

141

Left lateral bending

Right axial rotation

Extension

Left axial rotation

Flexion

Right lateral bending

LE, Max. Principal
(Avg: 75%)
0.43135
0.10000
0.09167
0.08333
0.07500
0.06667
0.05833
0.05000
0.04167
0.03333
0.02500
0.01667
0.00833
0.00000

Spine B
L4-L5
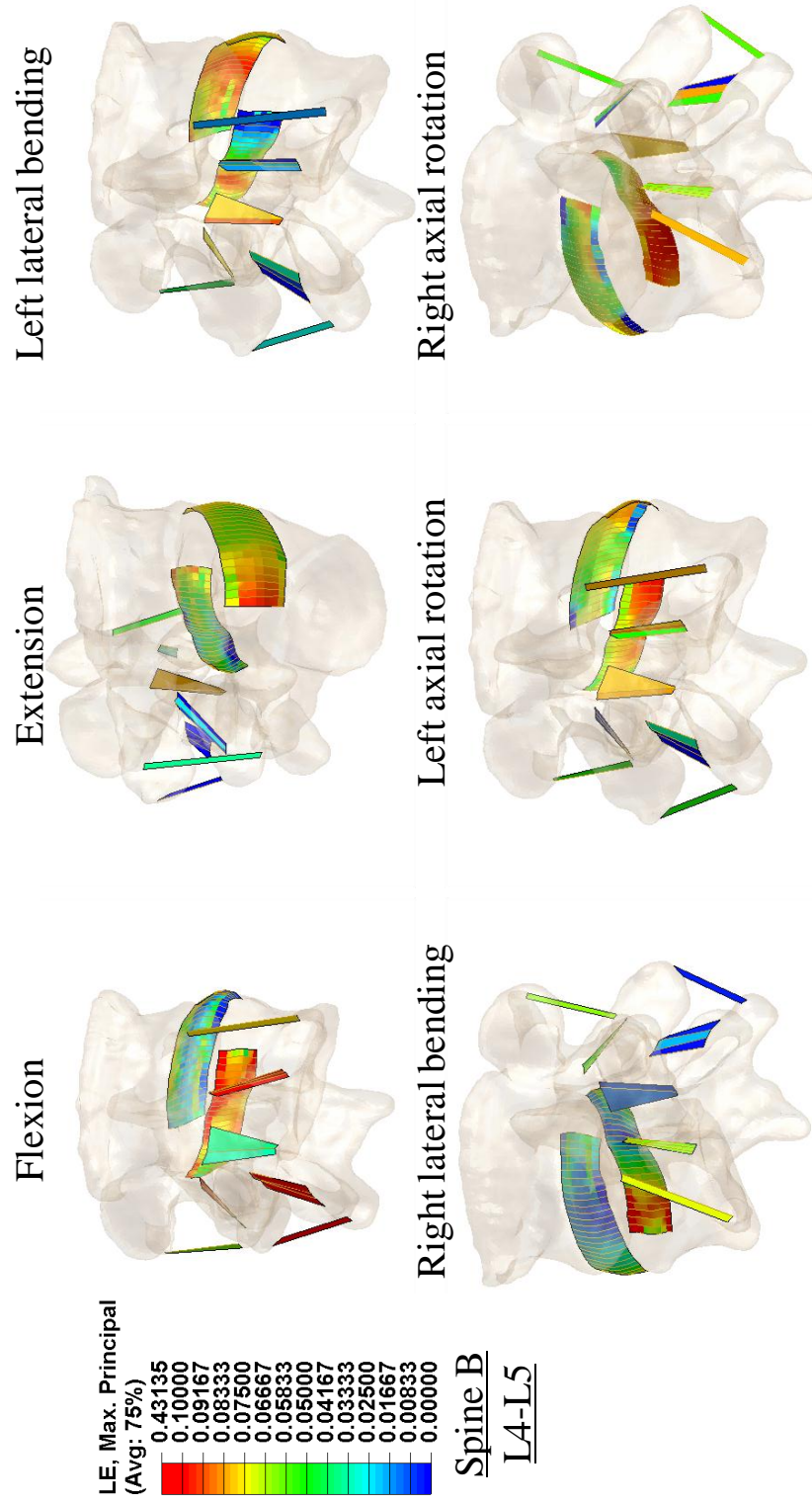
Figure A1.15 Representative strain contours in the fiber reinforced membranous ligaments for intact FSU L4-L5

142
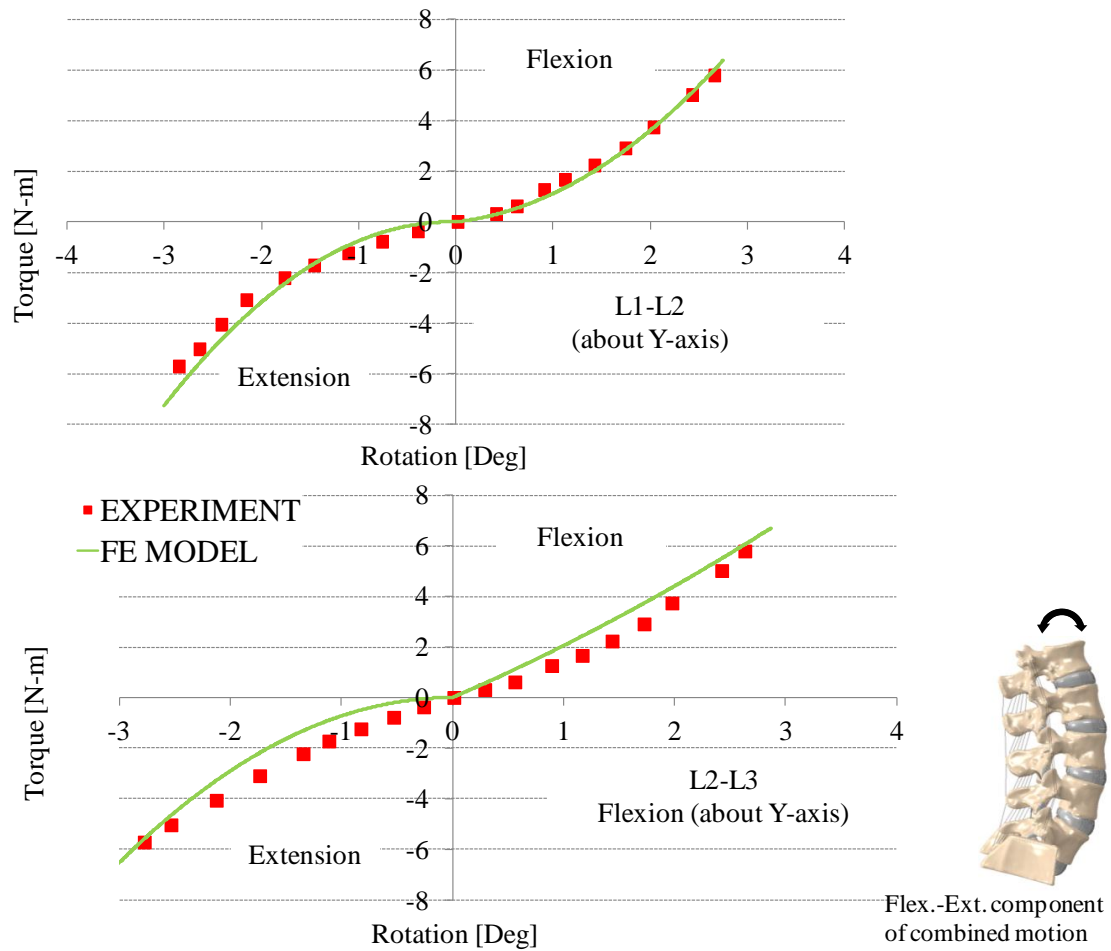
Figure A1.16 Representative torque-rotation response of intact combination motion during flexion and lateral bending at L1-L2 and L2-L3. Plots indicate the _flexion and extension_ components of this motion
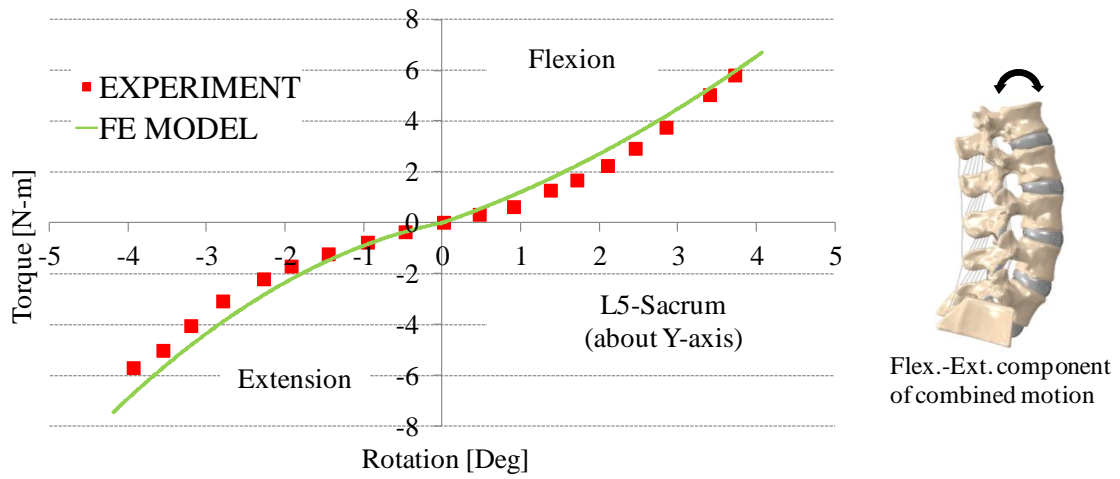
Figure A1.17 Representative torque-rotation response of intact combination motion during flexion and lateral bending at L5-Sacrum. Plots indicate the <u>flexion and extension</u> components of this motion
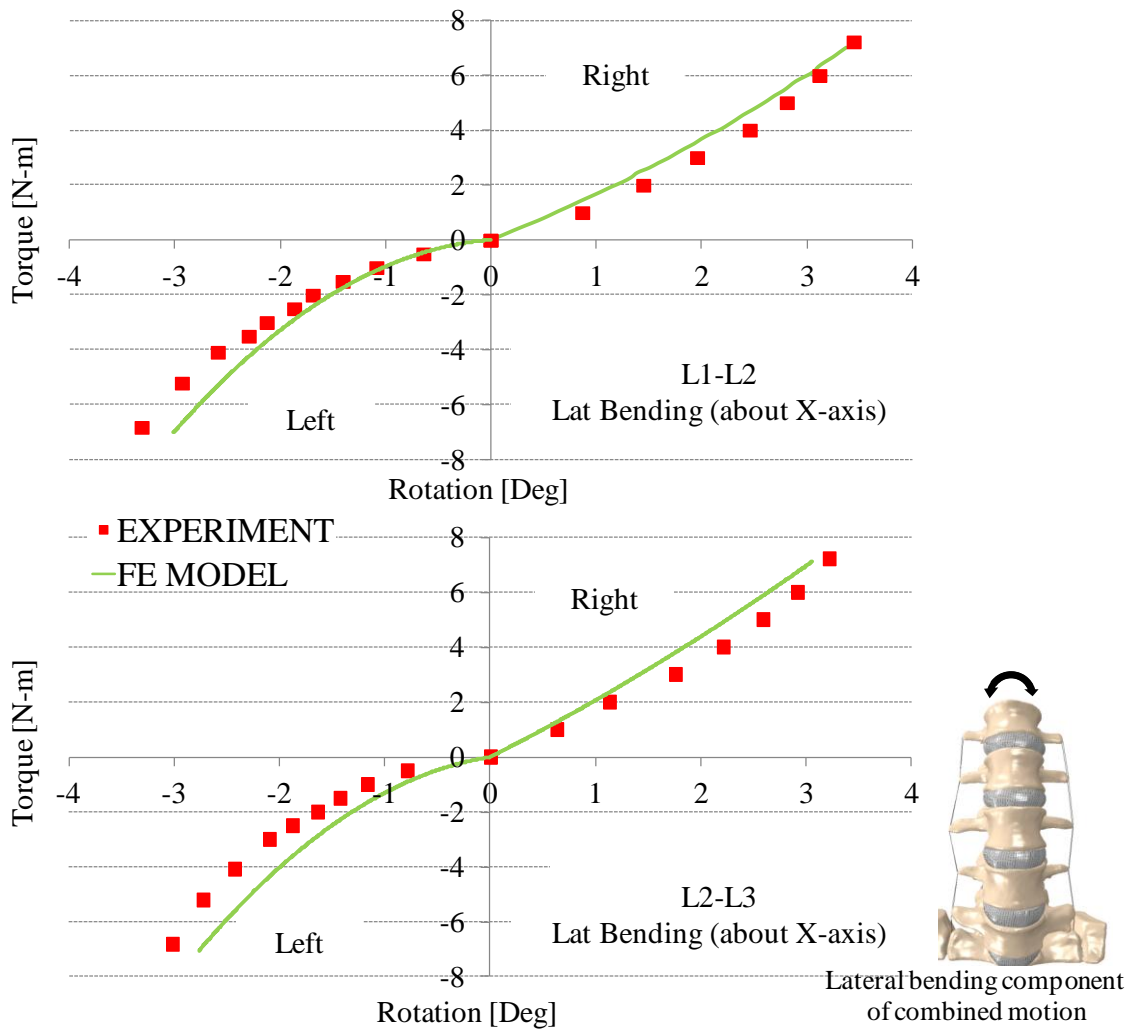
Figure A1.18 Representative torque-rotation response of intact combination motion during flexion and lateral bending at L1-L2 and L2-L3. Plots indicate the lateral bending components of this motion
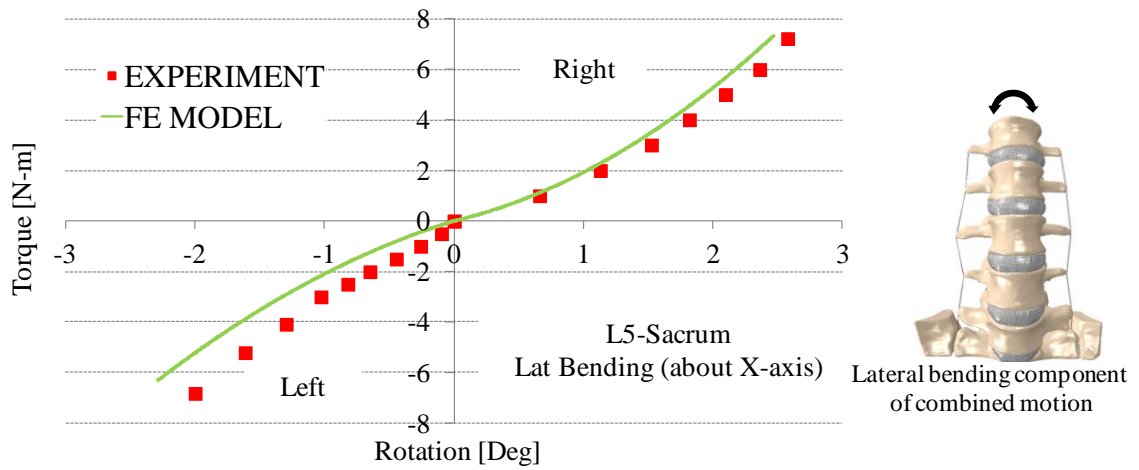
Figure A1.19 Representative torque-rotation response of intact combination motion during flexion and lateral bending at L5-Sacrum. Plots indicate the <u>lateral bending</u> components of this motion
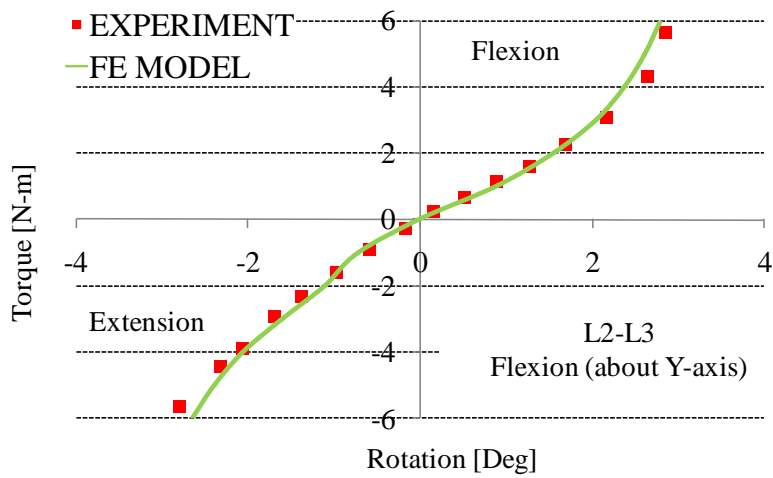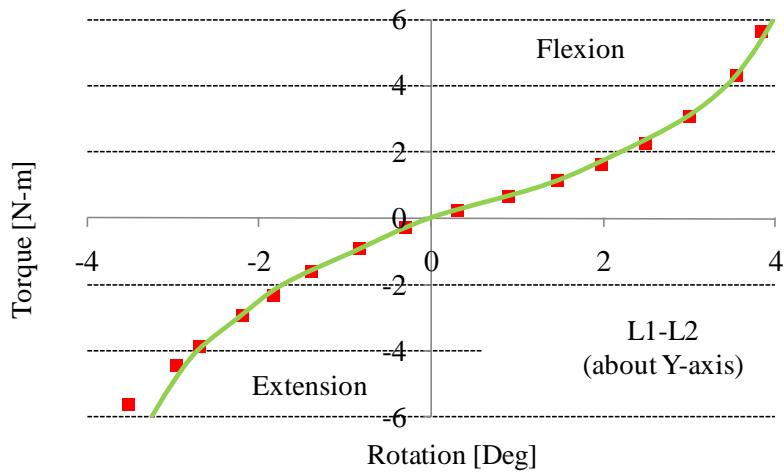
Figure A1.20 Representative torque-rotation response of intact combination motion during flexion and axial rotation at L1-L2 and L2-L3. Plots indicate the <u>flexion and extension</u> components of this motion
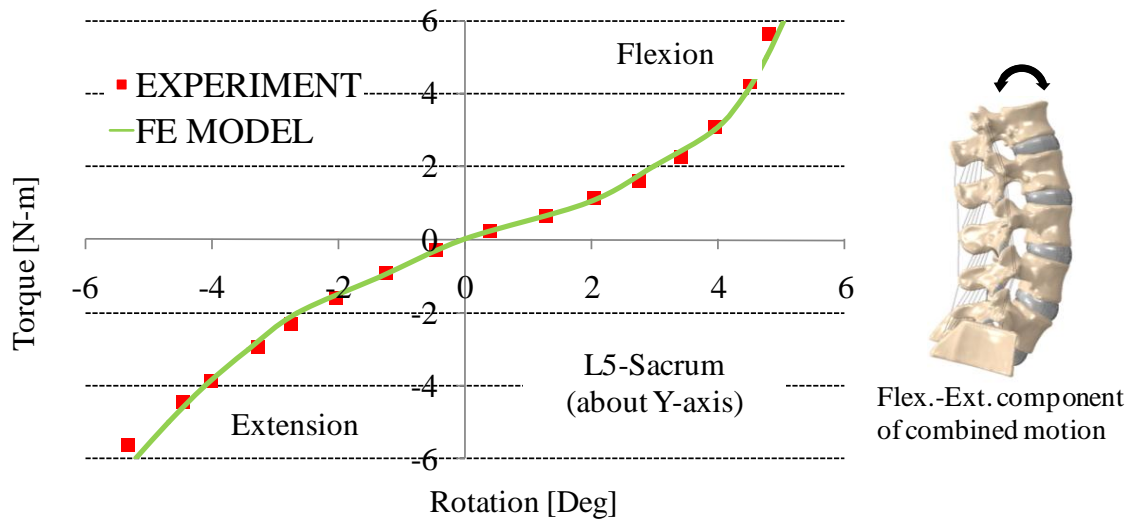
Figure A1.21 Representative torque-rotation response of intact combination motion during flexion and axial rotation at L5-Sacrum. Plots indicate the flexion and extension components of this motion
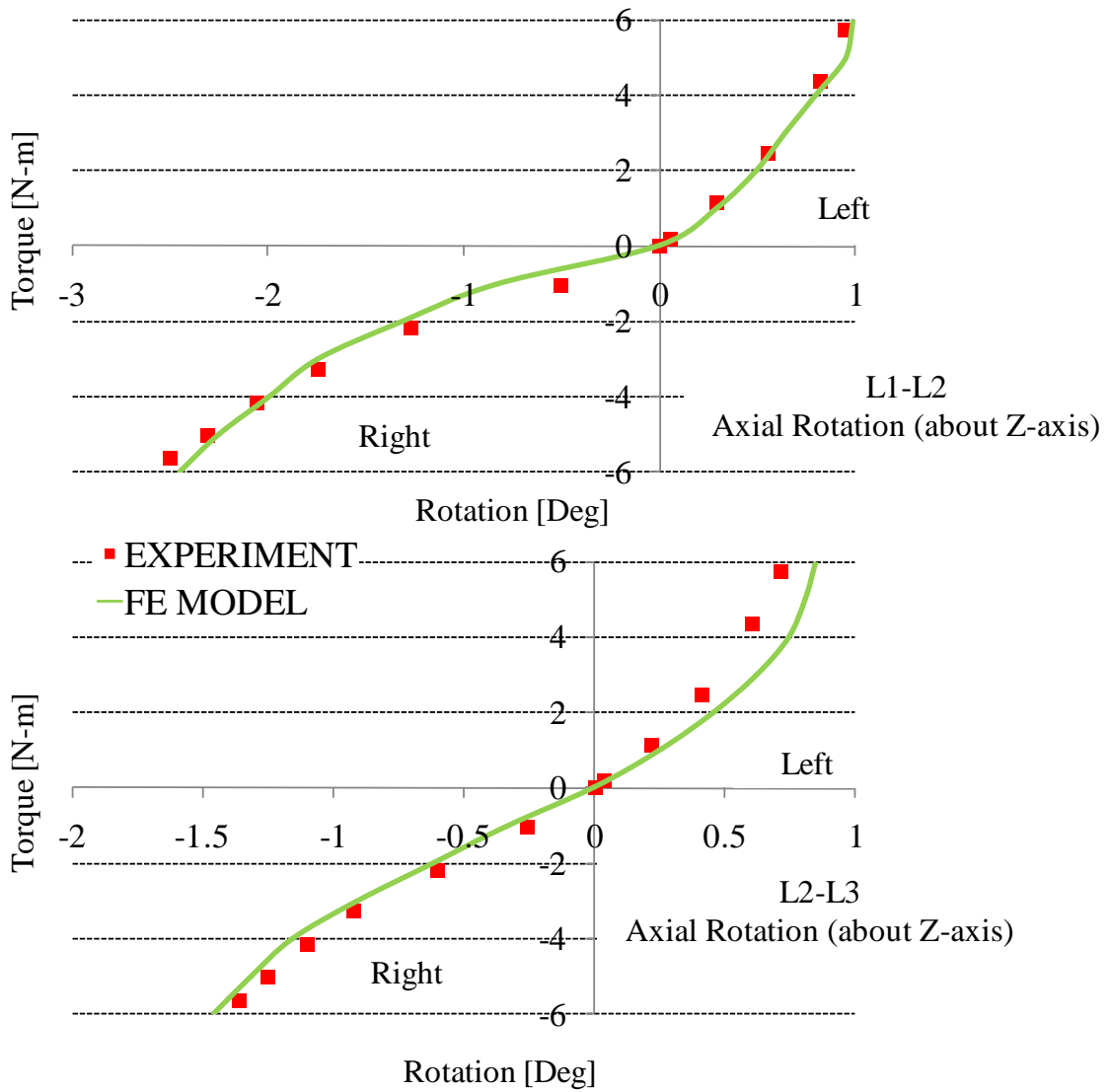
Figure A1.22 Representative torque-rotation response of intact combination motion during flexion and axial rotation at L1-L2 and L2-L3. Plots indicate the <u>axial rotation</u> components of this motion
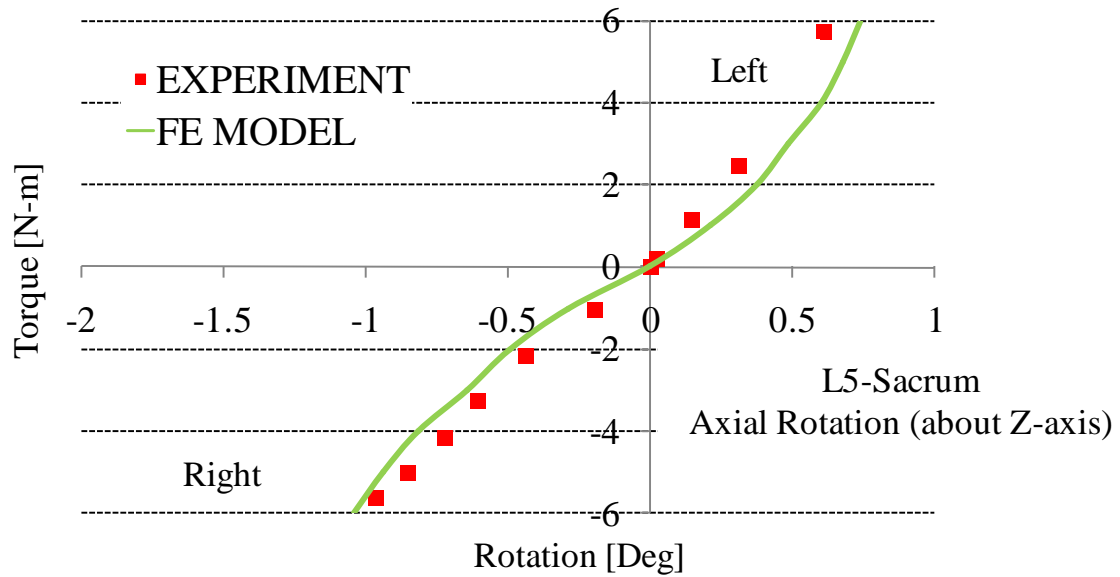
Figure A1.23 Representative torque-rotation response of intact combination motion during flexion and axial rotation at L5-Sacrum. Plots indicate the axial rotation components of this motion
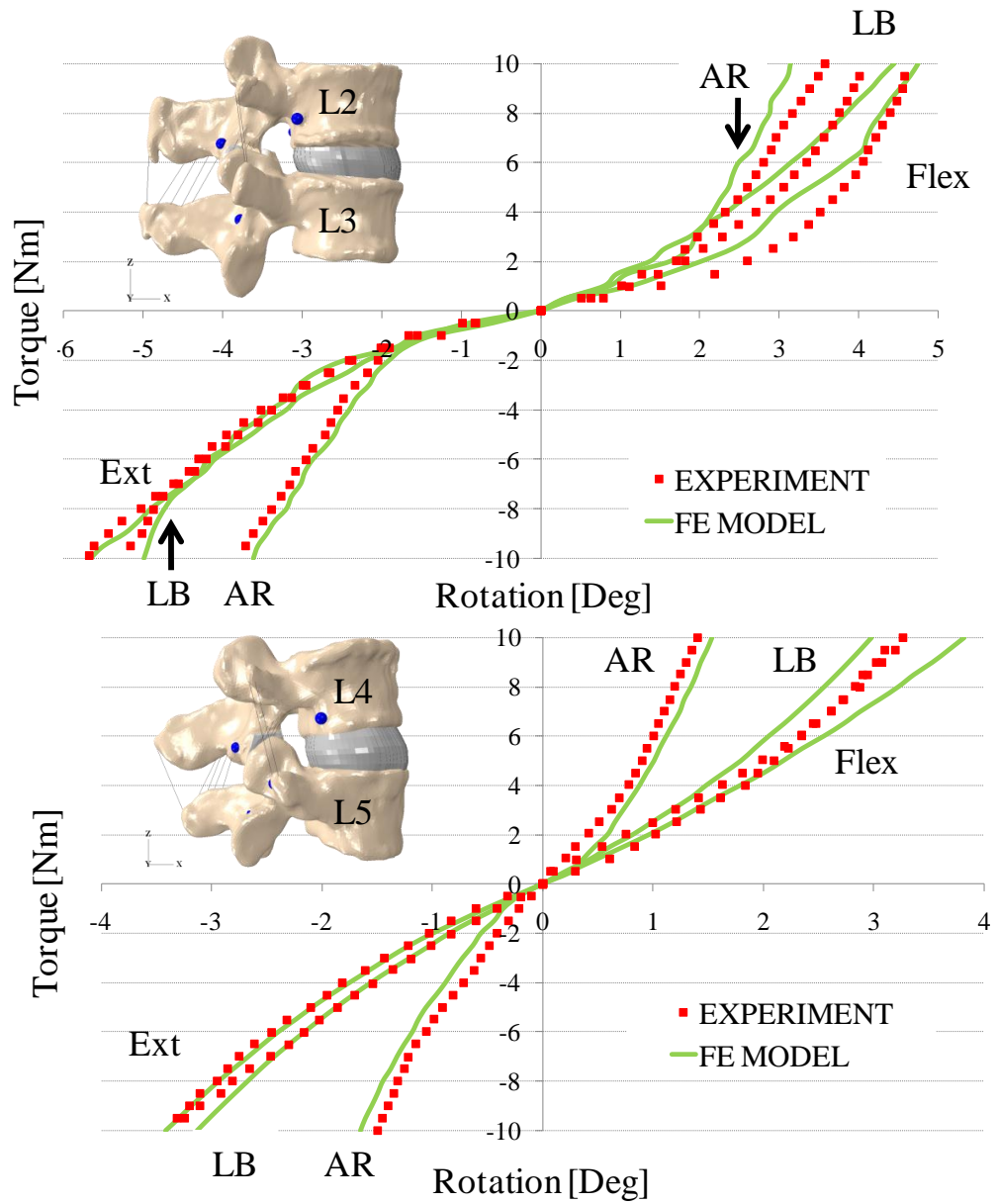
Figure A1.24. Torque-rotation response for intact *Spine B* - FSU L2-L3 (top) and

FSU L4-L5 (bottom)

| | L2-L3 | | | | | | L4-L5 | | | | | | Total RMSE [Deg] |
| | Spine A | | | Spine B | | | Spine A | | | Spine B | | | |
	Exp [Deg]	Model [Deg]	RMSE [Deg]	Exp. [Deg]	Model [Deg]	RMSE [Deg]	Exp. [Deg]	Model [Deg]	RMSE [Deg]	Exp. [Deg]	Model [Deg]	RMSE [Deg]	
Flexion	4.72	4.68	0.15	5.66	4.75	0.37	8.51	8.87	0.15	3.29	3.82	0.29	0.24
Extension	3.40	3.45	0.10	5.28	4.88	0.13	6.52	6.58	0.08	3.43	3.41	0.17	0.12
Left lateral bending	3.68	3.62	0.05	5.68	5.67	0.16	4.80	4.65	0.22	3.50	3.13	0.26	0.17
Right lateral bending	3.57	3.41	0.10	4.10	4.44	0.29	4.48	4.72	0.25	3.25	2.99	0.26	0.22
Left axial rotation	1.94	1.98	0.10	3.58	3.15	0.28	1.78	1.76	0.08	1.40	1.54	0.13	0.15
Right axial rotation	2.27	2.15	0.05	3.89	3.61	0.16	1.88	1.84	0.18	1.51	1.65	0.14	0.13

Figure A1.25. Comparison of range of motion (rotation) for intact L2-L3 (*Spine A* and *Spine B*) and L4-L5 (*Spine A* and *Spine B*) with the root mean squared error (RMSE) over the torque-rotation curve